PLASMA POSITION CONTROL IN THE STOR-M TOKAMAK: A FUZZY LOGIC APPROACH

A Thesis Submitted to the College of
Graduate Studies and Research
in Partial Fulfillment of the Requirements
for the Degree of

Doctor of Philosophy

in the
Department of Electrical Engineering
University of Saskatchewan
Saskatoon

by

Jordan Edwin Morelli

PERMISSION TO USE

In presenting this thesis in partial fulfilment of the requirements for a Postgraduate degree from the University of Saskatchewan, I agree that the Libraries of this University may make it freely available for inspection. I further agree that permission for copying of this thesis in any manner, in whole or in part, for scholarly purposes may be granted by the professor or professors who supervised my thesis work or, in their absence, by the Head of the Department or the Dean of the College in which my thesis work was done. It is understood that any copying or publication or use of this thesis or parts thereof for financial gain shall not be allowed without my written permission. It is also understood that due recognition shall be given to me and to the University of Saskatchewan in any scholarly use which may be made of any material in my thesis.

Requests for permission to copy or to make other use of material in this thesis in whole or part should be addressed to:

Head of the Department of Electrical Engineering

University of Saskatchewan

Saskatoon, Saskatchewan S7N 5A9

ABSTRACT

Adequate control of the position of the plasma column within the STOR-M tokamak is a chief requirement in order for experimental quality discharges to be obtained. Optimal control over tokamak discharge parameters, including the plasma position, is very difficult to achieve. This is due in large part to the difficulty in modelling the tokamak discharge parameters, as they are highly nonlinear and time varying in nature. The difficulty of modelling the tokamak discharge parameters suggests that a control system, such as a fuzzy logic based controller, which does not require a system model may be well suited to the control of fusion plasma.

In order to improve the quality of control over the plasma position within the STOR-M tokamak, the existing analog PID controller was modified. These modifications facilitate the application of a digital controller by a personal computer via the Advantech PCL-711B data acquisition card. The performance of the modified plasma position controller and an Arbitrary Signal Generator developed by the author was evaluated. This modified plasma position controller was applied successfully to the STOR-M tokamak during both normal mode and A.C. mode operation. In both cases, the modified controller provided adequate control over the position of the plasma column within the discharge chamber. Furthermore, the modified controller was more convenient to optimize than the original, existing analog PID controller.

By taking advantage of the modifications that were made to the plasma position controller, a fuzzy logic controller was developed by the author. The fuzzy logic based plasma position controller was also successfully applied to the STOR-M tokamak during both normal mode and A.C. operation. The fuzzy controller was demonstrated to reliably provide a higher degree of control over the position of the plasma column within the STOR-M tokamak than the modified PID controller.

ACKNOWLEDGEMENTS

I would like to acknowledge the support of my two co-supervisors: Dr. Akira Hirose and Dr. Hugh Wood; without their assistance this thesis would not have been possible. The guidance and training provided by Dr. Osamu Mitarai of the Kyushu Tokai University in Kumamoto, Japan was invaluable to the success of this research project. A special thanks also goes out to Dr. Andrei Smolyakov and Dr. Chijin Xiao for their assistance and for many stimulating discussions. To all the members of the Plasma Physics Laboratory, past and present, thank you for the friendly working environment and the many insightful discussions.

This research was funded through grants from the Natural Sciences and Engineering Research Council of Canada (NSERC), and from ITER Canada. The author also acknowledges the financial support that was provided by the University of Saskatchewan Graduate Scholarship.

DEDICATION

This thesis is dedicated to:

- my wife, Evelyn, and our son, Edwin, thank you for your patience and understanding throughout my academic career. I know that there were many times when I was not able to be with you because I was busy with my research.
- my parents, thank you for your undying support; it has made all the difference.
- those teachers whose classrooms I have had the great fortune of being in. Your dedication and commitment to your students is greatly appreciated.

TABLE OF CONTENTS

LIST OF TABLES

LIST OF FIGURES

LIST OF ABBREVIATIONS

$\boldsymbol{B}$	Magnetic flux density
B_i	Magnetic flux density internal to the plasma column due to the plasma current
B_V	Net vertical magnetic field required for equilibrium
$B_{VE,VF,HF}$	Vertical equilibrium field, vertical field and horizontal field
B_w	Magnetic field in the vertical direction produced by Eddy currents in the wall
B_ϕ, B_θ, B_ρ	Toroidal, poloidal and radial components of the magnetic field
d_w	Thickness of the wall of the discharge chamber
DCB	DC Bias
e	Elementary electric charge
$\boldsymbol{E}$	Electric field intensity
f_i	Maxwell distribution function
$F_{1,2,3,4,5}$	Forces acting on the plasma column
F_w	Force on the plasma column due to B_w
HN	High Negative
HP	High Positive
i	Counting index
I_{B_φ}	Toroidal magnetic field current
I_{i0}	Ion saturation current
I_{OH}	Ohmic heating current
I_P	Plasma current
$I_{VE,VF,HF}$	Vertical equilibrium, vertical field and horizontal field current
J	Plasma current density
J_i	Ion current density
J_{e0}	Electron saturation current density
l_i	Internal inductance parameter
L_{ext}, L_i	External and internal plasma inductance
LN	Large Negative
LP	Large Positive
m	Mass of a particle
MN	Medium Negative
MP	Medium Positive
n_c	Cutoff density
$n_{\mathrm{D,T}}$	Number density of deuterium and tritium
$n_{\mathrm{e,i}}$	Number density of electrons and ions
n_{i0}	Central ion density
N	Number of turns making up a winding
P_f	Fusion power produced
P_i	Total input power

q	Charge of a particle
q	Safety factor
Q_f	Fusion power gain
r_c	Radius of the transformer core
r_l	Larmor radius
r_m	Radial location of the plasma position sensing coils
R	Major radial coordinate
R,a	Major and minor radius of the plasma column
R,a_0	Major and minor radius of vacuum vessel
R_P,L_P	Plasma resistance and inductance
SN	Small Negative
SP	Small Positive
T	Tiny
T_{i0}	Central ion temperature
ΔV, ΔH	Vertical and horizontal displacement of the plasma column
V, V_f, V_s	Probe bias potential, plasma floating potential, and plasma space potential
V_P	Plasma loop voltage
V_{RC}	Voltage produced across the terminals of a Rogowski coil
Z_{eff}	Effective ion charge
β_θ	Poloidal beta factor
$\Delta\Phi$	Phase shift
ε_0	Permittivity of free-space
η	Plasma resistivity
η_α	Efficiency of power transfer from α-particles to the bulk plasma
θ	Poloidal coordinate angle
ι	Rotational transform angle
λ_D	Debye length
μ_c	Relative permeability of the transformer core
μ_0	Permeability of free-space
$\boldsymbol{v}$	Velocity
$v_\perp$	Velocity component in the plane perpendicular to the magnetic field
$v_\parallel$	Velocity component in the direction parallel to the magnetic field
ρ	Minor radial coordinate
σ	Fusion reaction cross-section
σ_w	Electrical conductivity of the wall of the discharge chamber
τ_E	Energy confinement time
$\tau_{d,\,w}$	Magnetic field wall penetration times
ϕ	Toroidal coordinate angle
ϕ	Magnetic flux
ϕ_{ext}	Magnetic flux external to the plasma column due to the plasma current
ω_c	Cyclotron frequency

1. INTRODUCTION

1.1 Controlled Thermonuclear Fusion

Since the end of the Second World War, scientists and engineers have been studying the release of enormous amounts of energy that occurs when light nuclei fuse together. Their research led them first to the successful development of the H-bomb. Many researchers at the time realized that rather than employing this uncontrolled explosive process to destroy humanity, they could put it to use to serve humankind if only they could find a way to confine the reaction. Thus, the dream of controlled thermonuclear fusion was born. While the progress has been slow, it has been steady. For example, in 1991 the controlled production of over a megawatt of fusion power (two megajoules of fusion energy were released) was demonstrated in the JET tokamak [8], and in 1999 the JT-60U tokamak reported the reproducible production of an equivalent fusion power gain of 1.25 [62]; that is, more power was released by the fusion reaction than was required to sustain it. As a result of these successes, it is anticipated that the next generation of experimental reactors, such as the ITER reactor that is being planned will yield the breakthrough that everyone involved in controlled thermonuclear fusion research has been struggling to achieve. Thus, while it has taken many years and requires still many more years, there is light at the end of the tunnel, and the dream seems increasingly certain to become a reality.

As with a thermonuclear explosion, controlled thermonuclear fusion involves a reaction in which light nuclei (usually hydrogen isotopes) approach each other closely

enough to fuse together thereby forming heavier nuclear species and releasing energy in the process. In order to accomplish this, however, the reacting nuclei must be moving towards each other fast enough so that the repulsive Coulomb force between them can be overcome. This requires extremely high temperatures, of the order of 100 million degrees Celsius. The principal difference between the explosive reaction and the controlled reaction is that with the former, there is no need to confine the reaction, while with the latter, confining the reaction is of the utmost importance.

The relevant quantity describing the production of energy for a given fusion reaction is the reactivity $\langle \sigma v \rangle_{12}$, where σ is the cross-section for the fusion reaction between species 1 and 2, v is their relative velocity, and the brackets indicate averaging over the Maxwell distribution, $f_i(\boldsymbol{v}_i)$, of the species involved; that is:

$$\langle \sigma v \rangle_{12} = \iint \sigma\left(\left|\boldsymbol{v}_1 - \boldsymbol{v}_2\right|\right)\left|\boldsymbol{v}_1 - \boldsymbol{v}_2\right| \mathrm{f}_1(\boldsymbol{v}_1)\mathrm{f}_2(\boldsymbol{v}_2)\mathrm{d}^3\boldsymbol{v}_1\mathrm{d}^3\boldsymbol{v}_2 \quad \mathrm{m}^3\mathrm{s}^{-1} \tag{1.1}$$

where $\boldsymbol{v}_1$ and $\boldsymbol{v}_2$ are the velocities of species 1 and 2 respectively [1]. The reactivity for several reactor relevant fusion reactions between hydrogen isotopes and ^{3}He versus temperature are shown in Figure 1.1. Clearly, the deuterium-tritium fusion reaction is the easiest to achieve in terms of the fusion reactivity and the temperature required for the reaction. This reaction is given by [2]:

$$\mathrm{T} + \mathrm{D} \rightarrow {}^4\mathrm{He}(3.5\ \mathrm{MeV}) + \mathrm{n}(14.1\ \mathrm{MeV}). \tag{1.2}$$

Deuterium is stable and is readily available as it occurs naturally in seawater from which it can easily be extracted. Tritium, however, is mildly radioactive; it decays through β-emission with a half-life of about 12.33 years [3]. As a result of its relatively short half-life, tritium must be manufactured. A fusion reactor can "breed" its own fuel if the fusion reaction chamber is surrounded by a lithium blanket. In this case, the neutrons produced

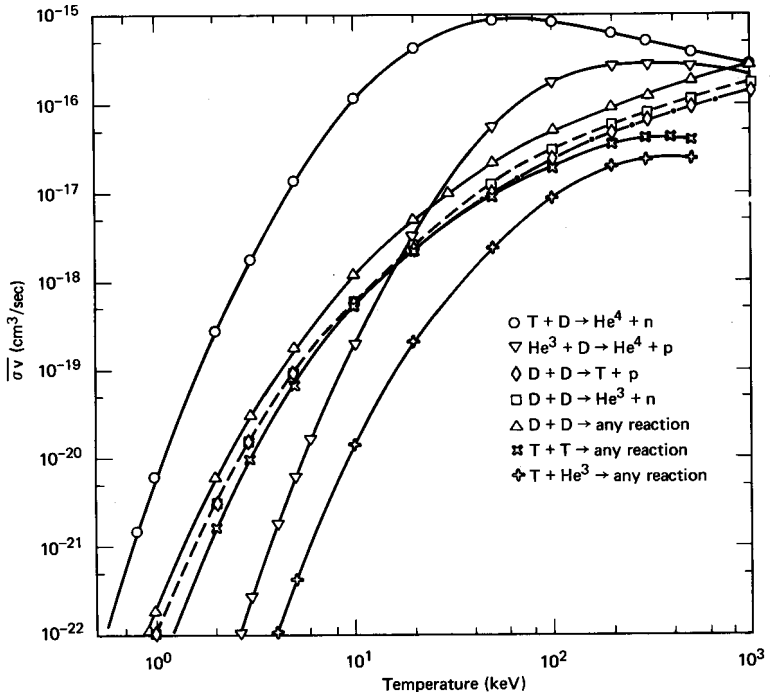

Figure 1.1 Maxwell averaged fusion reaction cross-sections. [E. Teller, "Fusion", Volume 1 Magnetic Confinement Part A, Academic Press, Inc., New York, 1981, p. 6.]

by the deuterium-tritium fusion reaction react with the lithium to produce tritium according to the following reaction [4]:

$$^6\mathrm{Li} + \mathrm{n} \rightarrow \mathrm{T}(2.7\ \mathrm{MeV}) + ^4\mathrm{He}(2.1\ \mathrm{MeV})\,. \qquad (1.3)$$

In order to achieve fusion, there are three important criteria that must be met. First, as was already mentioned, the temperature must be sufficiently high that the repulsive Coulomb force between the reacting nuclei can be overcome. However, wherever high temperatures are present, many technical difficulties arise. In fact, the high temperatures required for fusion reactions to occur are such that the gas is fully ionized; that is, it is plasma. Second, the density of the plasma must be high enough that the reaction rate is sufficient to ensure that the reaction is self-sustaining. Finally, the energy confinement time must be long enough that the reactions have enough time to

occur. The overall performance of a particular fusion device is typically assessed by the fusion triple product, $n_{i0}\tau_E T_{i0}$, where n_{i0} and T_{i0} are the central ion density and temperature respectively, and τ_E is the energy confinement time. The fusion triple product as a function of the central ion temperature obtained in several experimental reactors is shown in Figure 1.2. This figure clearly indicates the progress achieved over the years.

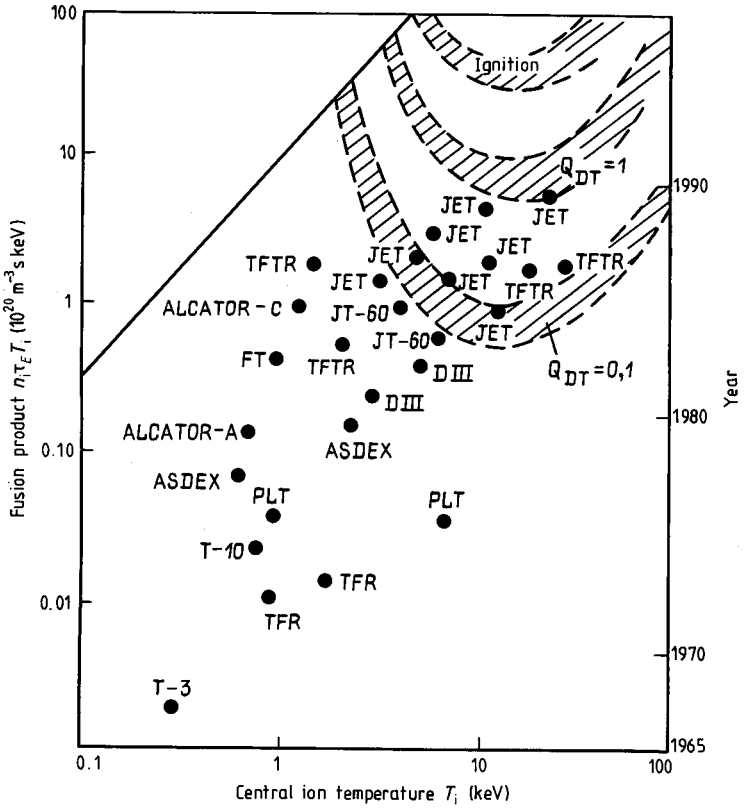

Figure 1.2 Progress of controlled fusion research. [B.B. Kadomstev, "Tokamak Plasma: A Complex Physical System", Institute of Physics Publishing, London, 1992, p. 48.]

In order to be economically viable, a fusion reactor must be capable of producing a net output of power with a sufficient gain over the total input power that is required to sustain the reaction. As well, the power must be produced at a sufficiently high power density and in the case of magnetic confinement schemes, at a realistic magnetic field

strength. In the steady-state the fusion power gain is given by: $Q_f = P_f \big/ P_i$, where P_f is the power produced as a result of the fusion reactions, and P_i is the input power. For the deuterium-tritium fusion reaction the power produced is given by [6]:

$$\mathrm{P_f} = 17.6\ \mathrm{MeV} \times \int \mathrm{n_D n_T} \langle \sigma \boldsymbol{v} \rangle \mathrm{dV} \quad \mathrm{eVs^{-1}}, \tag{1.4}$$

where n_D and n_T are the number densities of deuterium and tritium respectively, and the integral is taken over the volume of the plasma. The externally supplied input power must make up the difference between the power that is lost from the plasma as a result of radiation and particles leaving the plasma, and the power gained by the plasma due to the ^{4}He (α-particles) that are produced in the fusion reaction and captured by the plasma; this is given by [6] as:

$$\mathrm{P_i} = \frac{3}{2\tau_\mathrm{E}} \int (\mathrm{n_e T_e} + \mathrm{n_i T_i}) \mathrm{dV} - 3.5\ \mathrm{MeV} \times \eta_\alpha \int \mathrm{n_D n_T} \langle \sigma \boldsymbol{v} \rangle \mathrm{dV} \quad \mathrm{eVs^{-1}} \tag{1.5}$$

where n_e and n_i are the electron and ion number densities, T_e and T_i are the electron and ion temperatures (expressed in eV), and $\eta_\alpha \approx 1$ is the efficiency with which the power from the α-particles is transferred to the bulk of the plasma. To see the importance of the fusion triple product on the fusion power gain for the deuterium-tritium fusion reaction, Q_DT, the differences between the electron and ion densities and temperatures can be neglected, i.e. $n \approx n_e \approx n_i$ and $T \approx T_e \approx T_i$. As well, the differences between the density profiles and the temperature profiles of the electrons and the ions can be neglected. Furthermore, by noting from Figure 1.1 that for the deuterium-tritium fusion reaction that when T_i is in the 10 – 30 keV range, $\langle \sigma \boldsymbol{v} \rangle$ is approximately given by $\langle \sigma \boldsymbol{v} \rangle \cong \kappa T_i^2$, where κ, having units of $\mathrm{m^3 s^{-1} eV^{-2}}$, is a constant of proportionality. It follows, then, that by

dividing each term in Q_{DT} by nT/τ_E that Q_{DT} depends strongly on the fusion triple product; that is

$$Q_{DT} \cong \frac{(17.6\text{MeV})\int \kappa\left(\frac{n_D}{n_D+n_T}\right)\left(\frac{n_D}{n_D+n_T}\right)n\tau_E T dV}{\int\left\{3-(3.5\text{MeV})\eta_\alpha\kappa\left(\frac{n_D}{n_D+n_T}\right)\left(\frac{n_D}{n_D+n_T}\right)n\tau_E T\right\}dV} \tag{1.6}$$

The curve $Q_{DT} = 1$ represents energy break-even; this landmark has been approached (Q_{DT}=0.27) in the Tokamak Fusion Test Reactor (TFTR) at the Princeton Plasma Physics Laboratory in 1994 [7], and in the Joint European Torus (JET) tokamak (Q_{DT}=0.62) in 1997 [8,61]. The curve labeled ignition, $Q_{DT} = \infty$, represents the case in which the power balance is satisfied without the need for any external heating source and has yet to be achieved in a laboratory reactor. The following parameters would be required for a practical steady-state deuterium fusion reaction [6]:

$$T_{i0} \approx 30 \text{ keV},\ \tau_E \approx 3 \text{ s},\ n_{i0}T_{i0}\tau_E \approx 7\times10^{21} \text{ keV s m}^{-3}.$$

By taking into account the conversion of thermal power into electrical power and the power that is required to operate a power generating station, a fusion power gain $Q_f > 15$ is required in order for a tokamak reactor to be commercially successful [5]. A schematic diagram of a tokamak-based power plant is shown in Figure 1.3.

Following the discussion of the principal requirements for achieving a steady-state controlled thermonuclear fusion reaction, it is now appropriate to extend the discussion to examine methods of satisfying these requirements. Perhaps the most important issue to be resolved is that of confining the extremely hot plasma that is

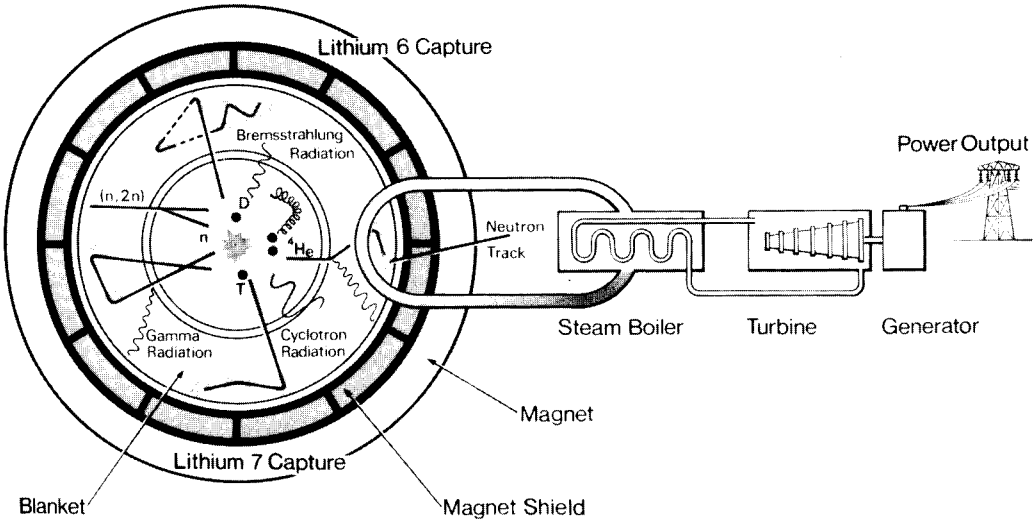

Figure 1.3 Schematic of a fusion power plant. [J. Hugill,*Nuclear Fusion Research*, "Plasma Physics and Nuclear Fusion Research, Edited by R.D. Gill, Academic Press Inc., London, 1981, p. 27.]

required for the fusion reactions to occur. Clearly, the use of any solid material for the confining walls is precluded, as at the temperatures required for the fusion reactions to occur any material would simply vapourize. Fortunately, however, as the plasma consists of charged particles (electrons and ions) it is possible to confine it using suitably arranged magnetic fields.

1.2 Magnetic Confinement – The Tokamak Configuration

Since research into thermonuclear fusion began in the 1950's, there have been several magnetic confinement configurations proposed to confine the plasma, including: mirror machines, stellarators (proposed by Spitzer), and tokamaks [10]. Of the various schemes proposed to date, the tokamak configuration is considered to be the most promising [9]; and the next generation tokamak, the International Thermonuclear Experimental Reactor (ITER) is expected to demonstrate controlled ignition [10,12]. First developed in Russia during the early 1950's, the tokamak configuration is a toroidal shaped system in which the plasma is confined magnetically. In the early years of fusion

research, progress was slow as a result of the secrecy that was imposed on the researchers, as their research was classified for reasons of national security. Fortunately, however, after the Second Atoms for Peace Conference in 1958, all fusion research was declassified [1,10]. Since then, work on controlled thermonuclear fusion research has been furthered by open and full cooperation among several countries [1]. For example, after the 1968 IAEA Conference at Novosibirisk, where Artsimovich reported the highly promising results of electron temperatures up to 2 keV in the T-3 tokamak, he invited a group of well reputed researchers from the Culham Laboratory in England to confirm his results using their newly developed laser diagnostic system, which they did [10,63].

It is well known that charged particles follow magnetic field lines by spiraling around them with an orbital frequency known as the cyclotron frequency, given by:

$$\omega_c = \frac{|q|B}{m} \quad s^{-1} \tag{1.7}$$

where $|q|$ is the charge of the particle, m is its mass, and B is the magnitude of the magnetic field density. Furthermore, the orbital radius of the particles about its guiding centre, commonly referred to as the Larmor radius, is given by:

$$r_L = \frac{v_\perp}{\omega_c} = \frac{mv_\perp}{|q|B} \quad m \tag{1.8}$$

where $v_\perp$ is the velocity component of the particle in the plane perpendicular to the magnetic field.

In considering a purely toroidal magnetic field, as shown in Figure 1.4, it is evident that the magnetic field lines are closed, and at first glance it appears that this configuration should be sufficient to confine the plasma. Upon closer examination, however, it becomes clear that this is not the case; in fact, this configuration does not

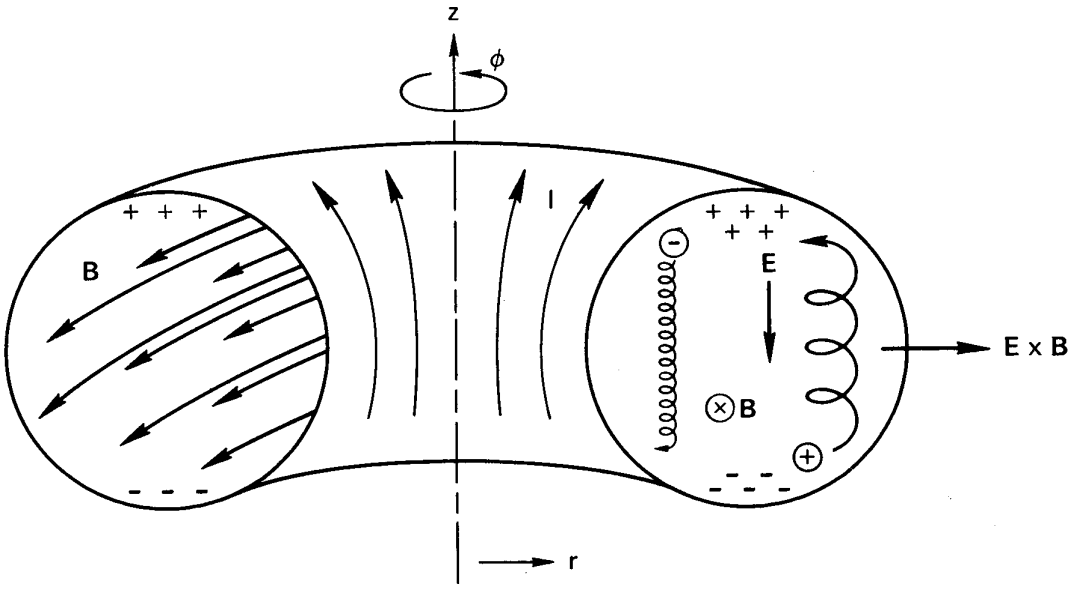

Figure 1.4 Particle motion in a toroidal field. [F.F. Chen, "Introduction to Plasma Physics", Plenum Press, New York, 1981, p. 284.]

have a stable equilibrium. This instability is the result of the fact that in any toroidal device the magnetic field is stronger at smaller radii than it is at larger radii, and since the particles will tend to move to regions of weaker magnetic field, they will not be confined. This can be seen by considering Equation 1.8 from which it is evident that as the particles spiral around the magnetic field lines, they will have slightly sharper orbits at smaller major radial positions (larger *B*) than at larger major radial positions (smaller *B*), causing them to drift vertically. This drift, which is due to both the curvature and the gradient of the magnetic field, is given by [4] as:

$$\boldsymbol{v}_{\boldsymbol{R}+\nabla B} = \frac{m}{q}\frac{\boldsymbol{B}\times\nabla B}{B^3}\left(\frac{1}{2}v_{\perp}^2 + v_{\parallel}^2\right) \quad ms^{-1} \tag{1.9}$$

where $v_{\parallel}$ is the velocity component of the particle in the direction parallel to the magnetic field. Furthermore, since this drift depends on the charge, the ions and electrons spiral in opposite directions; their guiding centres will tend to drift vertically in opposite directions as is shown in Figure 1.4. This drift results in a separation of charge and a corresponding

electric field $\boldsymbol{E}$; this electric field will eventually become strong enough to stop the drifting motion. Despite this, however, an electric field would exist that is perpendicular to the magnetic field; this gives rise to another type of particle drift known as $\boldsymbol{E} \times \boldsymbol{B}$ drift, in which the electrons and ions move in a direction that is perpendicular to both the electric and magnetic fields at a velocity given by:

$$\boldsymbol{v}_{\boldsymbol{E}\times\boldsymbol{B}} = \frac{\boldsymbol{E} \times \boldsymbol{B}}{\mathrm{B}^2} \quad \mathrm{ms}^{-1}. \tag{1.10}$$

The overall result, obviously, is that the plasma moves toward the outer wall, and is not confined.

It is possible to overcome the difficulty just described by superimposing a poloidal magnetic field, B_θ, on the toroidal magnetic field, B_ϕ. In the tokamak configuration a toroidal current, I_P, within the plasma, produces this poloidal magnetic field. This is traditionally accomplished inductively by transformer action, as shown schematically in Figure 1.5, with the plasma acting as the secondary winding of the transformer. The resultant helically shaped magnetic field lines now form nested closed magnetic surfaces, as shown in Figure 1.6. This helical magnetic field can confine the plasma; this is because as the electrons and ions spiral along the helical magnetic field lines, there will be a continuing change of the inhomogeneity of the magnetic field, and consequently, the drifts that had caused the separation of charges will only persist for a short time before being reversed, and in the time average they will cancel out. The resultant magnetic field has a helicity described by the rotational transform angle, ι, which is the poloidal angle traversed by the magnetic field line after one complete revolution in the toroidal direction and is shown in Figure 1.7. It can be shown that the

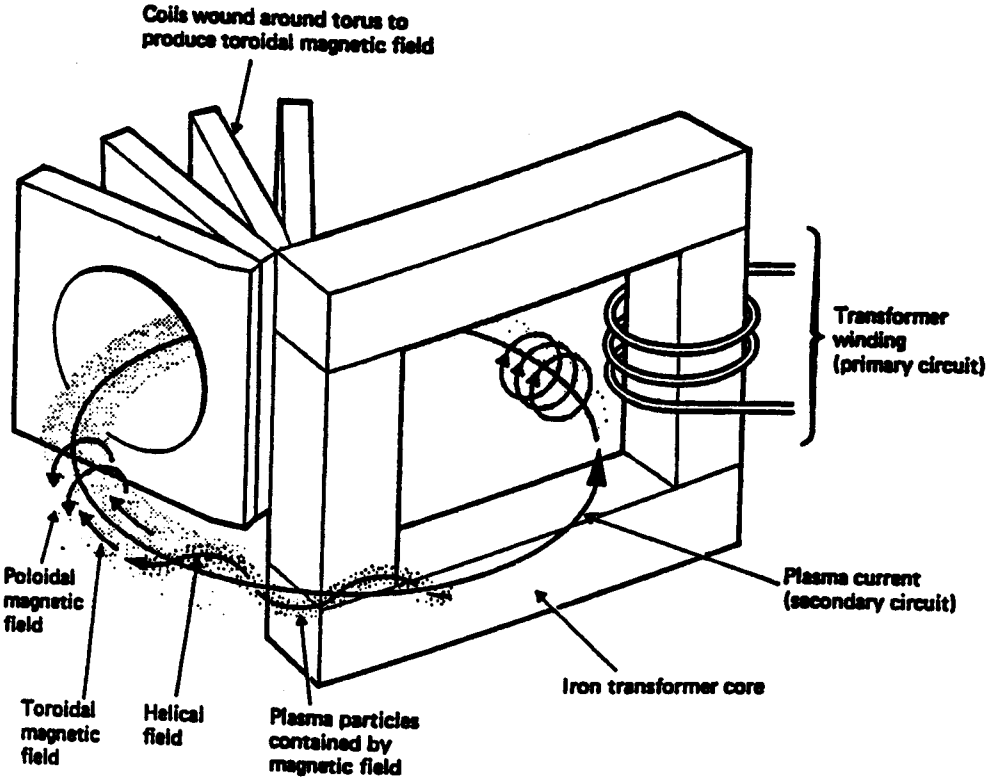

Figure 1.5 Resultant magnetic field in the tokamak configuration. [*J. Hugill, Nuclear Fusion Research*, "Plasma Physics and Nuclear Fusion Research, Edited by R.D. Gill, Academic Press Inc., London, 1981, p. 415.]

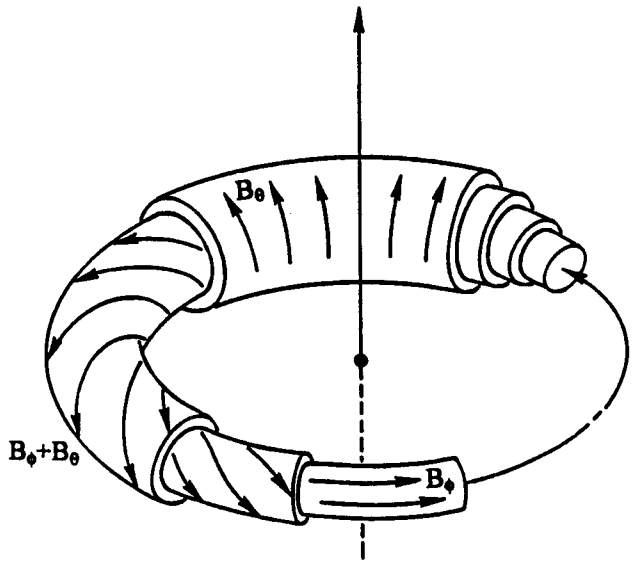

Figure 1.6 Resultant nested magnetic surfaces. [F.F. Chen, "Introduction to Plasma Physics", Plenum Press, New York, 1981, p. 287.]

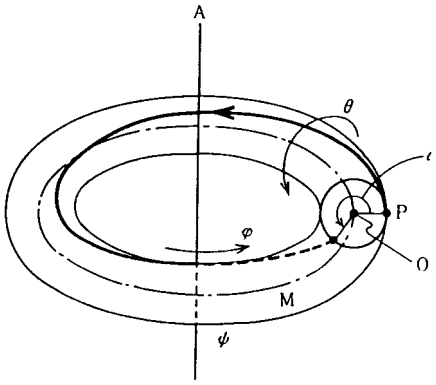

Figure 1.7 Rotational transform angle. [K. Miyamoto, "Fundamentals of Plasma Physics and Controlled Fusion", Iwanami Book Service Center, Tokyo, Japan, 1997, p. 46.]

rotational transform is given by [11]:

$$\iota = \frac{2\pi R}{\rho}\frac{B_\theta}{B_\phi}, \tag{1.11}$$

The stability provided by the rotational transform is only provided if the thermal motion of the particles is substantially larger than the $\boldsymbol{E} \times \boldsymbol{B}$ drifts. The rotational transform in the STOR-M tokamak, for example, is about 90° in the plasma edge region. Looking at it from another perspective, it can be said that the resultant helically shaped field lines connect regions of positive charge with regions of negative charge, thereby, short-circuiting the electric field which otherwise would result in the plasma not being confined [4].

It should be pointed out that there are also non-inductive means of producing the toroidal plasma current, but the transformer action described above is the simplest and most common technique; it is also the technique used in the STOR-M tokamak described in this thesis. In this case, a transformer having a primary current, I_{OH}, is used to induce the toroidal plasma current. In addition to producing the poloidal magnetic field, the toroidal plasma current serves to ohmically heat the plasma with ηJ^2 power being dissipated per unit volume, where: η is the resistivity of the plasma, and J is the plasma current density. In fully ionized plasma, as is the case in a tokamak, the resistivity is

given approximately by Spitzer as:

$$\eta = 5\times10^{-5}\,\frac{Z_{eff}\,\ln\Lambda}{T_e^{3/2}} \quad \Omega m \tag{1.12}$$

where T_e is in eV, Z_{eff} is the effective charge, and ln Λ is the Coulomb logarithm given by:

$$\ln\Lambda = \ln\left(12\pi n_e \lambda_D^3\right), \tag{1.13}$$

in which:

$$\lambda_D = \sqrt{\frac{\varepsilon_0 T_e}{n_e e^2}} \quad m \tag{1.14}$$

is the Debye length, where e is the elementary charge, ε_0 is the permitivity of free-space, and T_e is in J. Due to the strong dependence of the plasma resistivity on temperature, as seen in Equation 1.12, the resistivity rapidly decreases as the electron temperature increases. Consequently, beyond a certain temperature (≈1 keV), ohmic heating becomes ineffective as further increases in the plasma current do not significantly increase the plasma temperature. Additionally, the plasma current is limited in magnitude by magneto-hydrodynamic (MHD) instabilities such as the kink instability. It can be shown that the safety factor, q, against these instabilities occurring is given by:

$$q \approx \frac{2\pi}{\iota} = \frac{2\pi\rho^2 B_\phi}{\mu_0 R I_P} \tag{1.15}$$

and that the minimum value of safety factor for stability is given by q > 1 [36]. Clearly, any further increase in the plasma temperature beyond a certain device dependent level must be accomplished by employing supplementary heating techniques in order to achieve the temperatures necessary for fusion reactions to occur.

Figure 1.5 shows the main components of a tokamak; not shown is the toroidal vacuum chamber, which is usually constructed out of a conductor for reasons that will be discussed in Chapter 2. Consequently, ceramic breaks are inserted in the vacuum chamber to prevent any undesired toroidal currents from being induced within the chamber itself. The toroidal magnetic field is produced by a series of coils that are wound poloidally around the torus. Additional magnetic fields present on most tokamaks but not shown in Figure 1.5 are the vertical and horizontal fields. It will be shown in Section 2.3 that the vertical magnetic field provides the necessary $\boldsymbol{J} \times \boldsymbol{B}$ force to counter-balance the horizontally expanding plasma column due to the plasma pressure and magnetic forces. Similarly, the horizontal magnetic field acts to correct any plasma deviation from the vertical equilibrium position.

The vertical field present on the STOR-M tokamak consists of two components: the vertical equilibrium field, B_{VE}, which is pre-programmed, and the vertical feedback field, B_{VF}, which is dynamically applied by an active feedback control system. The horizontal magnetic field of the STOR-M tokamak consists of a pre-programmed field, the horizontal equilibrium field, B_{HE}. These fields play a very important role in ensuring the stability of the plasma position within the discharge vessel. If these fields are not properly optimized, the plasma will not be confined. Thus, it is critical in tokamak research that these fields be properly controlled. This has been the topic of much research over the decades, and the need to have a high quality of control over these fields is the primary motivation for, and the focus of, the research presented in this thesis.

1.3 Thesis Goals and Objectives

The primary goal of this thesis is to contribute to the advancement of research into controlled thermonuclear fusion and ultimately to the development of a controlled thermonuclear fusion reactor. To achieve this goal, three main objectives have been set out in the performance of the research described within this thesis. The first objective was to improve the current method of controlling the position of the plasma within the tokamak discharge chamber. The second objective of this research was to determine whether or not a fuzzy logic based controller could be successfully applied to control the position of the plasma within a tokamak device. The third objective was to develop a controller that would be capable of providing near optimal control in all modes of tokamak operation, particularly during transient conditions such as that which occurs during A.C. operation of the STOR-M tokamak.

1.4 Thesis Outline

From the discussion in Section 1.2 it should be clear that the requirement of confining extremely hot plasma is one of the most significant technical problems being faced by controlled thermonuclear fusion researchers. One issue that is closely related to the confinement problem is that of maintaining the position of the plasma as close to the centre of the torus as possible. In fact, the control of the plasma position is quite a complex problem and is the principle objective of the research described herein. In this first chapter a brief history of the research effort over the years towards the goal of producing a commercially viable controlled thermonuclear fusion reactor was given. The requirements for a fusion reactor were discussed, and an introduction to the tokamak,

magnetic confinement scheme, was presented. The first chapter also presented the objectives of the research described herein and outlined the remainder of the thesis.

Chapter 2 deals with the topic of plasma confinement in greater detail with emphasis being placed on the subject of plasma position control. The STOR-M tokamak is described in detail, and existing plasma position control schemes employed on various tokamaks around the world will be discussed. Chapter 2 also presents the two modes of STOR-M operation, namely: the normal mode and the A.C. mode. The design requirements for the plasma position controller on the STOR-M tokamak are also described in this chapter.

Chapter 3 discusses the classical analog Proportional-Integral-Differential (PID) controllers. More specifically, the existing analog PID controller developed for controlling the position of the plasma in the STOR-M tokamak will be discussed. Its performance during both steady-state and transient conditions will be examined. In addition, modifications made to enhance the existing analog PID controller will be presented.

In Chapter 4 the subject of fuzzy logic based controllers is discussed. A fuzzy controller developed by the author to control the position of the plasma within the STOR-M tokamak is presented in detail. Results of performance validation experiments are also presented in this chapter.

In Chapter 5 the performance of the modified analog PID controller is compared to that of the fuzzy controller. This comparison focuses on the quality of the plasma position control achieved by each controller during both modes of STOR-M operation.

Chapter 6 highlights significant conclusions made as a result of the research described herein and presents recommendations for future improvements.

2. PLASMA CONFINEMENT

2.1 Introduction

As was mentioned in Chapter 1, confinement of the plasma within the controlled thermonuclear fusion reactor is of the utmost importance. Consequently, it is necessary to investigate this issue in greater detail. One aspect of plasma confinement within the tokamak device is that of controlling the position of the plasma within the discharge chamber. Plasma position control is necessary to ensure that the plasma column does not approach too closely to the wall of the discharge chamber since if it did, the plasma would most certainly be disrupted or at least significantly degraded. Due to the symmetry of the tokamak device during equilibrium, the plasma position can be decomposed into two components: the vertical position, ΔV, and the horizontal position, ΔH, where the vertical position of the plasma represents the vertical displacement of the centre of the plasma column from the cross-sectional centre of the discharge chamber. Similarly, the horizontal position represents the horizontal displacement of the centre of the plasma column from the cross-sectional centre of the discharge chamber. The vertical and horizontal plasma positions are illustrated in Figure 2.1.

In the STOR-M tokamak, to be discussed in the next section, the position of the plasma in the vertical direction is adequately controlled by a pre-programmed open-loop analog controller and, therefore, will not be discussed in greater detail here. The horizontal position of the plasma in STOR-M, however, requires dynamic control in

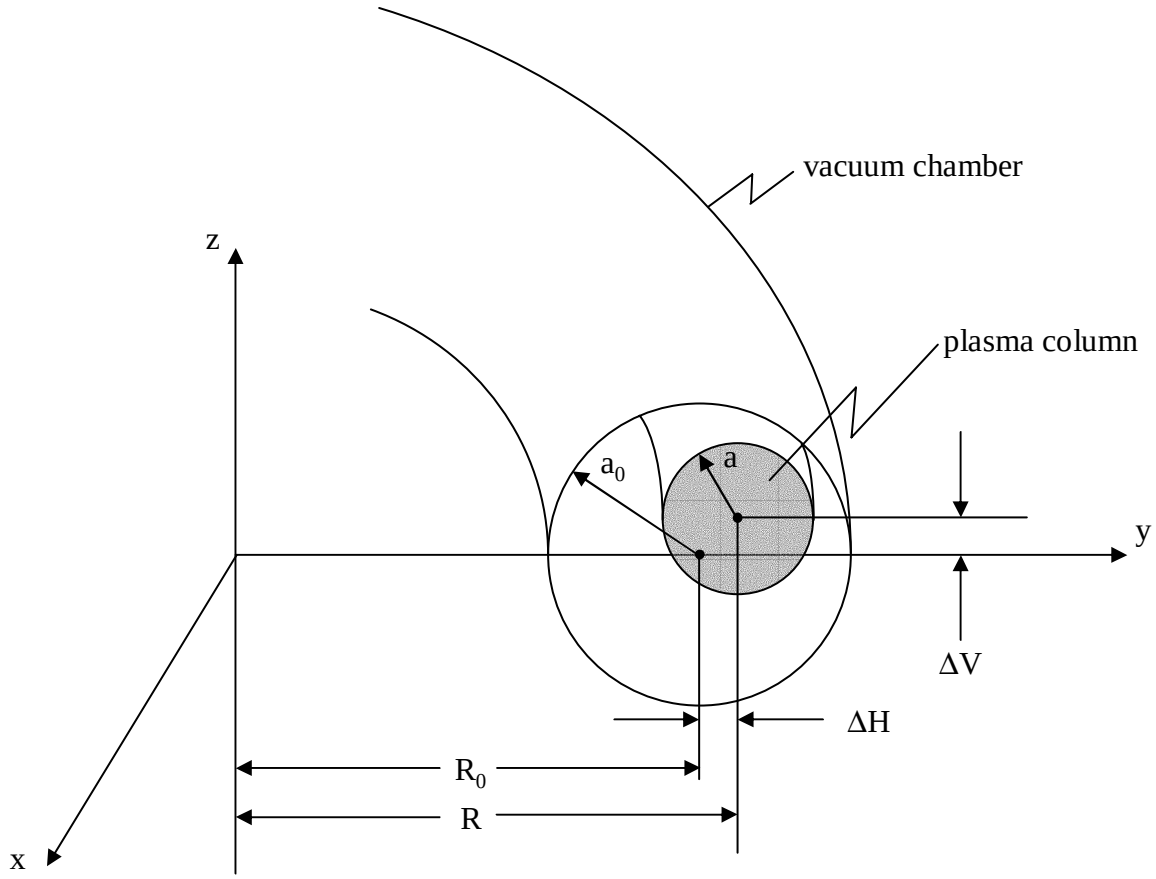

Figure 2.1 Plasma displacement inside the toroidal vacuum chamber.

order that the horizontal position of the plasma is maintained within suitable limits. The horizontal position of the plasma column in a toroidal device, such as a tokamak, will be discussed in detail in Section 2.3.

2.2 The STOR-M Tokamak

The Saskatchewan Torus - Modified, STOR-M, tokamak is the descendant of the smaller STOR-1M tokamak [22], Canada's first construction of a tokamak. STOR-M was completed in 1987 [14] and upgraded in 1994 [23]. The STOR-M tokamak, like its predecessor, was built primarily to study the effects of turbulent heating and the associated physics in tokamak plasmas [22]. The STOR-M tokamak is shown schematically in Figure 2.2, and Appendix A has a complete list of its parameters. Since its construction, over 140 000 discharges have been logged. In this section, the STOR-M tokamak and its diagnostic systems are presented.

2.2.1 Machine Description

The discharge chamber of the STOR-M tokamak is constructed of two 0.156″ (4 mm) thick type-304L stainless steel elbows with circular cross-section having an outer minor diameter of 12.750″ (324 mm) [24,25]. To reduce mechanical stresses each elbow is connected on one end to a stainless steel bellows to form the two halves of the discharge chamber. The two chamber halves are separated by two 20 mm thick alumina (Al_2O_3) ceramic breaks in order to prevent current from being induced in the walls of the discharge chamber by the ohmic heating current that forms the primary winding of the tokamak transformer [26]. The resulting discharge chamber is a toroid having a major radius of 460 mm [14] and an inner minor radius of 158 mm. The STOR-M tokamak is equipped with a combination of a circular and rail limiter. This limiter is segmented,

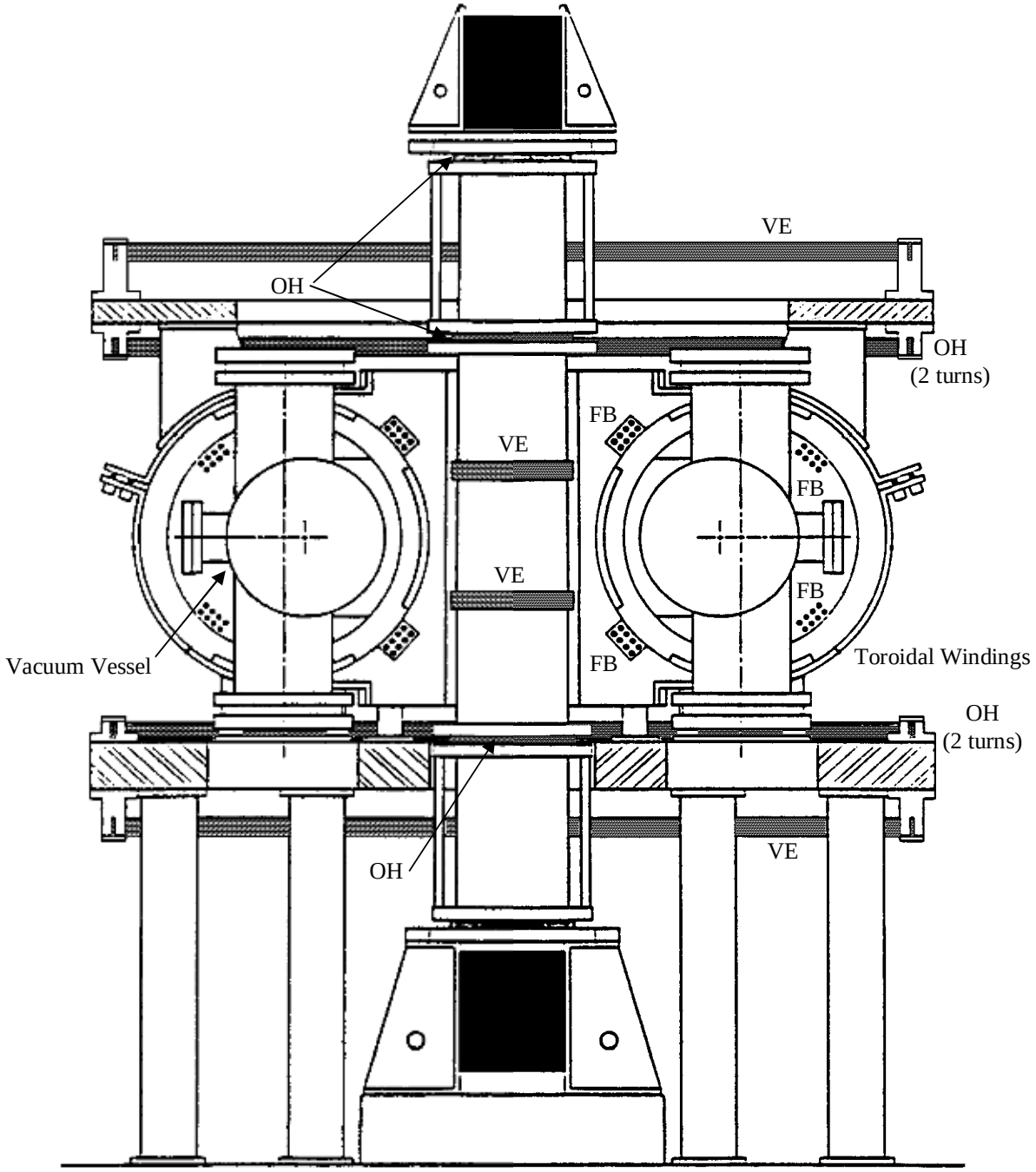

Figure 2.2 Vertical cross-section of STOR-M showing the locations of the Vertical Equilibrium (VE), Ohmic Heating (OH), and FeedBack (FB) windings. Not to scale.

allowing for either biasing or measuring of the floating potential while also measuring the limiter current [26]. The segmented limiter is shown in Figure 2.3 and limits the plasma column to approximately 11.7 cm in the vertical direction and 12.3 cm in the horizontal direction.

In order to minimize the amount of impurities in the plasma the use of ultra high vacuum compatible components is required for all components that come in contact with the vacuum. The vacuum chamber is evacuated by a turbomolecular pump with a pumping speed of approximately 1000 L/s [27] backed by a rotary vane pump [28]. The typical base pressure within the STOR-M tokamak is about 1.0×10^{-7} Torr; however, an ultimate pressure of 1.2×10^{-8} Torr has been achieved [14,15] after baking the system at about 60 °C. During operation the chamber is filled with ultra high purity hydrogen (99.999%) to a pressure of about 1.8×10^{-4} Torr. The chamber pressure is held constant using a Veeco Automatic Pressure Controller [29]. The vacuum chamber is filled through a PV-10 piezoelectric valve [30]. The PV-10 valve has a response time of about 2 ms. STOR-M is also equipped with two additional PV-10 valves, located approximately 180 toroidal degrees apart, which are used in conjunction with a pre-programmed open loop controller for the purpose of performing gas puffing during the discharge.

The discharge chamber is situated such that it encloses one leg of the tokamak transformer core as shown in Figure 2.2. The ohmic heating winding (transformer primary winding) consists of 8 turns of ¼" × 1½" copper busbar wound around the leg of the transformer core that is enclosed by the discharge chamber at the locations shown in Figure 2.2. The ohmic heating winding typically carries a peak current of about 3.5 kA

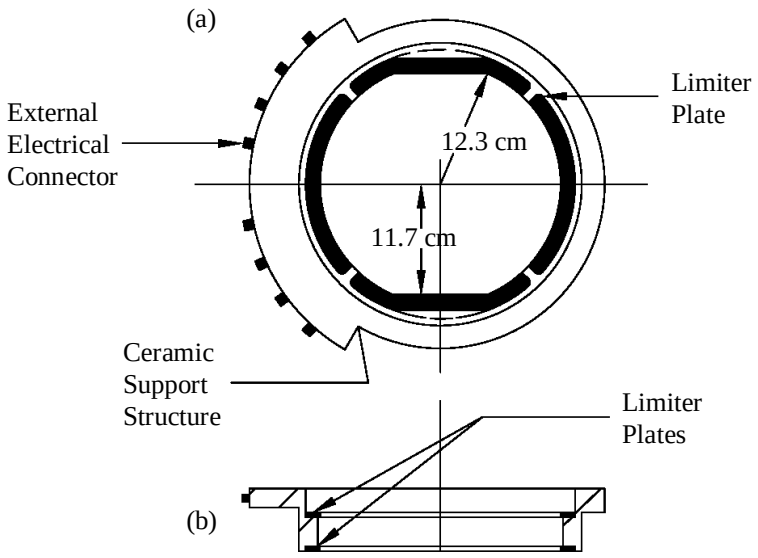

Figure 2.3 Segmented limiter (a) toroidal view (b) horizontal cross-section. [W. Zhang, C. Xiao, L. Zhang and A. Hirose, Physics of Plasmas, Volume 1, Number 11, Nov. 1994, p. 3647.]

with a rise time of about 8 ms. The circuit, which is used to produce the ohmic heating current I_{OH}, will be discussed in detail in Section 2.4. The ohmic heating current induces a voltage inside the tokamak, which causes the hydrogen gas filling it to break down. The resulting plasma then carries the induced plasma current, I_P. Figure 2.4 shows a typical time evolution of the initial stages of the discharge in the STOR-M tokamak.

The first stage of the discharge is the breakdown of the hydrogen gas filling the vacuum vessel. The sudden drop in the loop voltage, which corresponds to the drop in the plasma resistance as the hydrogen becomes fully ionized, characterizes this region. Following the breakdown, the plasma current increases until the peak current is reached; this is referred to as the current ramp-up stage of the discharge. The breakdown stage and the current ramp-up stage are collectively referred to in this thesis as the transient region of the discharge. The transient region of a typical STOR-M discharge typically lasts about 8 to 9 ms. The stages of the evolution of the discharge after the transient region has passed depend on whether the STOR-M tokamak is being operated in the normal mode or the A.C. mode and will be discussed further in Section 2.4.

Enclosing the discharge chamber of the STOR-M tokamak is the toroidal field winding. This toroidal winding consists of 16 spools each having 9 turns of ¼" × 2¾" copper for a total of $N = 144$ turns. The toroidal winding spools are evenly spaced along the toroidal direction. The temporal evolution of the toroidal field is shown in Figure 2.5(a). The toroidal field in the centre of the discharge chamber is given by:

$$B_\phi \, T = \frac{\mu_0 N I_{B_\phi}}{2\pi R} = 0.063 I_{B_\phi} \, kA \qquad (2.1)$$

and has a peak value of $B_\phi \approx 0.7\,T$ corresponding to a peak toroidal field current, I_{B_ϕ},

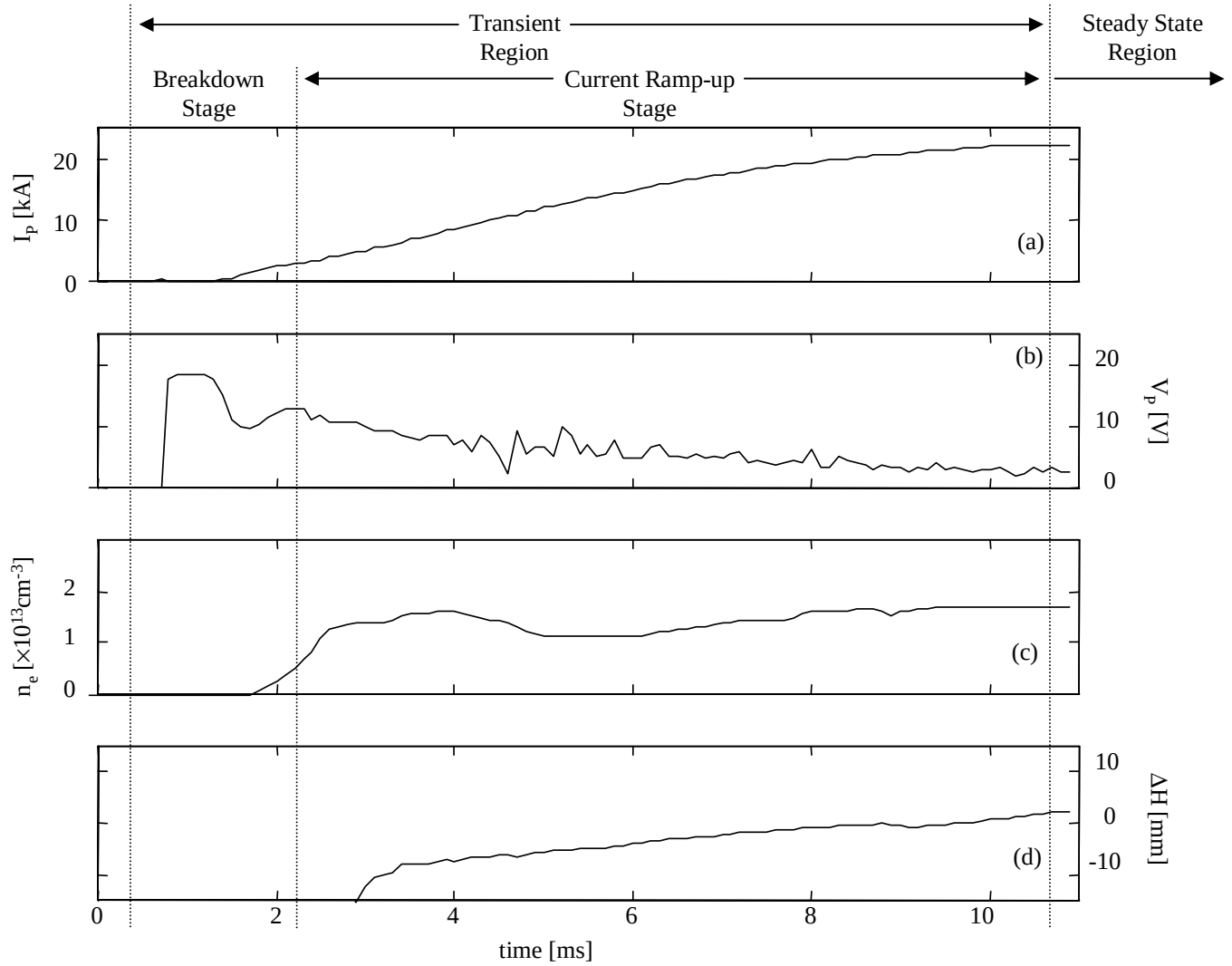

Figure 2.4 Evolution of the initial stage of a STOR-M discharge [J. Morelli, A. Singh, C. Xiao and A. Hirose, 43rd Annual DPP Meeting of the APS, Oct. 2001.]. (a) Plasma current, (b) Loop voltage, (c) Electron density and (d) Plasma position.

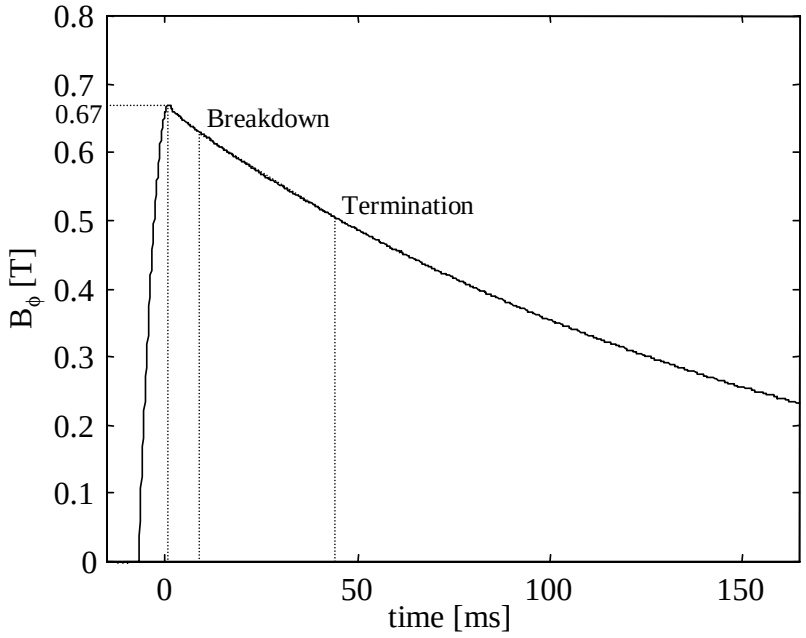

(a)

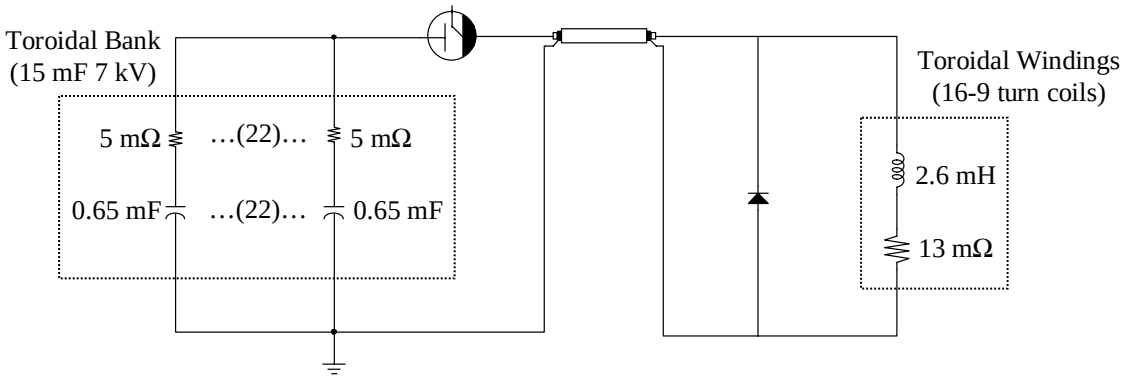

(b)

Figure 2.5 Toroidal magnetic field: (a) temporal evolution and (b) electric circuit.

of just over 12 kA. The toroidal field current is produced by the circuit shown in Figure 2.5(b) and has a rise time of about 6.5 ms and a decay time of about 400 ms. The ohmic heating circuit is usually triggered about 14 ms after the peak in the toroidal magnetic field has occurred.

The magnetic fields required to control the position of the plasma within the vacuum chamber are produced by three sets of windings. The vertical plasma position is controlled by a horizontal magnetic field, B_{HF}, which is produced by the current I_{HF} flowing in the horizontal field windings. The horizontal field windings are constructed from 2 AWG stranded copper cable. The horizontal field produced is shown in Figure 2.6. The horizontal plasma position is controlled by two vertical magnetic fields that are produced by separate sources. The vertical equilibrium field, B_{VE}, is produced by 4 turns of ¼" × 1½" copper busbar. The location of each of the four turns of the vertical equilibrium winding is shown in Figure 2.2. The current in the vertical equilibrium winding, I_{VE}, is proportional to the ohmic heating current and is produced by the circuit shown in Figure 2.7. The second source of vertical magnetic field is the vertical feedback current, I_{VF}, which produces the vertical feedback field, B_{VF}. This current flows in the windings, shown in Figures 2.6, which are made of 2 AWG stranded copper cable. The vertical feedback field that is produced is also shown in Figure 2.6. The locations of the horizontal field winding and the vertical equilibrium and vertical feedback windings are shown in Figure 2.2. The vertical feedback field and the horizontal field will be discussed in greater detail in Section 2.4.

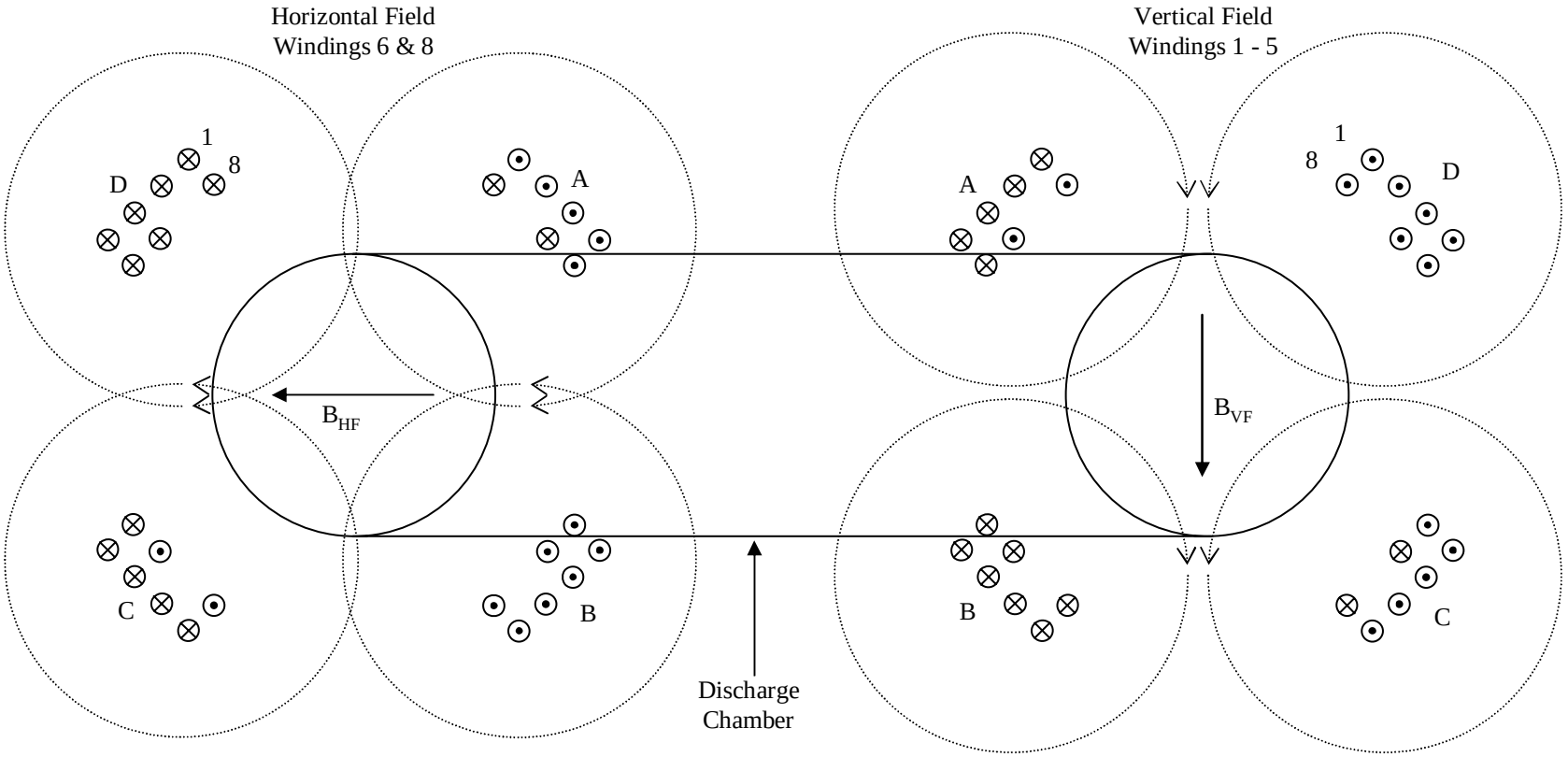

Figure 2.6 Production of the horizontal field B_{HF}, and the vertical feedback field, B_{VF}.

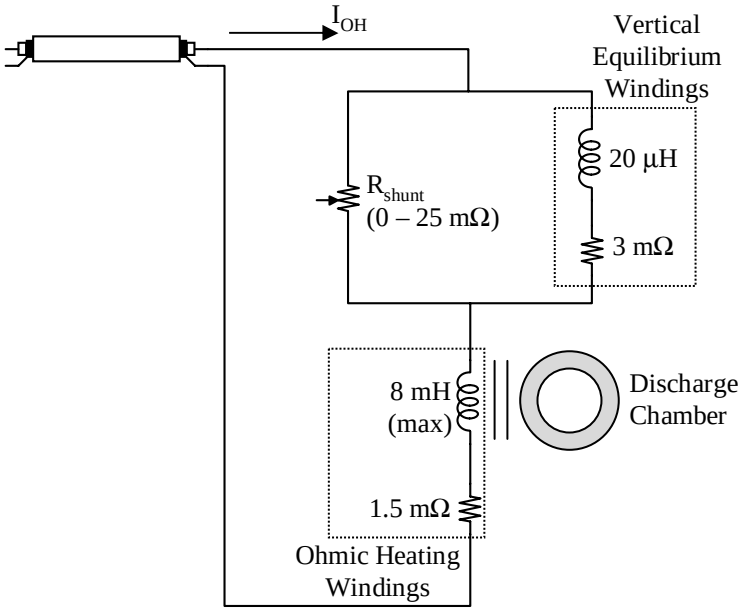

Figure 2.7 Circuit for the production of the vertical equilibrium field, B_{VE}.

2.2.2 Diagnostic Equipment

The STOR-M tokamak is equipped with a standard set of diagnostic equipment for measuring both the plasma parameters and the machine parameters. The majority of the diagnostics employ non-invasive techniques; in fact, it is highly desirable to determine as many of the plasma parameters as possible without significantly disturbing the plasma. This requirement stems from the fact that an object (probe or sensor) that is inserted into hot plasma will tend to be vapourized; thus, not only is the probe destroyed, but also the plasma is contaminated by the impurities that are released in the process. This contamination causes a degradation of the plasma, which then requires a long period of conditioning to become of a quality that is suitable for experimentation. Consequently, probes are only inserted into the cooler, plasma edge region ($\rho \approx 123$ mm), including the region that is in the shadow of the limiter known as the scrape off layer ($\rho > 123$ mm).

Diagnostic instruments used with the STOR-M tokamak include: a 4-mm microwave interferometer [16], a hard X-ray detector [14], a double array soft X-ray camera [14], an optical spectrometer [67], a set of Mirnov coils (m = 2) [67], Rogowski coils [15], and various configurations of Langmuir and magnetic probes [14], all of which are noninvasive except for the Langmuir and magnetic probes. Of these diagnostics, the hard X-ray detector, the soft X-ray camera, the Mirnov coils, and the magnetic probes are not routinely used on STOR-M and, therefore, will not be discussed further. What follows in this section is a general discussion of those diagnostics that are regularly used on STOR-M. In addition to these sensors, the signal conditioning circuits that are employed and the data acquisition system that is used to store the signals for later

analysis will also be presented. Figure 2.8 shows the locations of the diagnostic equipment on STOR-M.

2.2.2.1 Current Measurements - Rogowski Coils

Rogowski coils are used to measure the current in the various field windings of the STOR-M tokamak and within the plasma itself. A Rogowski coil is an N turn coil wound upon a nonmagnetic core, whose windings are perpendicular to the plane of the coil, and that completely encircles a conductor through which a time-varying current flows. The Rogowski coil produces a voltage signal, V_{RC}, that is proportional to the product of the number of turns, N, on the Rogowski coil and the time rate of change of the magnetic flux, ϕ, linking it; that is: $V_{RC} = -N\frac{d\phi}{dt}$. By integrating this signal the magnetic flux as a function of time is obtained. Ampere's Law gives the current enclosed by a Rogowski coil having a rectangular cross-section having width, a, and thickness, b, as:

$$I_{end} = \oint_c \overline{H} \bullet \overline{dl} = \frac{\frac{\phi}{ab} 2\pi R}{\mu_0} = \frac{-\int V_{RC} dt}{Nab} \frac{2\pi R}{\mu_0} \quad A \tag{2.2}$$

where R is the major radius of the Rogowski coil and μ_0 is the permeability of free space. The shape of a typical Rogowski coil is shown in Figure 2.9(a).

On the STOR-M tokamak, all of the Rogowski coils are constructed with 26 AWG enameled wire, except for the plasma current Rogowski coil, which is constructed with 18 AWG wire wound on a toroidal former having a rectangular cross -section. To reduce the pick-up of unwanted magnetic flux, a return winding is also wound on each Rogowski coil in the opposite toroidal direction. The number of turns and the

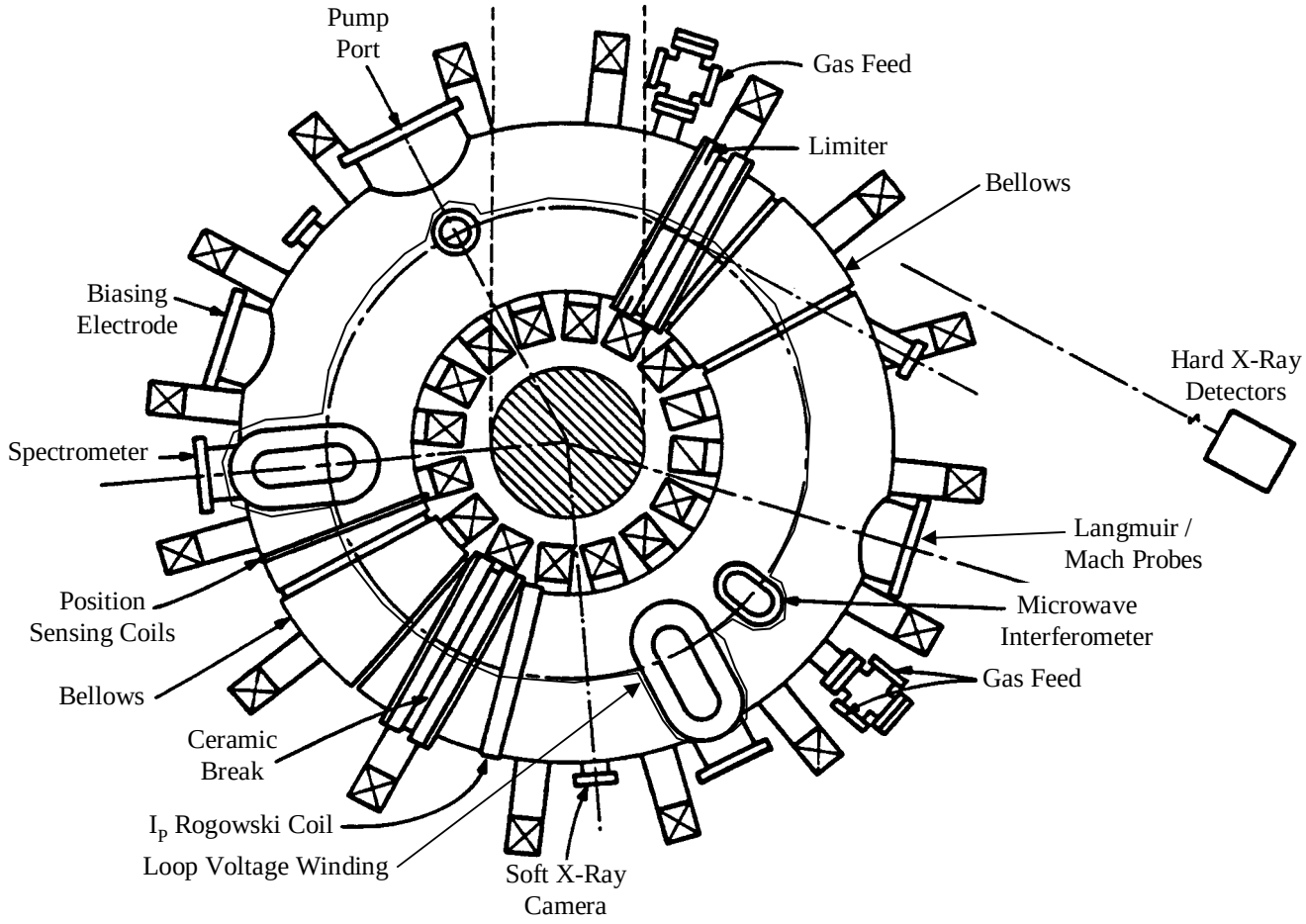

Figure 2.8 Locations of the diagnostic equipment on STOR-M.

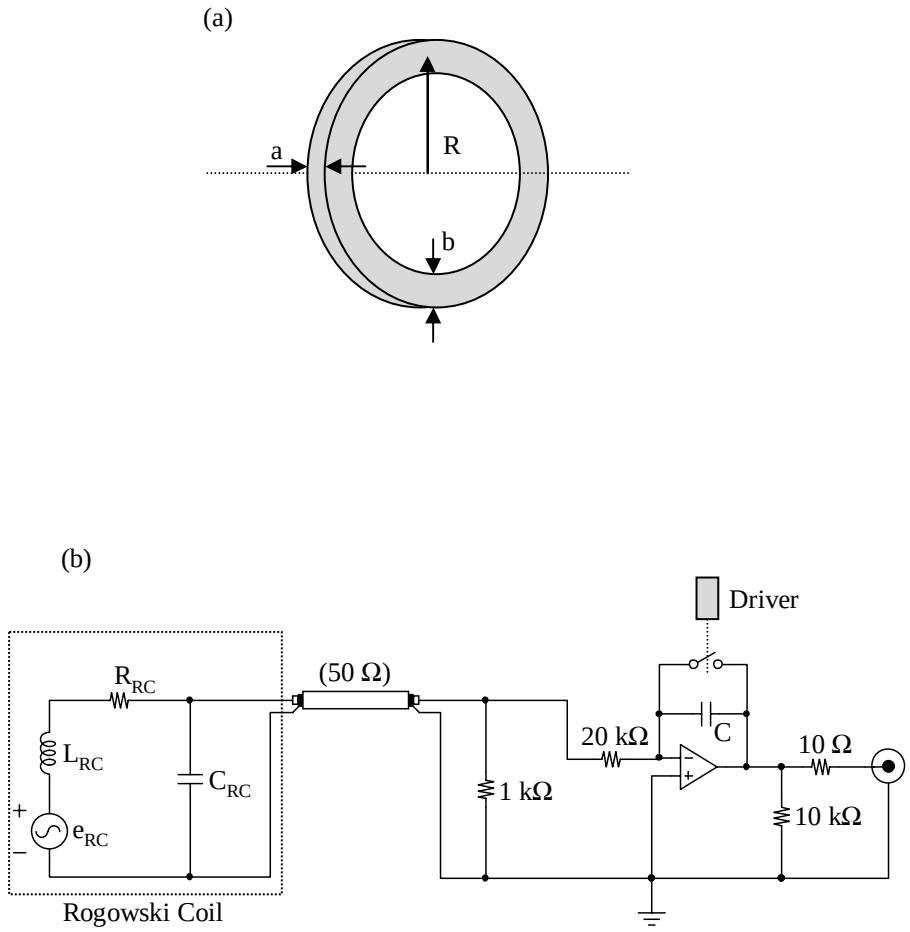

Figure 2.9 Rogowski coil: (a) dimensions and (b) schematic diagram.

dimensions of the former for each Rogowski coil used with STOR-M were chosen so that sufficient sensitivity could be obtained without sacrificing their high frequency performance [18]. Table 2.1 lists the main parameters of the Rogowski coils used on STOR-M. The measured signals are carried to the control room via 20 m of RG 58/U coaxial cable where they are integrated with gated, active integrators before being connected to the data acquisition system. The schematic diagram for the Rogowski coil circuit is shown in Figure 2.9(b). The frequency response of each coil is linear up to 800 kHz [14], which is more than adequate for the parameters of STOR-M that they monitor. The Rogowski coils on STOR-M were calibrated against a commercial Rogowski coil manufactured by Pearson Electronics before being installed, and the accuracy of each Rogowski coil is about 5% [14].

Table 2.1 STOR-M Rogowski coil parameters.

Current Measured	I_P	$I_{B\phi}$	I_{OH}	I_{VE}	I_{VF}	I_{HF}	I_{TH}
Resistance, R Ω	1.5	68.9	36.8	84.2	36.3	38.5	4.0
Inductance, L mH	0.11	6.93	5.15	9.34	4.78	5.09	0.02
Number of turns, N [14]	600	1187	750	1187	1187	1187	180
Major radius, R mm	170	70	70	70	70	70	170
Thickness, a mm	10	15	15	15	15	15	10
Width, b cm	35	25	25	33	25	25	35
Calibration Factor kA/V	100	10	10	10	10	10	100

2.2.2.2 Plasma Loop Voltage and Transformer Core Flux

A single loop on the top of the vacuum chamber, Figure 2.8, measures the plasma loop voltage. The voltage picked up by this single turn consists of both the resistive and inductive components of the loop voltage, and is given by: $V_P = I_P R_P + \frac{\mathrm{d}}{\mathrm{d}t}(I_P L_P)$, where R_P, the plasma resistance, and L_P, the plasma inductance are given by [1]:

$$\mathrm{R_P} = \eta \frac{2\pi \mathrm{R}}{\pi \mathrm{a}^2} \quad \Omega \quad \text{and} \quad \mathrm{L_P} = \mu_0 \mathrm{R}\left[\ln\left(\frac{8\mathrm{R}}{\mathrm{a}}\right) + \frac{\mathrm{l_i}}{2} - 2\right] \quad \mathrm{H} \tag{2.3}$$

where R is the major radius of the plasma column and a is its minor radius, η is the plasma resistivity, and l_i is the plasma internal inductance parameter, which will be discussed in Section 2.3.2. The plasma current and loop voltage can therefore be used to estimate the plasma resistivity, and with suitable approximations, the electron temperature which, as can be seen from Equation 1.12, is given by Spitzer [13] as:

$$\mathrm{T_e^{3/2}} \approx 5\times10^{-5}\,\frac{\mathrm{Z_{eff}}\,\ln\Lambda}{\eta} \quad \mathrm{eV^{3/2}} \tag{2.4}$$

where the Spitzer resistivity, η is in Ωm, the electron temperature, T_e is in eV, Z_{eff} is the effective ion charge, and for STOR-M the Coulomb logarithm may be assumed constant at $\ln\Lambda \approx 15$ [15].

On the STOR-M tokamak, this single turn loop consists of the centre conductor of a length of RG 59/U coaxial cable, with the outer conductor acting as an electrostatic shield. The resistance of the loop alone is 1.2 Ω and the inductance is 12 μH. The output voltage is attenuated using a 100:1 voltage divider (a 1000:1 voltage divider is used when turbulent heating experiments are being performed) and then carried to the control room via 20 m of RG 58/U triaxial cable, where it is connected directly to the data acquisition

system. The frequency response of this configuration is flat beyond 1 MHz. The schematic diagram of this measurement system is shown in Figure 2.10.

2.2.2.3 Position Sensing Coils

The quality of the discharge in the STOR-M tokamak is dictated by the quality of the control of the position of the plasma column within the vacuum vessel. In theSTOR-M tokamak, the position of the plasma column is measured using six magnetic probes, which are located just outside the vacuum vessel at a minor radius of 170 mm, as shown in Figure 2.11(a). Four of the probes are oriented to detect the poloidal magnetic field and are separated poloidally by 90°, as is shown in Figure 2.11(a). The remaining two magnetic probes are oriented to detect the radial component of the magnetic field at the poloidal angles of $\theta = \pm 90°$ and are also illustrated in Figure 2.11(a). Each of the magnetic coils has a resistance of about 22 Ω and an inductance of about 1 mH. The magnetic probes are constructed of 34 AWG enameled wire, wound on a cylindrical Teflon former [15]. When terminated by 2 kΩ, the frequency response of each coil extends to about 200 kHz [15], which is quite sufficient for the purpose of performing plasma position control.

The magnetic field measured by the position sensing coils consists of the desired magnetic field produced by the plasma current as well as unwanted magnetic fields such as that produced by the toroidal field coils. This happens primarily as a result of misalignments of the coils. In order to eliminate, or at least to reduce, these stray magnetic fields, the waveforms to which they correspond are added with suitable polarity to the measured signals via an adjustable gain passive mixer. To accomplish this, the gains are adjusted in the absence of the plasma, while all other fields are present, until the

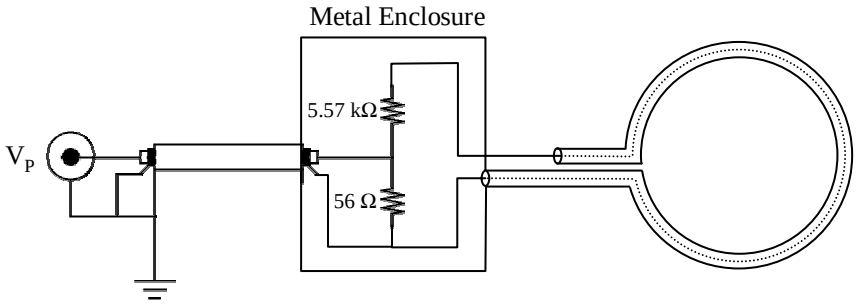

Figure 2.10 Loop voltage measurement circuit.

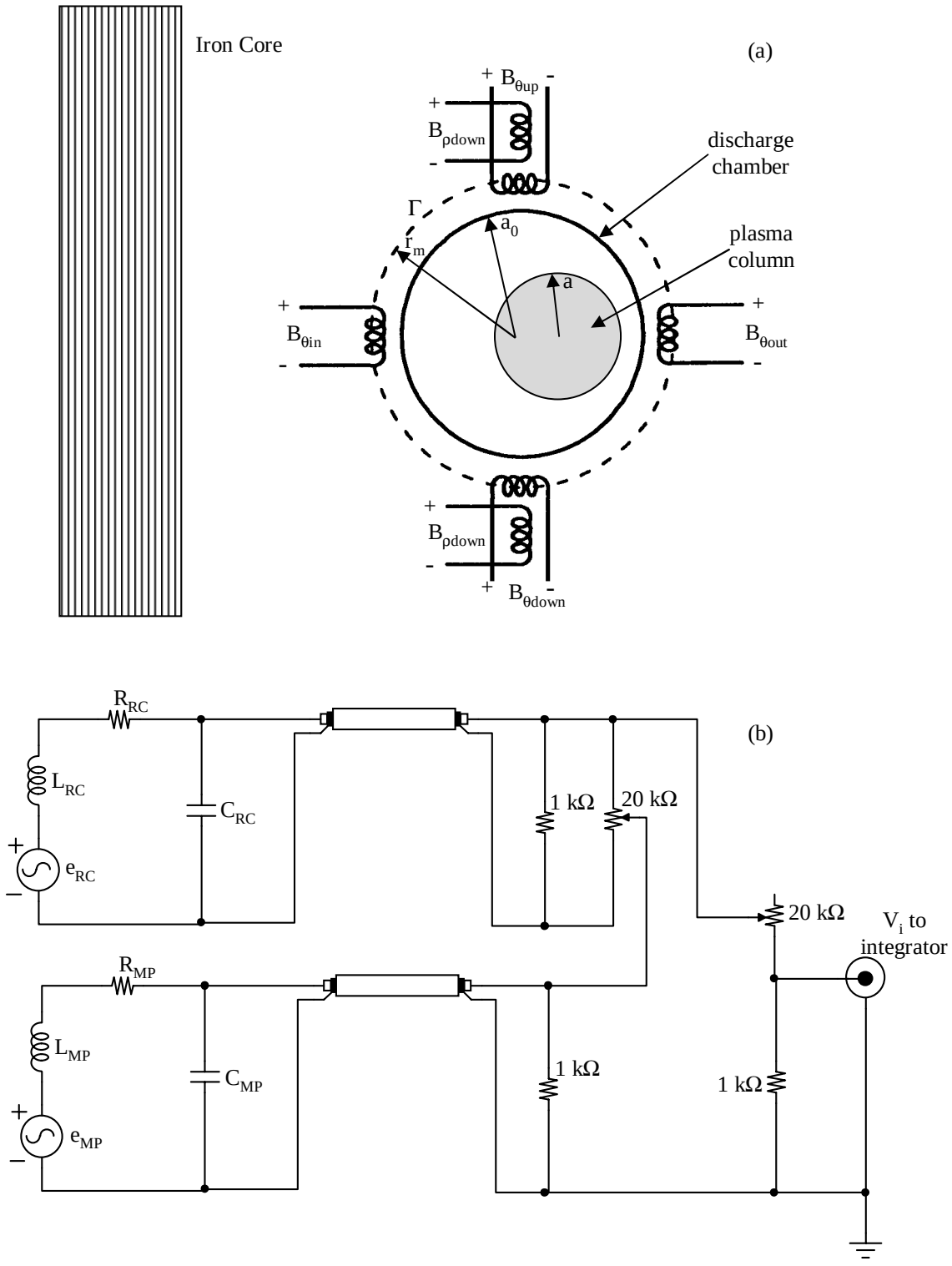

Figure 2.11 Plasma position: (a) sensing coils and (b) compensation circuit. Magnetic Probe signal (MP) and stray field compensation signal measured by a Rogowski Coil (RC).

coil signals are zero or as close to zero as possible. On the STOR-M tokamak, it is only necessary to cancel the contribution of the toroidal field from each of the position sensing magnetic probes. A schematic diagram of the probe and compensation circuit is given in Figure 2.11(b). The frequency response of the position sensing circuit including the compensation circuit has been reported to be linear up to about 100 kHz [14,15]. The probe signals are transmitted to the control room via 20 m of RG 58/U coaxial cable, where they are compensated and integrated by gated, active integrators. The integrated signals correspond to the magnetic field at the probe locations that is produced by the plasma current, as seen from $B_i = \frac{\phi_i}{A_i} = \frac{-\int V_i dt}{\pi a_i^2}$ where a_i is the radius of the i^{th} probe's cross-section, and V_i is the voltage induced in the i^{th} magnetic probe. The outputs of the integrated signals were calibrated against a known, uniform magnetic field produced by a Helmholtz coil. The details of how the vertical and horizontal plasma position signals are determined from these measurements will be presented in detail in Section 2.4.

2.2.2.4 Density – 4-mm Microwave Interferometer

The electron density in the STOR-M Tokamak is measured using a 4-mm microwave interferometer [16,31]. This system, shown in Figure 2.12, provides a direct reading, real-time output without the requirement of source modulation, thereby increasing the high frequency response. In this system a cavity stabilized IMPATT oscillator (ELVA-1) operating at 76 GHz and 100 mW [32] produces microwaves, which travel along the three paths, E_P, E_{R1}, and E_{R2} as shown in Figure 2.12. The reference signals E_{R1}, and E_{R2} are split off from E_P by 10 dB directional couplers. The signal E_P is guided to the chamber where it is vertically i ncident on the plasma through a horn antenna. After passing through the plasma, the transmitted wave is received by a

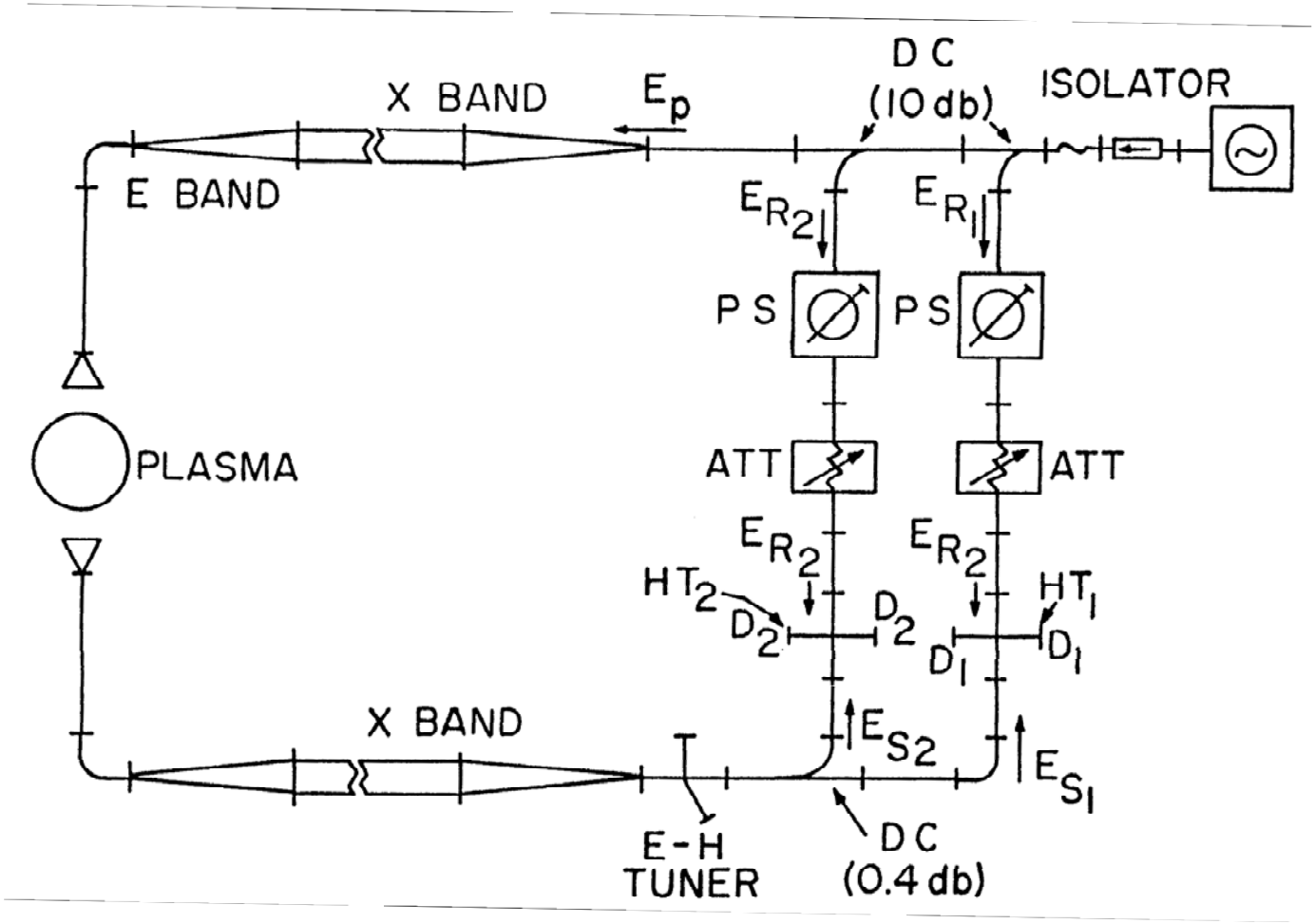

Figure 2.12 Plasma density measurement using a 4 mm microwave interferometer. [M. Emaami, O. Mitarai and S.W. Wolfe, PPL-86, June 1986.]

horn and passed through an E-H tuner before being split into the two paths, E_{S1} and E_{S2} by a 0.46 dB directional coupler [16]. The reference signals E_{R1} and E_{R2} are each passed through a phase shifter and an attenuator. Finally E_{S1} and E_{R1}, and E_{S2} and E_{R2} are then mixed in hybrid "magic" tees. The signals at the sum and difference ports of both of the hybrid tees are detected with 1N53 silicon point-contact diodes operating in the "square-law" regime. In order to compensate for the different efficiencies of each diode, the signals are then passed into buffer amplifiers with adjustable gains. The frequency response of this circuit is essentially limited by the frequency response of the detecting diodes [31]. It can be shown that the final output of each amplifier is given by: $V_{1,2} = K_{1,2}\cos\theta_{1,2}$, where $\theta_{1,2}$ are the phase angles of the detected microwave signals. When the phase shifters are correctly adjusted, the outputs become: $V_1 = K_1 \sin\Delta\Phi$, and $V_2 = K_2 \cos\Delta\Phi$, where $\Delta\Phi$ is the phase shift caused by the plasma itself. By measuring these two signals, the phase is determined, from which a fringe counting circuit is used to determine the line averaged electron density, as will be shown below. The fringe counting circuit is discussed in detail in [16] and [31] and has a resolution of a quarter fringe.

When the microwave signal passes through the plasma, it undergoes a phase shift as a result of the change in the index of refraction. This phase shift, which can be measured by the method just described, is given by [31]:

$$\Delta\Phi = \frac{2\pi}{\lambda}\int_{-a}^{a}\left[1-\sqrt{1-\frac{n_e(x)}{n_c}}\right]dx \quad \text{rad} \tag{2.5}$$

where $n_e(x)$ is the electron density, and n_c is the cutoff density which gives an upper limit to the density measurement. In STOR-M, with the use of a 76-GHz microwave source,

$n_c = 7.0\times10^{19}$ m^{-3}; thus, this interferometer can measure densities up to 7.0×10^{19} m^{-3}, and if the plasma is assumed to extend up to the limiter, then the fringe counting circuit can resolve the measured density in steps of 5.6×10^{17} m^{-3}. If the plasma position is assumed to be stationary then, since $n_e(x)$ and $\Delta\Phi$ are related by an integral, the measurable quantity is the central line averaged electron density and is given by:

$$\overline{n_e} = \frac{1}{2a}\int_{-a}^{a} n_e(x)dx \quad m^{-3} \tag{2.6}$$

The output of the fringe counting circuit therefore corresponds to the line averaged electron density. This signal is transmitted to the control room via 20 m of RG 58/U coaxial cable where it is received by the data acquisition system.

2.2.2.5 Quality of Confinement - Spectrometer

Measuring the intensity of line emissions from hydrogen and from impurity elements can give a qualitative indication of the quality of the plasma confinement and the plasma purity. The H_α emission corresponds to the recycling process of the plasma particles in the edge region [14,67]; thus, a lower H_α emission indicates better plasma confinement. In addition, since carbon and oxygen outgas from the inner surface of the vacuum vessel, they are often used for impurity studies in tokamaks.

The STOR-M tokamak is equipped with a SPEX-1702, 0.75 m focal length Czerny-Turner scanning spectrometer having a relative aperture of f/7 and a dispersion of 10 Å/mm at 5000 Å [33]. The diffraction grating, manufactured by Bausch & Lomb, has 1200 lines/mm and is blazed at 5000Å [33]. A fiber optic probe is used to transmit the radiation emitted from the plasma to the entrance slit of the spectrometer. The optical probe is made of bundles of glass fibers with optical lenses at each end. The

spectrometer has a lens at the entrance to image the plasma onto the entrance slit and a diaphragm to match the relative aperture of the lens with that of the spectrometer. The entrance and exit slits of the spectrometer have a width of 100 μm and a height of 10 mm [33]. The dispersed light is detected by a photomultiplier, which is shielded by a μ-metal from the magnetic field, and is enclosed in a brass and copper housing. Figure 2.13(a) is a schematic diagram of the spectrometer system. The photocathode and the shield are both negatively biased with 1.2 kV, while the anode is grounded through the 5.6 kΩ output resistor, as shown in Figure 2.13(b). Since only the relative intensity is important, it is not necessary to have a calibrated output signal. The raw signal is transferred to the control room via 20 m of RG 58/U coaxial cable where it is amplified to an acceptable level before being received by the data acquisition system.

2.2.2.6 Langmuir Probes

Langmuir probes are widely employed to study various plasma parameters in the edge region of tokamak plasmas. These probes are rather diverse as, depending upon how they are configured, they can provide information about the electron density, the electron temperature, and the floating potential of the plasma, as well as the fluctuation of these parameters. Langmuir probes are also highly favoured because they are relatively inexpensive and simple to construct, they are easy to use, and they provide good spatial resolution. Their use, however, is restricted to the cooler edge region of the plasma where their presence does not cause significant perturbations of the plasma.

Langmuir probes essentially consist of a conductor (or an array of conductors) that is inserted into the plasma and biased relative to the wall of the discharge chamber, as shown in Figure 2.14(a). In order to maintain the quasi-neutrality of the plasma a

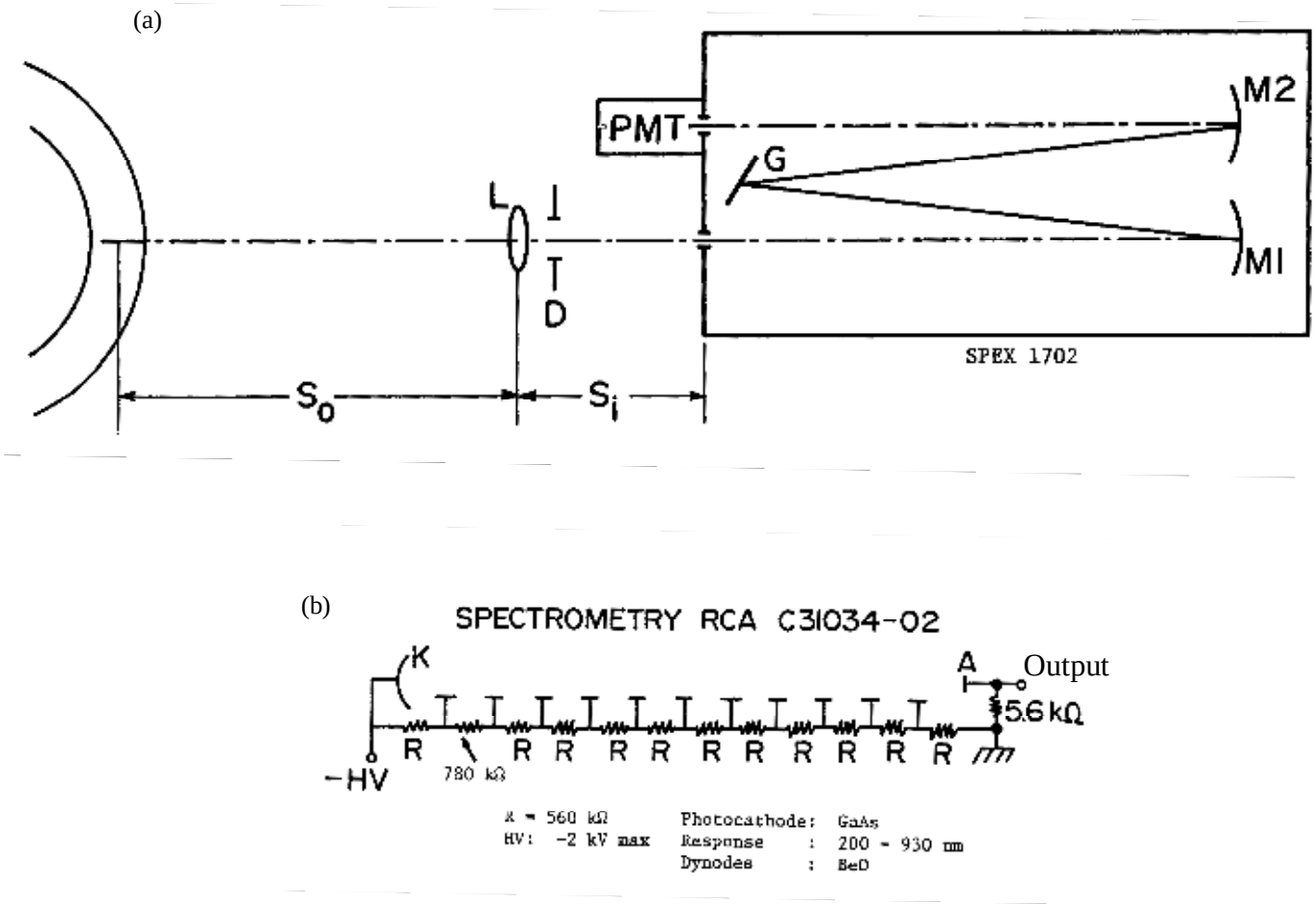

Figure 2.13 Spectrometer: (a) schematic diagram and (b) photomultiplier tube circuit. [S.W. Wolfe, PPL-101, July 1988, p. 66.]

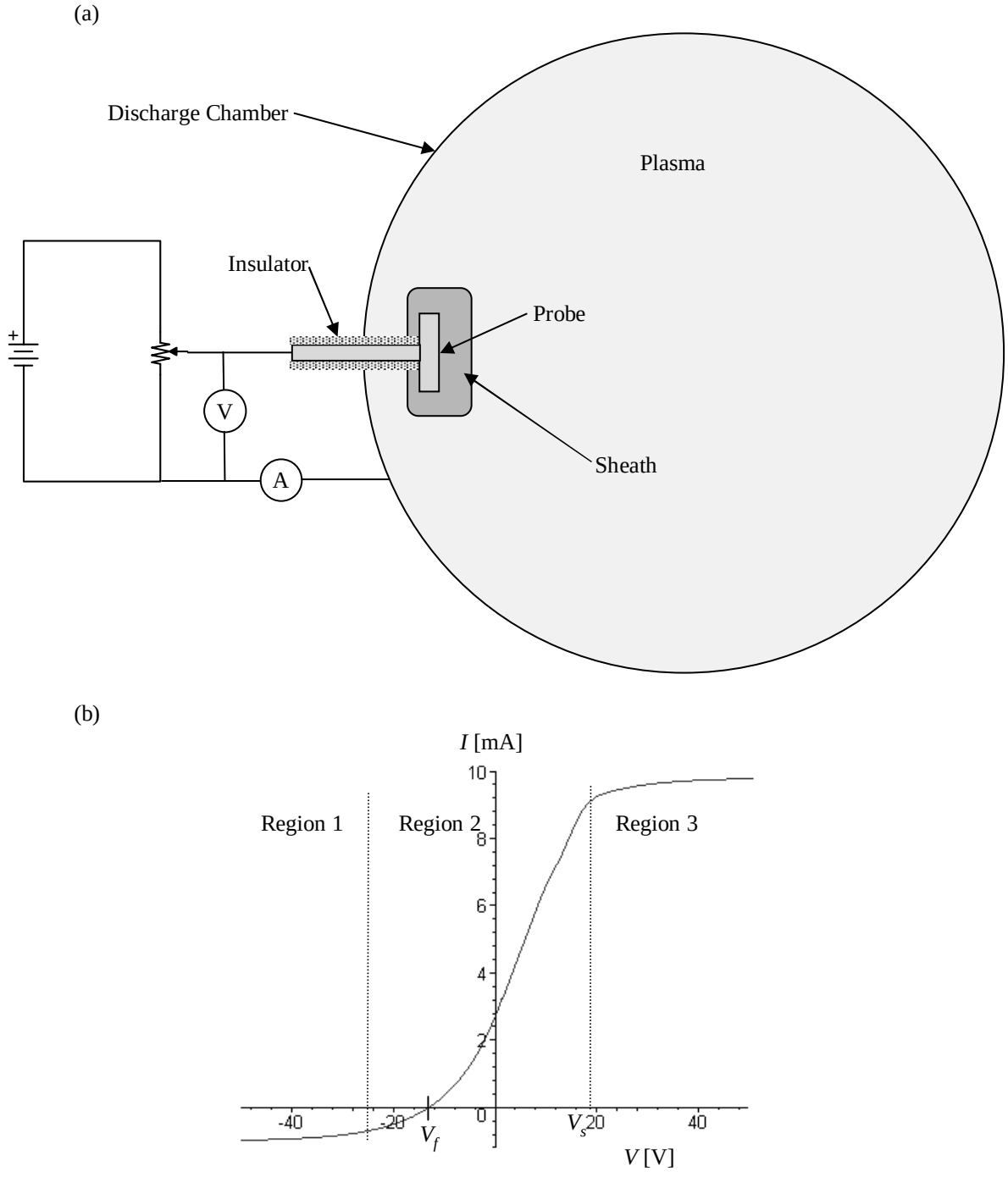

Figure 2.14 Langmuir probe: (a) schematic diagram and (b) characteristic I-V curve.

Bohm sheath is developed around the biased conductor. If the undisturbed ions and electrons both follow a Maxwellian distribution, ignoring the effects of the magnetic field, the current density that flows into the surface of the probe is given by [65]

$$J = J_{i0} + J_{e0}\, e^{\left(\frac{e(V-V_s)}{T_e}\right)} \quad Am^{-2} \tag{2.7}$$

where J_i is the ion current density, J_{e0} is the electron saturation current density, V is the potential to which the probe is biased, V_s is the plasma space potential, and T_e is the electron temperature in units of eV. Depending upon how the probe is biased, as will be shown below, any of the parameters mentioned above can be obtained.

A typical I-V characteristic for a Langmuir probe inserted into plasma is shown in Figure 2.14(b). This curve can be divided into three regions, as shown in Figure 2.14(b). The first region corresponds to the probe being sufficiently negatively biased such that all electrons are repelled and, hence, the probe collects only ion current. Thus, this region is called the ion saturation region. Under this operating condition, the electron density can be obtained from:

$$I_{i0} = J_{i0}S = n_i e v_i S = n_e e \sqrt{\frac{2kT_e}{m_i}} S \tag{2.8}$$

where I_{i0} is the ion saturation current (the current collected by the probe), and S is the surface area of the probe.

From Figure 2.14(b) it can be seen that as the probe bias voltage is increased from that in the ion saturation region, a point where the probe current is equal to zero will be reached. The bias voltage at which the probe current is zero is the floating potential, V_f, of the plasma at that location. As the bias voltage continues to increase, the expon ential

term of Equation 2.7 is dominant. In this region the electron temperature can be determined from:

$$T_e = \frac{e(V_f - V_s)}{\ln\left(\frac{I_{i0}}{I_{e0}}\right)} \quad eV \tag{2.9}$$

This situation corresponds to region two of Figure 2.14(b)

As the bias voltage of the probe is further increased, the probe will eventually become so positively biased that all of the ions are repelled. In this third region, as shown in Figure 2.14(b), the probe current is solely due to electrons. Thus, this region is known as the electron saturation region. As shown in Figure 2.14(b), the plasma space potential marks the beginning of the electron saturation region.

2.2.2.7 Data Acquisition System

As has already been indicated, all data signals are routed to the control room via 20 m of either coaxial or triaxial RG 58/U cable. Once in the control room, all required signal conditioning, such as amplification and integration, is performed. The conditioned signals are then passed to the data acquisition system for analog to digital conversion and subsequent storage. All of the data signals reported in this thesis were sampled and digitized by a LeCroy 8212A Fast Data Logger module. This module has 32 input channels and is capable of simultaneous sampling at a sampling rate of up to 40 ksamples per second (25 μs per sample). However, as is normally the case during the operation of STOR-M, all of the signals reported here were sampled at 100 μs per sample using 16 channels of the LeCroy 8212A module. In addition, the LeCroy 8212A has 12-bit resolution which for the ±5.0 V input range corresponds to 2.4 mV resolution. The input impedance of the LeCroy 8212A is 1 MΩ. The sampled, digitized signals are stored in a

LeCroy 8800A Memory module until they are transferred to a 486 PC computer via the LeCroy 8901A GPIB (IEEE-488) Interface module, where they are ultimately stored on the hard drive for later analysis. All of the LeCroy modules are mounted in a LeCroy CAMAC Instrumentation Mainframe 8013A. The data transfer is facilitated by the LeCroy Catalyst software package, which saves the data as a FORTRAN binary file. These binary files are opened by a MATLAB routine written by the author. Once the files are opened any analysis of the data, including plotting that is required, may be performed using MATLAB, or the data may be saved in a suitable format for use with any other package or platform.

2.3 Plasma Confinement in STOR-M

As was discussed in Chapter 1, the tokamak configuration is the most promising candidate for a viable commercial fusion reactor. Before this very promising energy source can be harnessed, many scientific and engineering problems must first be resolved. One of the principal problems facing magnetic confinement schemes such as the tokamak configuration is the issue of stably maintaining the plasma column within the discharge chamber. In order to accomplish this, a suitably shaped magnetic field structure must be produced. What follows in this section is a discussion of the plasma confinement issue in general and the maintenance of the equilibrium of the plasma column in the major radial direction in the STOR-M tokamak in particular.

2.3.1 Plasma Confinement

The confinement of the plasma within the discharge chamber of a tokamak requires a suitably structured magnetic field configuration. This magnetic field will act as a magnetic bottle only as long as certain conditions are satisfied. The confinement of

the plasma within the discharge chamber can be thought of as a problem of controlling the equilibrium position of the plasma column and the position of the plasma column with respect to its equilibrium position. If the equilibrium position of the plasma column can be made to be at the cross-sectional center of the discharge chamber, then a necessary condition for the plasma to be well confined is that the position of the plasma column from the center of the discharge chamber be maintained to be less than a suitably small displacement. For the STOR-M tokamak it has been found that a displacement of ±5 mm can be tolerated without significantly affecting the quality of the discharge. The displacement of the plasma column from the cross-sectional center of the vacuum vessel can be decomposed into a vertical displacement component and a horizontal displacement component, as was shown in Figure 2.1. The control of the vertical plasma displacement in the STOR-M tokamak is relatively straightforward and is adequately controlled by a pre-programmed, open-loop, analog controller. The control of the horizontal displacement, however, is nontrivial and forms the impetus of the research discussed in this thesis.

2.3.2 Expansion Forces in the Major Radial Direction

The tokamak plasma is subjected to several forces in the major radial direction that must be dynamically counterbalanced by an appropriate magnetic Lorentz force in order to maintain equilibrium in the horizontal direction. The mechanism of plasma confinement in the tokamak device was described briefly in Chapter 1; in what follows a detailed discussion of the forces acting on the plasma column in the major radial (horizontal) direction will be presented. The majority of these forces tend to cause the

plasma to expand in the major radial direction and must be counteracted if the plasma is to be confined.

The current carrying tokamak plasma tends to expand radially so as to increase its inductance. The self inductance of the plasma column can be separated into two components: the external self inductance, which is due to the magnetic flux outside of the plasma column, $L_{ext} \approx \frac{\phi_{ext}}{I_P}$, and the internal self inductance, which results from the magnetic energy within the plasma column ($\int \frac{B_i^2}{2\mu_0} dV = \frac{1}{2} L_i I_P^2$). With the plasma column being modelled as a thin conducting ring, it can be shown that the plasma external self-inductance, L_{ext}, is given by [34,35]:

$$L_{ext} = \mu_0 R \left[\ln\left(\frac{8R}{a}\right) - 2 \right] \quad H \tag{2.10}$$

where μ_0 is the permeability of free-space, and R and a are the major and minor radii of the plasma column respectively. The force, F_1, acting on the plasma due to the external self-inductance, is given by:

$$F_1 = \frac{\partial}{\partial R}\left(\frac{1}{2} L_{ext} I_P^2\right) \quad N \tag{2.11}$$

Substituting (2.10) into (2.11) and simplifying gives:

$$F_1 = \frac{\mu_0 I_P^2}{2}\left[\ln\left(\frac{8R}{a}\right) - 1 \right] \quad N \tag{2.12}$$

It can also be shown that the internal self-inductance of the plasma column is given by [35]:

$$L_i = \mu_0 R \frac{l_i}{2} \quad H \tag{2.13}$$

where l_i is the internal inductance parameter given by [36]:

$$l_i = \frac{\overline{B_\theta^2}}{B_\theta^2(a)} = \frac{2\pi \int_0^a \left(\frac{B_\theta^2(\rho)}{2\mu_0} \right) \rho d\rho}{\pi a^2 \left(\frac{B_\theta^2(a)}{2\mu_0} \right)} \tag{2.14}$$

where $B_\theta(\rho)$ and $B_\theta(a)$ are the poloidal magnetic field as a function of distance, ρ, from the center of the plasma column and at the edge of the plasma column, $\rho = a$, respectively. The internal inductance parameter depends on the toroidal current density profile; the internal inductance parameter ranges from zero for a skin current, to greater than one for a centrally peaked current distribution, and $l_i = 0.5$ for an uniform current profile. Figure 2.15 shows the internal inductance parameter for various radial profiles of the toroidal plasma current. The force, F_2, acting on the plasma column as a result of the internal inductance of the plasma is:

$$F_2 = \frac{\partial}{\partial R}\left(\frac{1}{2} L_i I_P^2 \right) = \frac{\mu_0 I_P^2}{2}\left(\frac{l_i}{2} \right) \quad N \tag{2.15}$$

There is also a force, F_3, acting on the plasma as a result of thermal energy of the plasma. This force, the so-called ballooning force, tends to expand the plasma column. Only the plasma pressure perpendicular to the plasma column can contribute to the expansion of the plasma column. The force, F_3, that results is the radial component of the thermal expansion force, F_T, and is given by:

$$F_T \cdot dR = \overline{P} \int_{\theta=0}^{2\pi} 2\pi (R + a\cos\theta) a d\theta \, dR \cos\theta = F_3 dR \quad J \tag{2.16}$$

where $\overline{P} = \frac{1}{\pi a^2} \int_0^a P(\rho) 2\pi \rho d\rho$ is the mean value of the plasma pressure averaged over the

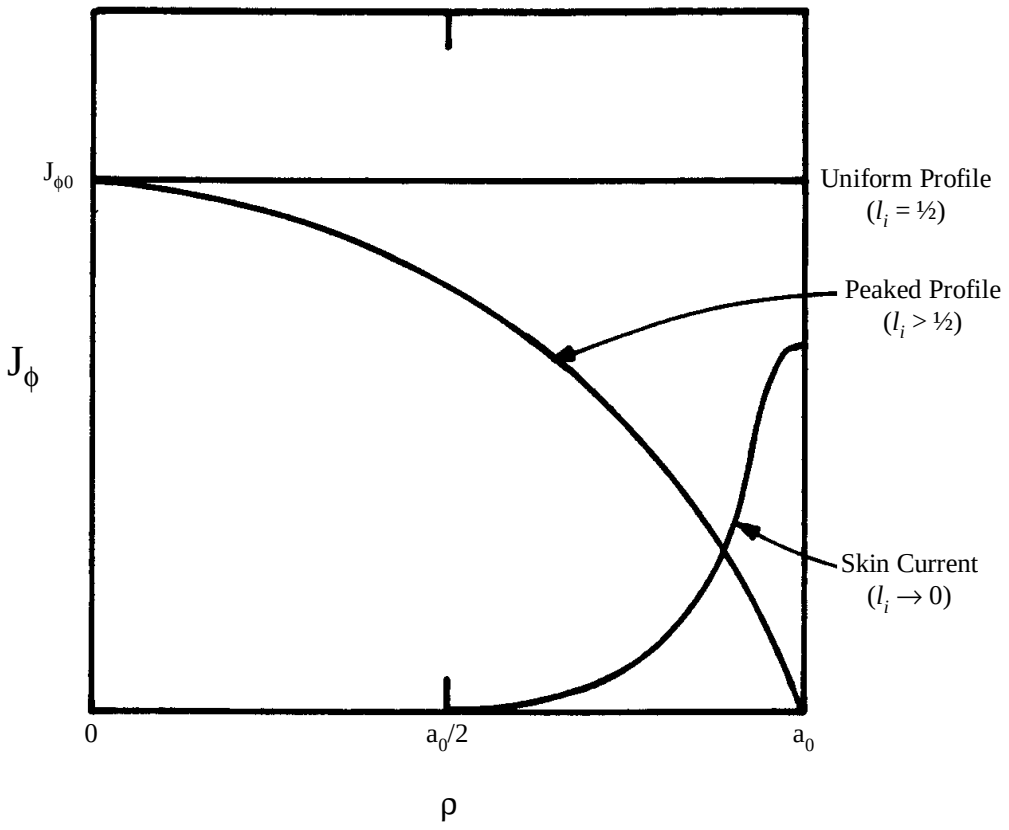

Figure 2.15 Dependence of the internal inductance parameter on the radial profile of the toroidal plasma current. [K.C. Mark, M.A.Sc. Thesis, University of Saskatchewan, Apr. 1993, p. 34.]

cross-section of the plasma column. Integrating Equation 2.16 and simplifying gives:

$$F_3 = 2\pi^2 a^2 \overline{P} \quad \text{N} \tag{2.17}$$

As a result of the variation of the toroidal magnetic field over the plasma column, the tokamak plasma will experience a radially outward force, F_4, given by:

$$F_4 = \frac{\partial}{\partial R}\left\{\frac{1}{2\mu_0}\left(B_\phi^2(a) - \overline{B_\phi^2}\right)\left(2\pi^2 R a^2\right)\right\} \quad \text{N} \tag{2.18}$$

where $\frac{1}{2\mu_0}\overline{B_\phi^2}$ is the mean energy density (toroidal magnetic pressure) stored in the toroidal magnetic field averaged over the cross section of the plasma column. Furthermore, the force balance in the minor radial direction requires that:

$$\overline{P} = \frac{B_\theta^2(a)}{2\mu_0} + \frac{B_\phi^2(a) - \overline{B_\phi^2}}{2\mu_0} \quad \text{Pa} \tag{2.19}$$

In addition, it can be shown from Ampere's Law that the poloidal magnetic field at the edge of the plasma column is given by:

$$B_\theta(a) = \frac{\mu_0 I_P}{2\pi a} \quad \text{T} \tag{2.20}$$

Substituting Equations (2.19) and (2.20) into Equation (2.18) and simplifying gives:

$$F_4 = (\beta_\theta - 1)\left(\frac{\mu_0 I_P^2}{4}\right) \quad \text{N}. \tag{2.21}$$

where the β_θ is the poloidal beta factor defined as the ratio of the average thermal pressure to the poloidal magnetic pressure [36], and is given by:

$$\beta_\theta \equiv \frac{2\pi\int_0^a P(r) r dr}{\pi a^2\left(\frac{B_\theta^2(a)}{2\mu_0}\right)} = \frac{\overline{P}}{\left(\frac{B_\theta^2(a)}{2\mu_0}\right)} \tag{2.22}$$

From Equation 2.21 and 2.22 it is evident that if on the one hand the thermal pressure of the plasma column exceeds the magnetic pressure on the plasma column, then the plasma column will expand and F_4 is directed outward; however, if the thermal pressure of the plasma column is less than the magnetic pressure on the plasma column, then the plasma column will be compressed and F_4 will be directed inward.

2.3.3 Major Radial Force Equilibrium

The net force, F_R, tending to cause the tokamak plasma to expand in the radial direction is given by:

$$F_R = F_1 + F_2 + F_3 + F_4 = \frac{\mu_0 I_P^2}{2}\left[\ln\left(\frac{8R}{a}\right) - 1 + \frac{l_i}{2} + \frac{2}{\mu_0 I_P^2}\left(2\pi^2 a^2 \overline{P}\right) + \frac{1}{2}\left(\beta_\theta - 1\right)\right] \qquad (2.23)$$

which can be simplified further by recognizing that:

$$\frac{2}{\mu_0 I_P^2} 2\pi^2 a^2 \overline{P} = \frac{\overline{P}}{\left(\frac{\mu_0 I_P^2}{4\pi^2 a^2}\right)} = \frac{1}{2}\frac{\overline{P}}{\left(\frac{B_\theta^2(a)}{2\mu_0}\right)} = \frac{1}{2}\beta_\theta \,. \qquad (2.24)$$

Thus, substituting (2.24) into (2.23) and simplifying gives the net radially outward force acting on the tokamak plasma column as:

$$\mathrm{F_R} = \frac{\mu_0 \mathrm{I_P^2}}{2}\left[\ln\left(\frac{8\mathrm{R}}{\mathrm{a}}\right) - \frac{3}{2} + \left(\beta_\theta + \frac{\mathrm{l_i}}{2}\right)\right] \quad \mathrm{N}\,. \qquad (2.25)$$

In order for the position of the plasma column to be in equilibrium, the Lorentz force that is induced by the net vertical magnetic field must counterbalance this force; that is:

$$\mathrm{F_R} = 2\pi \mathrm{R I_P B_V} \quad \mathrm{N}\,. \qquad (2.26)$$

Thus, the net vertical field, B_V, that is required for the position of the plasma column to be in equilibrium in the major radial (horizontal) direction is obtained by substituting

Equation (2.25) into Equation (2.26) and rearranging to give [34]:

$$B_V = \frac{\mu_0 I_P}{4\pi R}\left[\ln\left(\frac{8R}{a}\right) - \frac{3}{2} + \left(\beta_\theta + \frac{l_i}{2}\right)\right] \quad T \tag{2.27}$$

From Equation (2.27) it becomes obvious that the control of the plasma position in the horizontal direction is quite complicated. Not only does the net vertical field required for equilibrium depend on the magnitude of the plasma current; it also depends on the poloidal beta factor and the internal inductance parameter, both of which are also dependent on the plasma current. Further complicating matters is the fact that the plasma parameters, including the plasma current, are not static. The temporal variation of the plasma parameters demands continuous, dynamic regulation of the net vertical field that is required for equilibrium. This is a very difficult technical problem, particularly if the parameters of the plasma column change quickly. This is the primary motivation for the research presented in this thesis.

For a tokamak such as STOR-M, eddy currents that are induced in the conducting wall of the discharge chamber by the motion of the plasma column will produce a significant portion of the net vertical field required for equilibrium. In addition, image currents in the conducting transformer core will produce a significant portion of the vertical field. For STOR-M it has been estimated that nearly half of the required vertical field is produced by the image currents in the transformer core [15]. Finally, to ensure the equilibrium of the position of the plasma column, a portion of the requisite vertical magnetic field is produced by two sets of external windings: the vertical equilibrium winding and the vertical feedback winding. In STOR-M the majority of the remaining vertical field required is provided by the vertical equilibrium field, B_{VE}, which is roughly

proportional to the plasma current. The vertical feedback field, B_{VF}, provides the remaining vertical field.

When the plasma column expands in the major radial direction, it approaches the outer wall of the discharge chamber, which for STOR-M is made of stainless steel, a good conductor. As the plasma column approaches the outer wall, so to do the poloidal magnetic field lines that are produced by the plasma current. As these magnetic field lines begin to cut across the chamber wall, an electromotive force is induced in the conducting wall that is proportional to the rate of approach. This emf produces eddy currents in the chamber wall. The net image current flows in the direction opposite the plasma current and produces a magnetic field equal in magnitude and opposite in direction to the magnetic field that is trying to penetrate the conducting wall, thereby cancelling the component of the magnetic field that is normal to the surface of the chamber wall [2]. This effect is illustrated in Figure 2.16 [37]. Since the wall of the discharge chamber does not have infinite conductivity, the poloidal magnetic field of the plasma column will eventually penetrate the chamber wall. While for an ideally conducting, unbroken discharge chamber the equilibrium position of the plasma column is stable, for a practical discharge chamber this method of stabilizing the position of the plasma column does not have a steady state equilibrium position, and it becomes ineffective after the poloidal magnetic field of the plasma column penetrates the wall. The time required for the magnetic field to reach the wall, τ_d, and the time required to penetrate through the wall, τ_w, are given by [2,34,38] respectively as:

$$\tau_d = \frac{\mu_0 a_0 d_w \sigma_w}{2} \quad \text{and} \quad \tau_w = \mu_0 d_w^2 \sigma_w \quad \text{s} \tag{2.28}$$

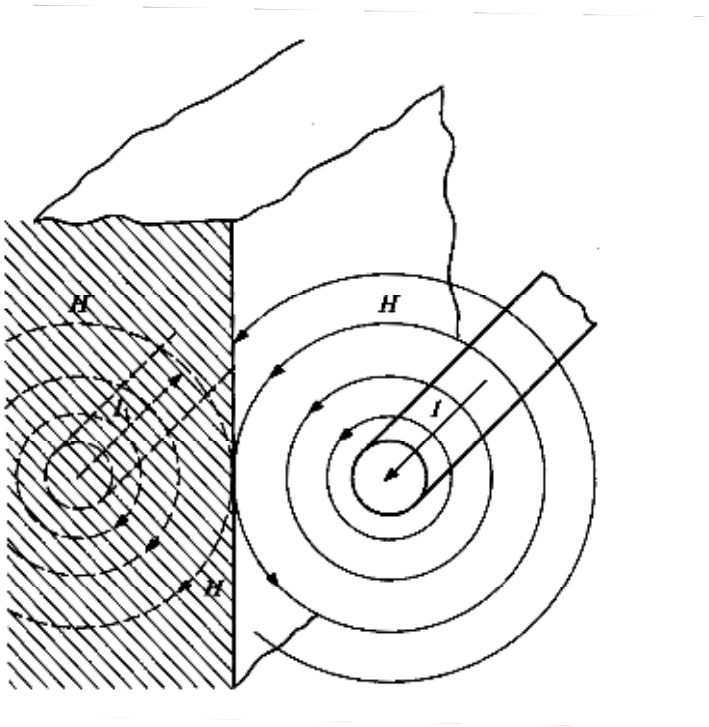

Figure 2.16 Image current produced in the conducting wall of the discharge chamber upon the displacement of the plasma column from the equilibrium position. [L.A. Artzimovich, "Elementary Plasma Physics", Blaisdell Publishing Company, Waltham, Massachusetts, 1965, p. 151.]

For the stainless steel vacuum chamber of STOR-M the conductivity is $\sigma_w \approx 1.39\times10^6\ \mathrm{Sm}^{-1}$ [66] which corresponds to the time required for the magnetic field to reach the wall of $\tau_d \approx 550\ \mu\mathrm{s}$, and the time required for the magnetic field to penetrate through the wall of $\tau_w \approx 28\ \mu\mathrm{s}$. The stabilizing effect of the conducting chamber wall is further reduced by the insulating breaks that are necessary to prevent a toroidal current from being induced in the wall. The magnetic field produced by the eddy currents in the wall of a discharge chamber having two insulating sections, as is the case with STOR-M, can be estimated by treating the conductivity of the wall as being infinite; in this case, the magnitude of the magnetic field in the vertical direction is approximately [2,34]:

$$B_w \approx \frac{\mu_0 I_P \Delta H}{2\pi a_0^2}\left(1+\frac{2a_0}{2\pi R_0}\right)\ \mathrm{T}. \tag{2.29}$$

Assuming that the plasma current is constant, and allowing for the finite conductivity of the chamber wall, the force on the plasma column in the horizontal direction that results from this magnetic field is approximately:

$$F_w \approx -\frac{\mu_0 R_0 I_P^2}{a_0^2}\left(\Delta H-\frac{\partial \Delta H}{\partial t}\tau_d\right)\left(1+\frac{2a_0}{2\pi R_0}\right)\ \mathrm{N}. \tag{2.30}$$

The equilibrium position of the plasma core is also maintained, in part, by the interaction between the transformer core and the plasma current. This effect occurs because a core having a high relative magnetic permeability, $\mu_c >> 1$, tends to concentrate the magnetic field lines surrounding the plasma column. The concentration of magnetic field lines generates a force that attracts the plasma column towards the core, that is, inwards in the major radial direction. By modelling the transformer core as an

infinite cylinder of radius r_c, then, the force in the major radial direction is approximately given by [34] as:

$$F_c \approx -\mu_0 I_P^2 f\left(\frac{R}{r_c}\right) \quad N \tag{2.31}$$

where $f\left(\frac{R}{r_c}\right)$ is a complicated function expressed in terms of the integral of modified Bessel functions [34]. Furthermore, this force does not lead to a stable equilibrium since the accidental displacement of the plasma column from the equilibrium position towards the core results in a directly proportional increase in the force of attraction, while an accidental displacement away from the core relative to the equilibrium position results in an inversely proportional decreasing force of attraction. Nevertheless, this force aids in the horizontal equilibrium of the plasma column.

The facts that the wall of the STOR-M discharge chamber is not an ideal conductor and that it has toroidal gaps not only means that the magnetic field due to the plasma column can penetrate the wall of the dscharge chamber, but it also means that the magnetic field of the various current carrying windings outside of the discharge chamber (such as the ohmic heating winding and the various control windings) can penetrate the wall of the discharge chamber and exert forces on the plasma column. In addition, the forces due to these external currents are augmented by the presence of the iron transformer core. This augmentation is the result of the image currents that exist in the iron core. The exact forces that are produced are very difficult to express analytically and, therefore, must be measured experimentally; it has been estimated that for STOR-M these image currents account for about 50% of the vertical magnetic field that is required to maintain the position of the plasma column in a stable equilibrium [15]. The

remaining portion of the required vertical field must be supplied by the magnetic field produced by the control windings.

As has already been mentioned, the vertical magnetic field necessary to ensure the stable equilibrium position of the plasma column in STOR-M is provided by two sets of control windings: the vertical equilibrium winding and the vertical feedback winding. The magnetic fields produced by the control windings are subject to a delay due to the penetration time of the stainless steel discharge chamber and are approximately given by:

$$B_{VE} = -\frac{\mu_0 K_{VE} I_{VE}}{2\pi} - \frac{\partial B_{VE}}{\partial t}\tau_w \ \text{T} \quad \text{, and} \quad B_{VF} = -\frac{\mu_0 K_{VF} I_{VF}}{2\pi} - \frac{\partial B_{VF}}{\partial t}\tau_w \ \text{T} \qquad (2.32)$$

where K_{VE} and K_{VF} depend on the number and locations of the vertical equilibrium windings and the vertical feedback windings respectively. The resulting forces due to these fields in the major radial direction are then:

$$F_{VE} = 2\pi R I_P B_{VE} \ \text{N} \quad \text{, and} \quad F_{VF} = 2\pi R I_P B_{VF} \ \text{N} \qquad (2.33)$$

Thus, it is clear that provided that suitable control currents are used, the position of the plasma column in the horizontal direction can be maintained in, or around, a stable equilibrium position. For STOR-M, the force produced by the vertical equilibrium field is roughly proportional to the plasma current; thus, the vertical equilibrium field can be thought of as providing coarse control of the position of the plasma column, while the vertical feedback winding provides fine control. Adjusting the shunt resistance shown in Figure 2.7 controls the relative magnitude of the vertical equilibrium current. The quality of the discharge in the STOR-M tokamak is actually quite sensitive to the quality of the fine control of the plasma position, and this requires the use of a good controller. Furthermore, as will be discussed in greater detail in Section 2.5, the analysis of the forces acting on the plasma column just presented requires the use of several

assumptions, most of which are only marginally valid in a practical system such as the STOR-M tokamak, and their experimental measurement is very complicated in practice.

2.4 Determination of ΔH

In order to control the position of the plasma column within a device, such as the STOR-M tokamak, it is necessary to have some way of measuring it. Not surprisingly, given the analysis of the previous section, the theory regarding the experimental determination of the position of the plasma column is quite complicated. For the approximation of a tokamak device with a thin walled discharge chamber having toroidal gaps (as is the case with the STOR-M tokamak), it can be shown in the first order of the inverse aspect ratio (*a*/*R*) that the poloidal and radial components of the magnetic field on the contour Γ which is defined by a circle of radius r_m, whose center coincides with that of the discharge chamber (refer to Figure 2.11), are given by [34,39]:

$$B_\theta = \frac{\mu_0 I_P}{2\pi r_m} - \frac{\mu_0 I_P}{4\pi r_m}\left\{\ln\left(\frac{a}{r_m}\right) + 1 - \left(\Lambda + \frac{1}{2}\right)\left(\frac{a^2}{r_m^2} + 1\right) - \frac{2R\Delta H}{r_m^2}\right\}\cos\theta \quad T \qquad (2.34)$$

$$B_\rho = -\frac{\mu_0 I_P}{4\pi r_m}\left\{\ln\left(\frac{a}{r_m}\right) + \left(\Lambda + \frac{1}{2}\right)\left(\frac{a^2}{r_m^2} - 1\right) + \frac{2R\Delta H}{r_m^2}\right\}\sin\theta \quad T \qquad (2.35)$$

respectively, where $\Lambda = \beta_\rho + \frac{l_i}{2} - 1$. Thus, by measuring $B_\theta(\theta = 0)$, $B_\theta(\theta = \pi)$, $B_\rho(\theta = \pi/2)$, and $B_\rho(\theta = 3\pi/2)$ using appropriately aligned magnetic probes placed at these poloidal locations on the contour Γ, the plasma position signal ΔH and $\beta_\rho + \frac{l_i}{2}$ can be estimated. Using this four probe method it can be shown by rearranging Equations 2.34 and 2.35 that [39]:

$$\Delta H = \frac{a}{4R_0}\left\{\left(\frac{r_m^2}{a^2}-1\right)-2\ln\left(\frac{a}{r_m}\right)\right\}+\frac{\pi r_m^2}{2\mu_0 I_P}\left\{\left\langle B_\theta\right\rangle\left(1-\frac{a^2}{r_m^2}\right)-\left\langle B_\rho\right\rangle\left(1+\frac{a^2}{r_m^2}\right)\right\} \quad \text{m} \quad (2.36)$$

$$\beta_\rho + \frac{l_i}{2} = 1 + \ln\left(\frac{a}{r_m}\right) + \frac{\pi R_0}{\mu_0 I_P}\left\{\left\langle B_\theta\right\rangle + \left\langle B_\rho\right\rangle\right\} \quad (2.37)$$

where $\langle B_\theta \rangle \equiv B_\theta(\theta = 0) - B_\theta(\theta = \pi)$ T and $\langle B_\rho \rangle \equiv B_\rho(\theta = \pi/2) - B_\rho(\theta = 3\pi/2)$ T. The determination of the horizontal plasma position in the STOR-M tokamak is accomplished using this technique. In fact, since this technique is relatively simple, it is often used in tokamaks [39]. In STOR-M, however, this measurement is complicated somewhat by the unique ability of STOR-M to be operated in the A.C. mode.

2.4.1 Normal Mode Operation of STOR-M

Most of the world's tokamaks operate in a pulsed manner. They have a discharge time that lasts anywhere from a few milliseconds in smaller tokamaks like STOR-1M [40] and SINP [41] to several seconds in larger tokamaks such as JET [42] and TFTR [43]. The discharges in these tokamaks all have a relatively long duty cycle, with several minutes between discharges. This pulsed operation is the normal mode of tokamak operation. In the STOR-M tokamak, the normal mode lasts up to 200 ms and has a peak current of about 50 kA (during turbulent heating). The ohmic heating circuit used for the normal mode operation of STOR-M is shown in Figure 2.17. Waveforms of a typical normal mode discharge are shown in Figure 2.18. The normal mode discharge can be broken into three main regions. The first region, the transient region, was discussed in Section 2.2.1 and consists of the breakdown stage and the current ramp-up stage. Following the transient region is the steady state region of the discharge. Relatively constant plasma current and a nearly constant, low loop voltage characterize the steady

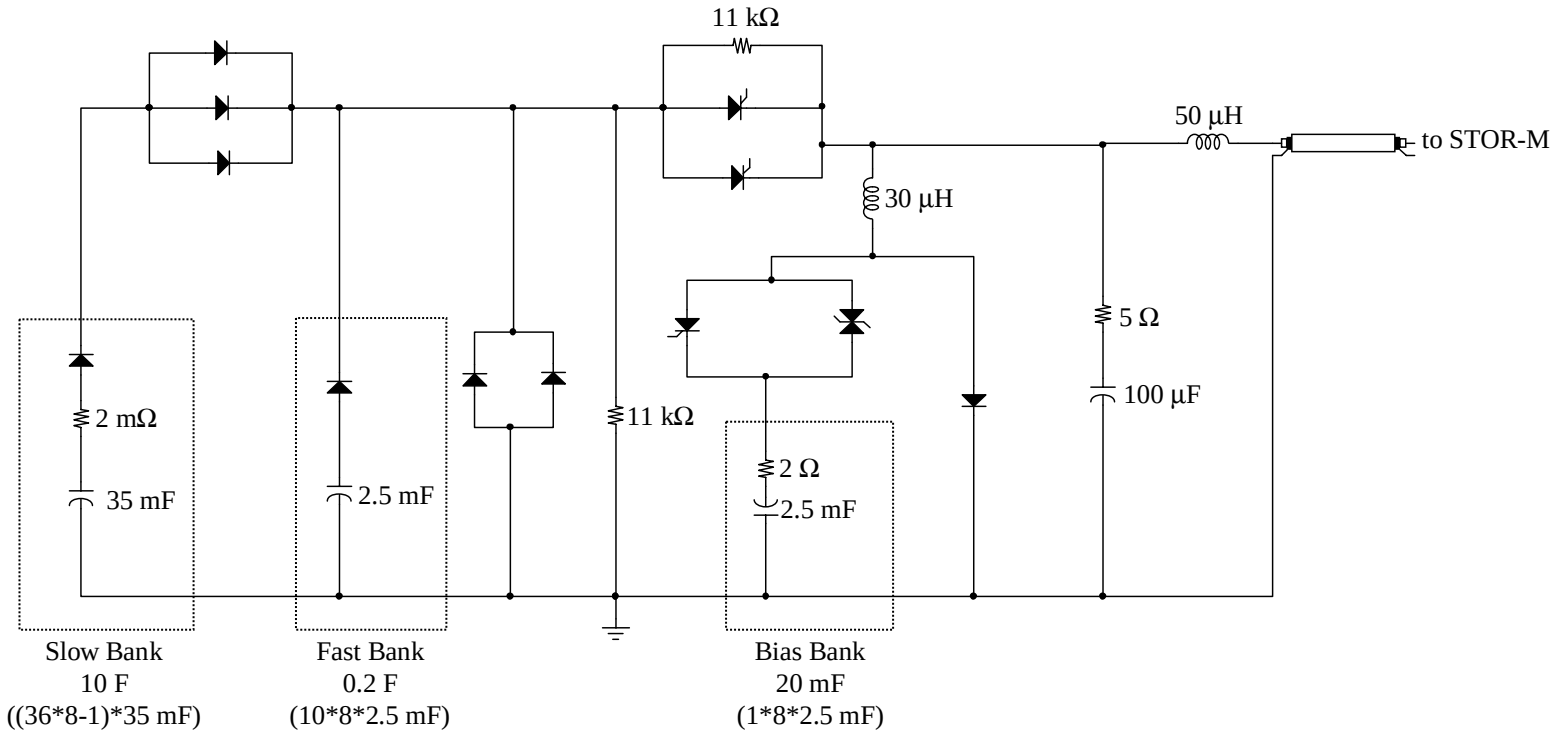

Figure 2.17 Ohmic heating circuit for normal mode operation of STOR-M.

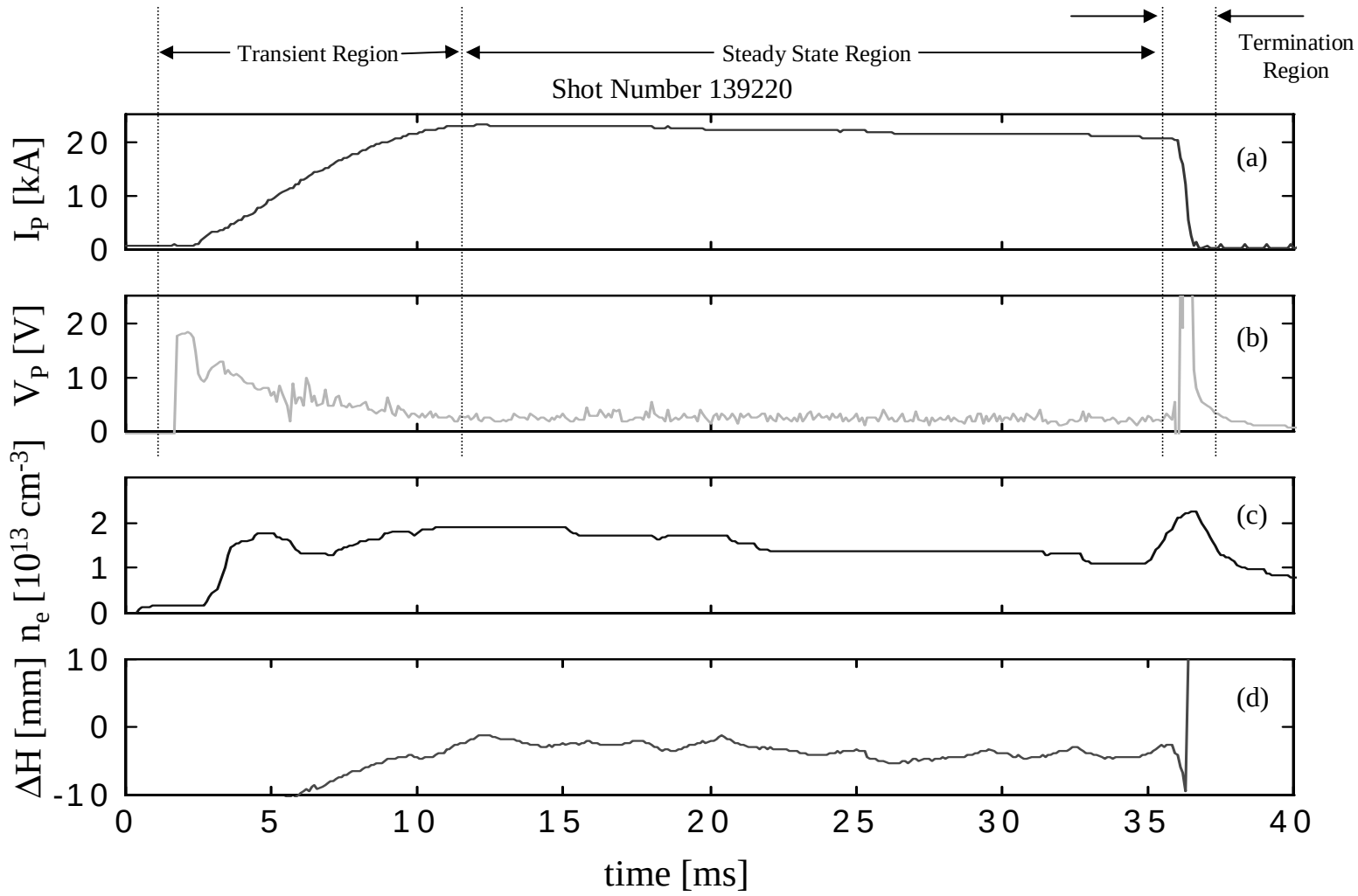

Figure 2.18 Typical parameters of a normal mode STOR-M discharge. [J. Morelli, A. Singh, C. Xiao and A. Hirose, 43rd Annual DPP Meeting of the APS, Oct. 2001.]

state region. The final region of the discharge is the termination region. Typically the normal mode discharge in STOR-M is terminated after about 35 ms by applying a strong gas puffing pulse in order to prevent the production of runaway electrons. The three regions of a typical normal mode discharge are shown in Figure 2.18.

In order to measure the position of the plasma column during the normal mode of operation of STOR-M, instrumentation based on the theory discussed in the previous section was developed by Emaami-Khonsaari et al. [21]. The measurement of $B_\theta(\theta = 0)$, $B_\theta(\theta = \pi)$, $B_\rho(\theta = \pi/2)$, and $B_\rho(\theta = 3\pi/2)$ is accomplished using the magnetic probes and the compensation circuit that was discussed in Section 2.2.2.3. The plasma position signal is determined from these signals using the analog circuit shown in Figure 2.19, where the gains are obtained by rearranging Equation 2.36 as follows:

$$\Delta H = \Delta H_0 + \frac{K_2}{K_3 I_p}\left\{\langle B_\theta \rangle - K_1 \langle B_\rho \rangle\right\} \quad m \tag{2.38}$$

This represents the original horizontal plasma position measurement circuit developed for use with STOR-M.

2.4.2 A.C. Mode Operation of STOR-M

The toroidal plasma current that is necessary for plasma confinement in tokamak devices may be either driven inductively or non-inductively. Inductive current drive is when the plasma current is produced by transformer action, as is the case in STOR-M. Inductive current drive has the advantage of being technologically simple; however, it is restricted by the fact that the flux capability of the transformer is limited. This gives rise to the pulsed nature of tokamaks that defines the normal mode of operation. As a fusion

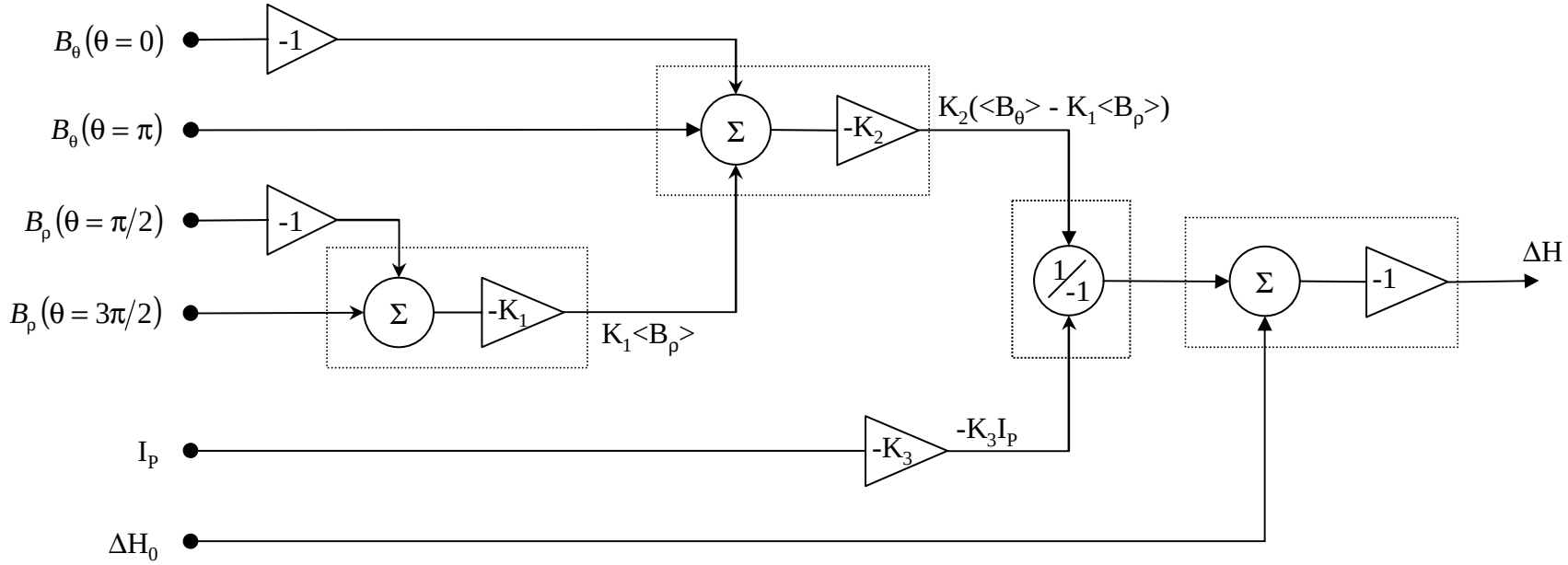

Figure 2.19 Block diagram of the original circuit for determining the horizontal position of the plasma column in STOR-M.

power generator, the pulsed nature of tokamak operation has the disadvantages that in order to maintain continuous electricity production, a large thermal energy storage system is required [44]. While the problems related to inductive current drive can be alleviated using non-inductive current drive techniques [45], the fusion power produced per unit capital investment would likely prohibit such techniques from a commercial tokamak based fusion reactor [46].

In order to reduce the requirements of the thermal storage unit, it is desirable to reduce the downtime of the fusion burn in inductive current drive tokamaks. Using A.C. tokamak operation can significantly reduce this downtime [44,47]. In A.C. tokamak operation there is no need to recharge the transformer flux as after the available flux has been consumed in one direction of plasma current, the current is terminated and smoothly reversed in direction. Thus, in A.C. operation the downtime is reduced to the sum of the plasma current ramp-down time, the dwell time, and the current rise times. The world's first successful demonstration of A.C. tokamak operation was achieved at the Plasma Physics Laboratory at the University of Saskatchewan in the STOR-1M device [48,49]. This demonstration prompted the JET team to perform A.C. operation experiments in order to evaluate this mode of operation under reactor relevant conditions [46]. In JET a full cycle of A.C. operation was achieved with a plasma current of ±2 MA with a period of nearly 30 s and dwell times as short as 50 ms with no apparent degradation of the plasma purity [46]. Thus, A.C. mode operation holds the promise of a tokamak fusion reactor with a minimum plant recirculating power.

Further studies into the A.C. mode of operation have been performed both on the STOR-1M [50] and the STOR-M [51-53] tokamak at the University of Saskatchewan, as

well as at other institutions [54,55]. One of the important issues related to A.C. tokamak operation revolves around the current reversal regime. In order to reduce the dwell time, or to eliminate it altogether, it is necessary to control the position of the plasma during this regime [44,53]. While the exact mechanism(s) that maintain the equilibrium of the plasma during the current reversal regime are not well understood, it is clear that the proper optimization of the horizontal plasma position during this regime is quite important.

2.4.2.1 Requisite Hardware Modifications

In order to produce Alternating Current operation in the STOR-M tokamak it was necessary to modify the ohmic heating circuit. The modified ohmic heating circuit used for 1.5 cycle A.C. operation of STOR-M is shown in Figure 2.20, and waveforms of a typical A.C. mode discharge are shown in Figure 2.21. Furthermore, in order to control the position of the plasma during A.C. operation it is necessary to have a method of accurately measuring it. The plasma position measuring circuit described above was designed only to measure the plasma current during the normal mode. In order for the plasma position in STOR-M to be measured during both the positive and negative half-cycles of A.C. operation, the circuit had to be modified in order to account for both the change in the current direction and the change in the stray fields during each half-cycle. Mitarai et al. [53] developed the modified plasma position measuring circuit, and it is presented in Figure 2.22. In this circuit, ΔH_{0+} is added to ΔH_1 when the plasma current is positive and ΔH_{0-} is added to ΔH_1 when the plasma current is negative. In addition, the absolute value of the plasma current is used in order to prevent misinterpretation of the position signal. Using this circuit, the plasma position signal ΔH_2 will be positive when

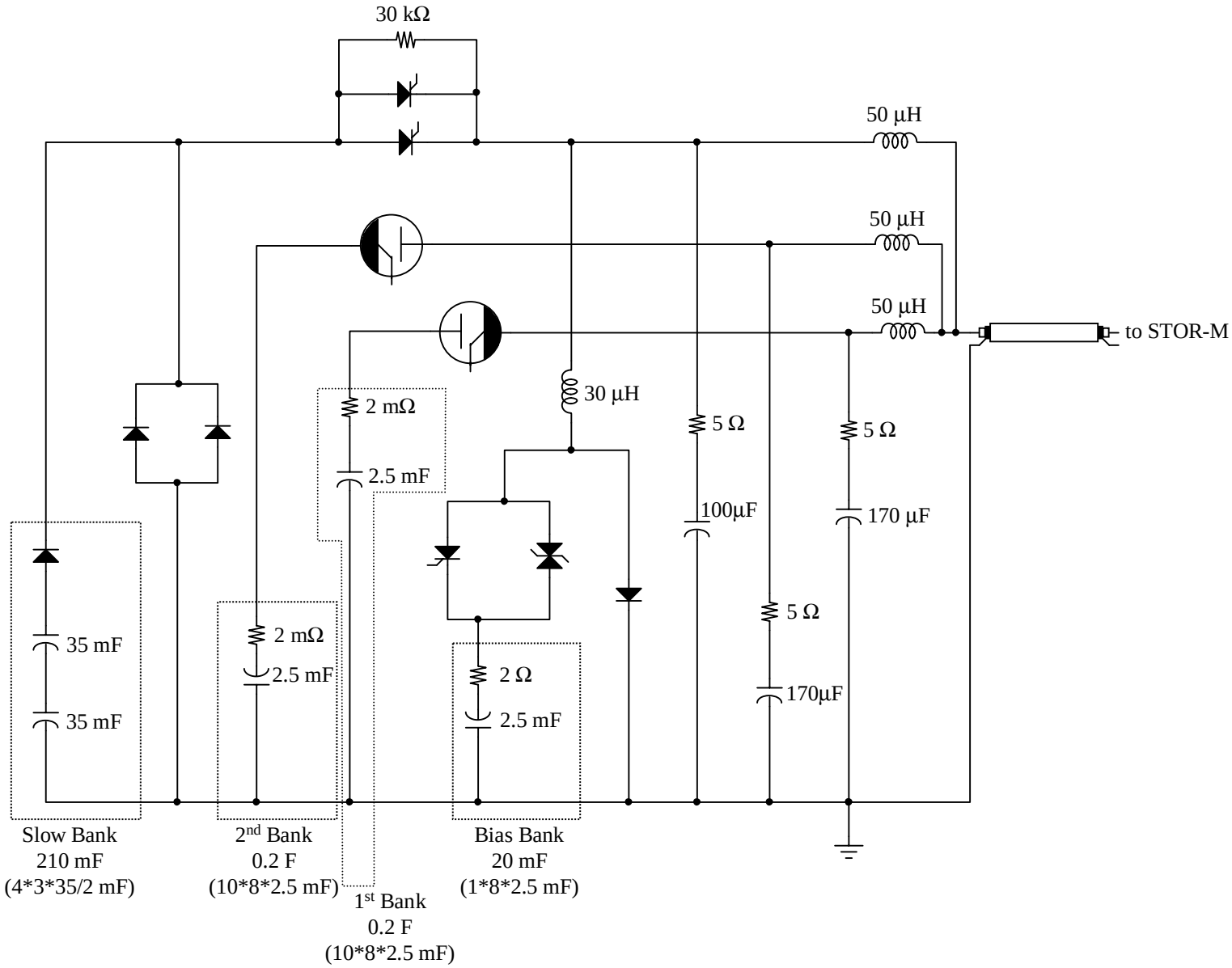

Figure 2.20 Ohmic heating circuit for 1.5 cycle A.C. operation of STOR-M.

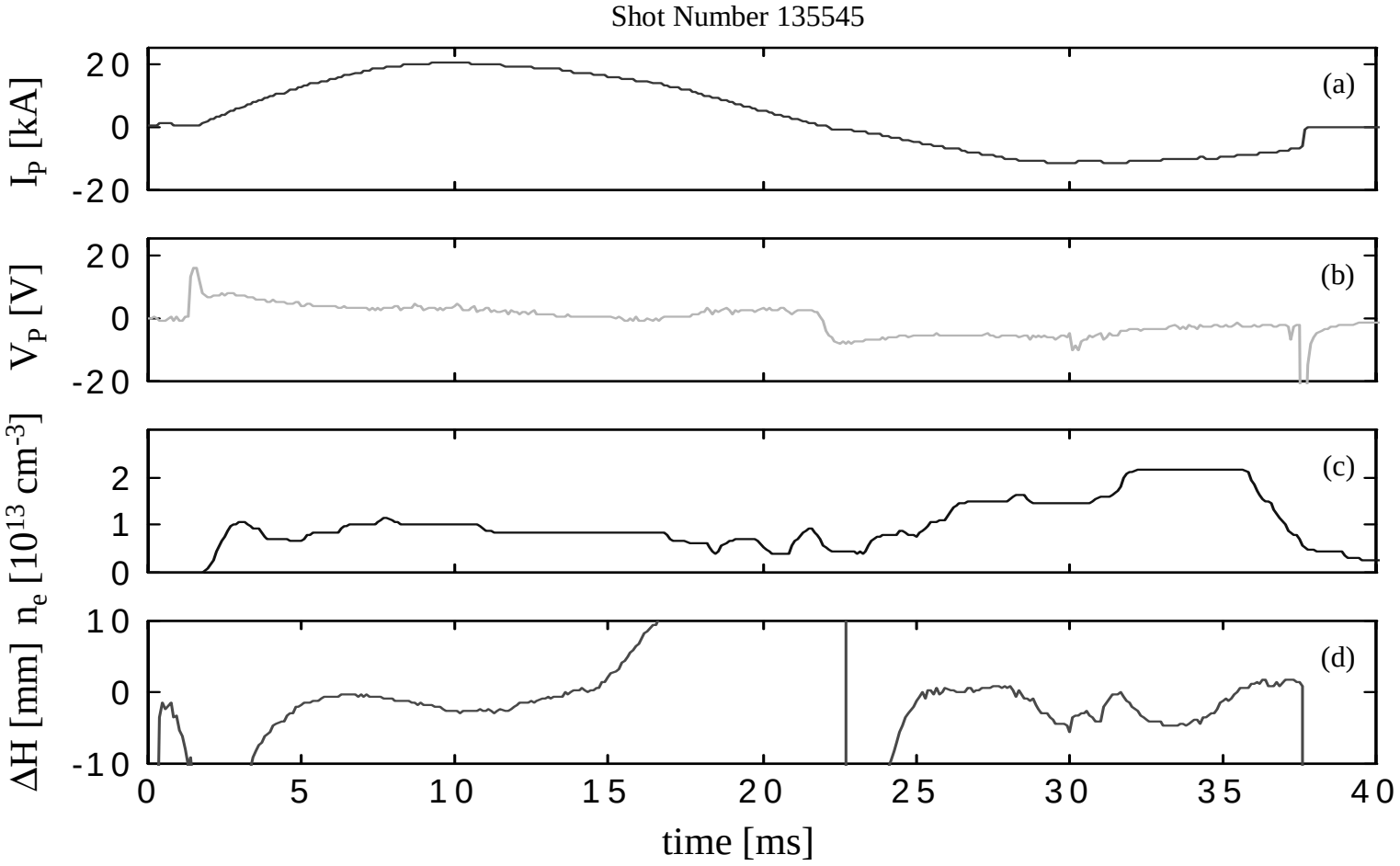

Figure 2.21 Typical parameters of an A.C. mode STOR-M discharge [J. Morelli, A. Singh, C. Xiao and A. Hirose, 43rd Annual DPP Meeting of the APS, Oct. 2001.]. (a) Plasma current, (b) Loop voltage, (c) Electron density and (d) Plasma position.

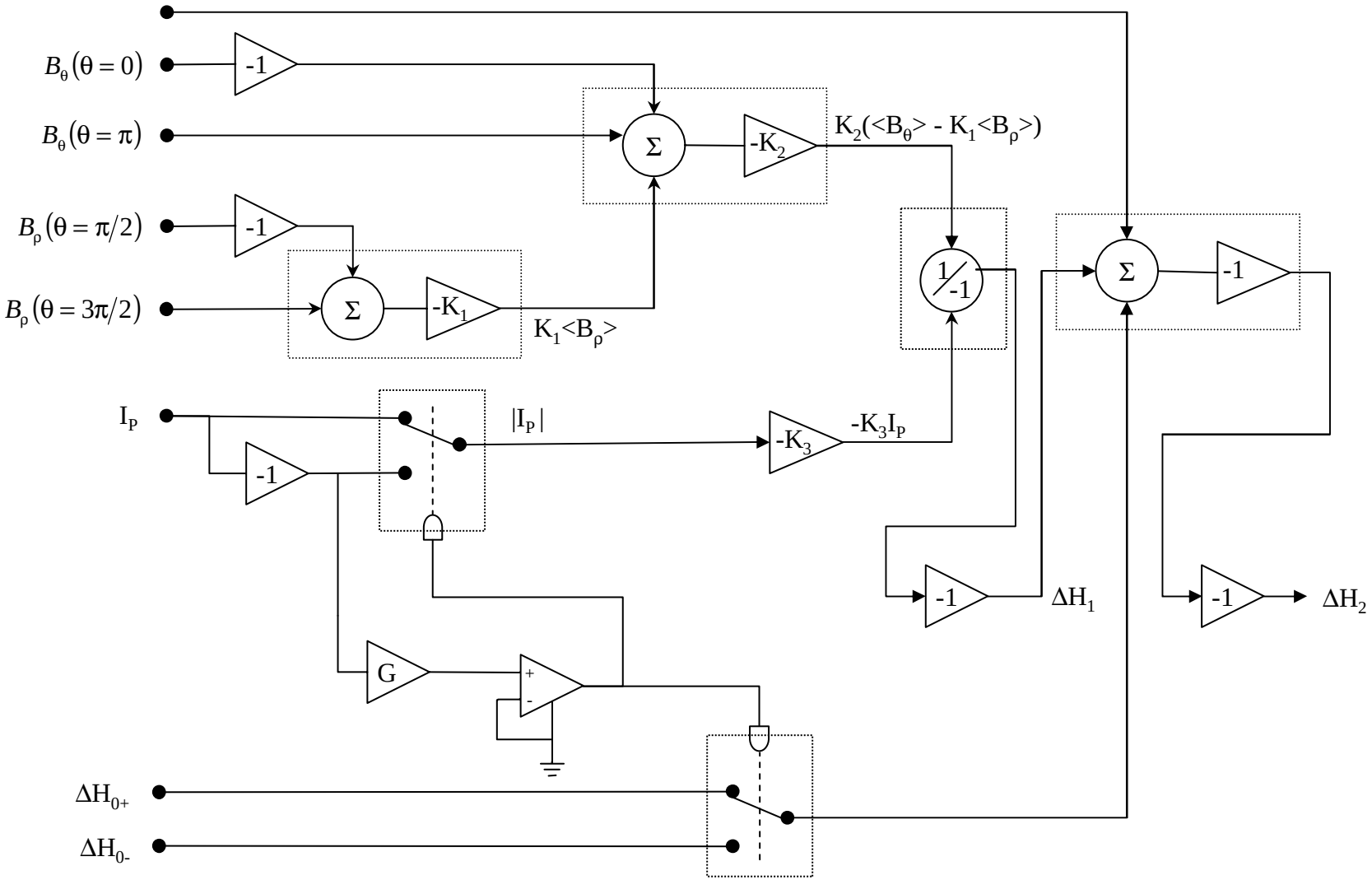

Figure 2.22 Block diagram of the modified circuit for determining the horizontal position of the plasma column in STOR-M.

the plasma column is major radially outward and the plasma current is positive, whereas it will be negative when the plasma column is major radially outward and the plasma current is in the negative direction. This was done because when the plasma current is in the reverse direction, the vertical field required for equilibrium must also be in the reverse direction; in this way, the analog PID plasma position controller can be fooled into providing the correct polarity control signal without also having to be modified.

2.5 Existing Position Control Schemes on Other Tokamaks

The control of the parameters and properties of the plasma column in a tokamak discharge is quite complex. Not only are the properties difficult to measure, they are highly interdependent. Thus, changing or attempting to change one of the plasma parameters results in changes to several of the other plasma parameters. Further complicating the matter is the fact that the system is highly nonlinear, making a high quality controller difficult to design.

In early tokamaks the plasma position was maintained in equilibrium by the use of a conducting discharge chamber. As was shown in Section 2.3.3, the resulting eddy currents are able to maintain the equilibrium position of the plasma. This equilibrium, however, is not stable as once the poloidal magnetic field of the plasma column penetrates the chamber wall the equilibrium is lost. Thus, these early tokamak discharges were limited in duration by the resistive diffusion time of the discharge chamber, which was typically less than a few tens of milliseconds. While technically simple, this configuration is not suitable for use as a commercial reactor, and thus, the use of an externally produced vertical magnetic field is required to stably maintain the position of the plasma column in the major radial direction.

One method of adjusting the externally produced vertical magnetic field is to use an open loop controller. That is, the temporal evolution of the magnitude of the vertical field is pre-programmed based on the expected plasma parameters. While this technique may be suitable for some tokamak discharges, it lacks the ability to take into account unexpected changes in the plasma parameters. In reactor relevant tokamaks, and in fact in most modern tokamaks, the plasma parameters are quite dynamic and may change quite drastically during a discharge. For example, when the STOR-M plasma is turbulently heated, it is common for the plasma current nearly to double in less than a millisecond [14,67]. Clearly, it is quite difficult to pre-program the vertical field for each type of discharge that may be performed in a particular tokamak device. Therefore, it is desirable to have closed loop feedback control of the plasma position.

In addition to being able to measure the position of the plasma within the discharge chamber (a difficult task itself) in order to design a traditional controller, it is necessary to have a model of how the actuators affect the quantity to be controlled; that is, the transfer function of the plant must be known. The transfer function describing plasma position as a function of the applied vertical feedback field can be obtained by linearizing the equations that were obtained in Section 2.3; however, the assumptions required to accomplish this are seldom valid in reality. The result is generally a moderately good controller, which requires considerable fine-tuning in order to provide merely adequate, not optimal, control of the plasma position.

One of the obvious difficulties associated with controlling the position of the plasma within the discharge chamber is that of accurately measuring it. As has been shown above, this requires a system model that has to be simplified before it can be

implemented. Furthermore, it is necessary to have accurate models describing the dynamics of the system being controlled. The controllers implemented to date for controlling the position of the plasma within tokamaks have almost exclusively had a PID structure [68]. The design of these controllers was facilitated by the introduction of assumptions to simplify the physical system model. They employed detailed enough models that the primary physical phenomena were still represented but simple enough to keep the design of the controller straightforward. The systems of Partial Differential Equations (PDEs) describing the system dynamics were decoupled in order that Ordinary Differential Equations (ODEs) were obtained. The system models were often further simplified so that single input single output (SISO) controllers could be employed. Once implemented, these controllers were optimized during tokamak operation. This is the method of controller design that was originally performed for use with the STOR-M tokamak. There has been considerable interest in recent years in evaluating existing tokamak parameter controllers in order that a suitable controller can be designed for the next generation of tokamaks. Consequently, there are several very good literature surveys discussing this subject. Rather than repeating that information here, the reader is referred to references [68-70].

It would be highly desirable to have a plasma position controller that does not require an analytical system model. Artificial Intelligence (AI) based controllers, such as: Artificial Neural Networks (ANNs), Genetic Algorithms (Gas), Fuzzy Logic Controllers, and Expert Systems offer this feature. In fact, one of the primary goals of this thesis is to determine if equivalent or better control over tokamak parameters can be obtained using a controller that does not require a system model; that is a fuzzy

controller. To date, the application of AI based controllers to fusion plasmas has been quite limited. This is quite likely to change in the near future, as recently, the Office of Science of the United States Department of Energy "has asked the Fusion Energy Sciences Advisory Committee (FESAC) to assist in defining a major new initiative … recognizing the programmatic importance of developing predictive capabilities for fusion systems, the goal of the initiative would be to improve substantially the capabilities for integrated simulation of fusion systems based on verified and validated models of the underlying physical processes". For a discussion of the plasma controllers being proposed for use with the next generation of tokamaks the reader is referred to references [71-74].

The application of AI based control techniques is already being considered for fusion plasma. For example, the Large Helical Device (LHD) has been designed with the goal of evaluating fuzzy logic controllers and ANN controllers for the feedback control of plasma current, position, and cross-sectional shape [76-78]. In addition, recently, an ANN has been developed for fast, reliable plasma position control in KSTAR tokamak [79,80]. The ANN that was developed was applied to a simulation of the KSTAR plasma, and was successfully demonstrated to predict the plasma position , thus, indicating that ANNs may be capable of serving as a reliable plasma position control system. Certainly the application of AI based techniques such as ANNs and fuzzy logic controllers to the control of fusion plasma merits investigation. It was with this in mind that the research described herein was performed.

Fuzzy logic controllers are known for their ability to provide a high quality of control over systems that are both nonlinear and time varying [84]. Fuzzy controllers

have recently been applied to several electrical power systems control problems. For example the Electrical Power Research Institute (EPRI) Inc. holds a patent for a "Steam Turbine Fuzzy Logic Cyclic Control Method and Apparatus Therefor" [92]. In addition to their application to electrical power generation, fuzzy logic controllers have also been applied to the optimal distribution of electric power [93,94]. Given the success of fuzzy logic controllers to the control of these nonlinear, time varying electrical power systems problems, it is natural that the suitability of fuzzy logic controllers to fusion plasmas be investigated.

2.6 Design Requirements for STOR-M Plasma Position Controller

In designing the fuzzy logic based plasma position controller for use with the STOR-M tokamak, several performance criteria had to be met. First, and most importantly, the fuzzy logic based controller had to be able to reliably maintain the position of the plasma column within ±5 mm from the equilibrium position. Furthermore, the controller had to be capable of providing near optimal control in all modes of STOR-M operation, especially during transient conditions such as that which occurs during A.C. operation. As a reference, the fuzzy logic based controller should be able to provide a quality plasma column position control within STOR-M that is as good as, or better than, that provided by the original analog PID controller.

Based on the author's experience with the STOR-M tokamak, it was decided that the controller should be capable of producing a new control decision at the most every 800 μs, but it was felt that anything faster than 200 μs was not necessary. It should be pointed out here that the rise time of the vertical feedback current driver circuit ranges from 100 μs to a few milliseconds depending on the current demand. A constraint that

was imposed on the design of the fuzzy controller was that it had to interface with the existing hardware without permanently changing it. That is, any hardware changes that were made had to be transparent and easily reversible. This restriction resulted in the development of slightly awkward actuator design modifications, as will be discussed in the next chapter.

The process of designing a fuzzy logic based controller for maintaining the position of the plasma within the STOR-M tokamak began with the modifications to the hardware of the existing analog PID controller. As a part of validating the modifications, the modified analog PID controller was optimized in order to control the position of the plasma during A.C. mode STOR-M tokamak operation. Aside from verifying the hardware modifications, this stage of the development permitted the modified controller to be evaluated and its performance compared with its effectiveness before the modifications were made. The process followed during this stage of the development of the plasma position controller will be discussed in detail in Chapter 3.

2.7 Summary

In this chapter, the issue of plasma confinement within a tokamak device has been addressed. The STOR-M tokamak has been presented, and its primary operating parameters and diagnostic complement have been introduced. The forces acting on the plasma column in the major radial direction were discussed in detail. This led to the consideration of force balance in the major radial direction. From this, it became apparent that in order to maintain the horizontal position of the plasma column stably within a tokamak device it is nec essary to apply an externally generated, dynamic, vertical magnetic field. The modes of operation of the STOR-M tokamak were discussed

next, and the unique requirements that they impose on the plasma position measurement and control were considered. This was followed by a look at the existing position control schemes that have been implemented on other tokamaks, and a discussion of future AI based control schemes. Finally, the design requirements of the fuzzy logic based plasma position controller developed for use with the STOR-M tokamak were presented.

3. ANALOG PID CONTROLLER

3.1 Overview

Traditional automatic feedback controllers operate in a simple manner. They compare the actual value of some property of the system to be controlled (the plant) with the desired value for that property. The difference between these two values is computed and called the error signal. The controller then produces a control signal that is suitable to reduce the error signal to zero, or to less than some acceptable value. The block diagram of a typical analog feedback control system is shown in Figure 3.1.

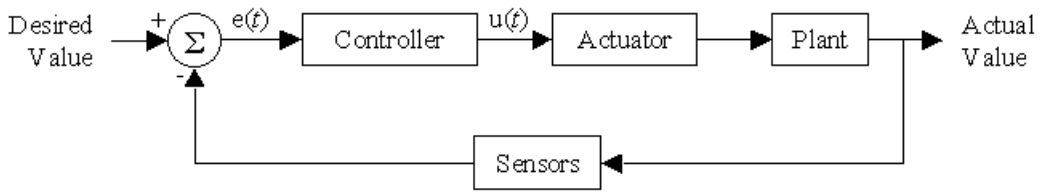

Figure 3.1 A typical analog control system.

There are various techniques by which the control signal can be produced. The simplest of the traditional analog control techniques is that the controller simply produces a control signal that is Proportional to the error signal. A proportional controller has the advantage that it is simple, and thus, easy to implement; however, it is limited in its ability to control a system. Furthermore, increasing the gain of a proportional controller reduces the rise time (the time required to respond to a sudden change in the error signal), and also reduces, but never eliminates, the steady state error. A related drawback with proportional controllers is that they may require a long time to converge to a stable control signal for a given set of system parameters, and while settling down, a

proportional controller oscillates around the steady state control signal. It should also be mentioned that the magnitude of the overshoot during this transient period might be quite large for a purely proportional controller.

For a system where the transient performance of the proportional controller alone is not satisfactory, marked improvement can be obtained by adding Derivative control. As its name implies, a derivative controller produces a control signal that is proportional to the time rate of change (derivative) of the error signal. When combined with a proportional controller, it is commonly referred to as a PD controller, and can be optimized to have an improved transient response over pure proportional control. The PD controller, while offering improved transient performance, still suffers from a less than ideal steady state performance; that is, the PD controller, like the proportional controller, may have an unacceptably high error signal during the steady state for a given set of system parameters.

In order to reduce the steady state error to zero, or to a value that is smaller than some acceptable value, an Integral controller may be used. Combining an integral controller with a PD controller gives a PID control. The PID controller is probably the most versatile and most commonly used of the traditional analog controllers. By varying the relative weighting of the proportional, integral and differential contributions to the control signal (that is by adjusting their respective signal gain), an optimal controller may be obtained. The block diagram of a traditional analog PID controller is shown in Figure 3.2. A PID controller is the type of controller that was originally implemented for the purpose of controlling the horizontal position of the plasma within the STOR-M

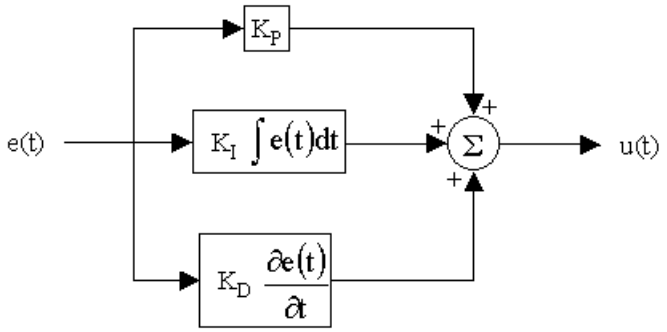

Figure 3.2 An analog Proportional-Integral-Derivative (PID) controller.

tokamak, and one of the main objectives of the work presented in this thesis was to improve the performance of this controller.

3.2 Analog PID Position Controller

Various design techniques for PID controllers are well established as control systems engineers have studied these systems for decades. References [56-58] provide very good information and analysis of these controllers, although there are countless other references from which to choose. In order to use a PID controller most effectively, consideration must be given to the system to be controlled, the actuators that are to affect the control, and the sensors that will detect the behaviour of the system being controlled. Each of these subsystems is represented by a transfer function, and these transfer functions can be substituted into the respective blocks of Figure 3.1. In this way, a complete model of the entire system is obtained. The modelling of each of these subsystems, that is, the determination of their appropriate transfer functions, will be discussed in the next section.

Once the system model has been obtained, the analog PID controller must be optimized. In essence, the optimal design of a PID controller involves the determination of the values of the controller gains, K_P, K_I and K_D, such that the properties of the plant that are to be controlled are controlled as desired. There are several well-established

techniques for accomplishing this task such as the "root locus" technique or the "state-space" approach, and again the author refers the reader to References [56-58] for further information on these approaches. It should also be pointed out that when designing a controller, one must not be only concerned with the system performance but also with the system stability.

3.2.1 System Modeling

In order to optimally design a PID controller, one must first have a model of the system to be controlled; as mentioned above, this includes not only the plant but also the sensors and the actuators. Typically the determination of the respective models (transfer functions) requires the linearization of the behaviour of each subsystem. From the discussion in Chapter 2 it should be evident that for a system such as a tokamak, this is not a trivial process. An additional point that must be mentioned is that a PID controller is optimized based on a particular system model. If the parameters of the system change, the PID controller will no longer be optimally configured. Thus, the optimal design of a PID controller requires that the system being controlled is both linear and time-invariant; that is, the system must be a Linear Time-Invariant (LTI) system.

Obtaining a complete system model for a complicated device such as the STOR-M tokamak is extremely difficult. Making several simplifying approximations, however, can make the task manageable. In the design of the existing PID controller used to control the position of the plasma column in STOR-M two major assumptions were first made. The first assumption that was made in the design of the existing PID controller used for STOR-M is that the system is in fact a time-invariant system. This approximation is reasonable during the steady state of the normal mode of operation;

however, it fails completely during A.C. operation. Thus, the existing analog controller that had been previously designed is only suitable for use during normal mode STOR-M operation. It should be pointed out, however, that the designer of the existing PID controller did not have A.C. mode STOR-M operation in mind while designing the controller. The second assumpti on that was made in the design of the existing PID controller was that the system could be modelled by a set of linear ordinary differential equations. This assumption is also not strictly valid for STOR-M, but if one restricts the analysis to small perturbations around the equilibrium, then this approximation becomes less unreasonable. Using these two approximations, the system transfer functions for STOR-M were obtained by Emaami-Khonsaari [15], and it was based on this analysis that the existing analog PID controller was developed. The reader is referred to References [15,21] for a complete description of the system modelling that was performed in the design of the existing PID controller.

The existing analog PID controller was designed and implemented based on the analysis of the major radial force equilibrium presented in Chapter 2, and the approximation that for the STOR-M tokamak they, along with the sensors and actuators could be treated as an LTI system. Since this controller was based on only partially valid approximations, its performance is not very good unless the controller gains are empirically tuned. This is a rather tedious and time-consuming process, often requiring several weeks. The problem of the control of the horizontal plasma position in STOR-M is further compounded by the fact that the existing analog controller is only capable of providing optimal control (or near optimal control) when the system parameters are near their equilibrium values. Thus, the problem arises as to how to arrive at the equilibrium

with a controller that is incapable of providing good control away from the equilibrium. Using a signal generator to pre-program the control signal during the initial stages of the STOR-M discharge initially solved this problem. With this technique, the PID controller would be switched on once the discharge reached the steady state.

3.2.2 Existing Hardware Implementation

The original analog PID controller circuit is shown in Figure 3.3 and Figure 3.4. This controller has a single input and a single output. The input, the plasma position signal, is determined from the circuit that was described in Section 2.4. The first stage of the PID controller calculates the error signal by comparing the plasma position signal with the "Set Point" (the desired valued). The REF input is not connected. The error signal is held at zero at all times except for a 100-ms control window during the discharge. This window is delayed from the positive going edge of the trigger signal by a 4-ms delay. During the control window the error signal is split into three paths. The first path multiplies the error signal by the proportional gain. The proportional gain can be adjusted by a ten-turn potentiometer to take any value in the range: $-1.7 \leq K_P \leq 0.0$.

The second path performs the integration and has the following transfer function:

$$\frac{V_I}{E} = \frac{K_I}{\tau_I s + 1} \tag{3.1}$$

That is, the output is essentially given by the average of the input signal taken over the time τ_I [59]. This differs from pure integration in that an integrator ideally averages over an infinite amount of time. This circuit implementation has the advantage, however, of eliminating or reducing the output drift voltage offset that results from both the input offset voltage and the input bias current of the active integrator. The integrator also features a reset that is active outside of the control window. In fact, the integrator is reset

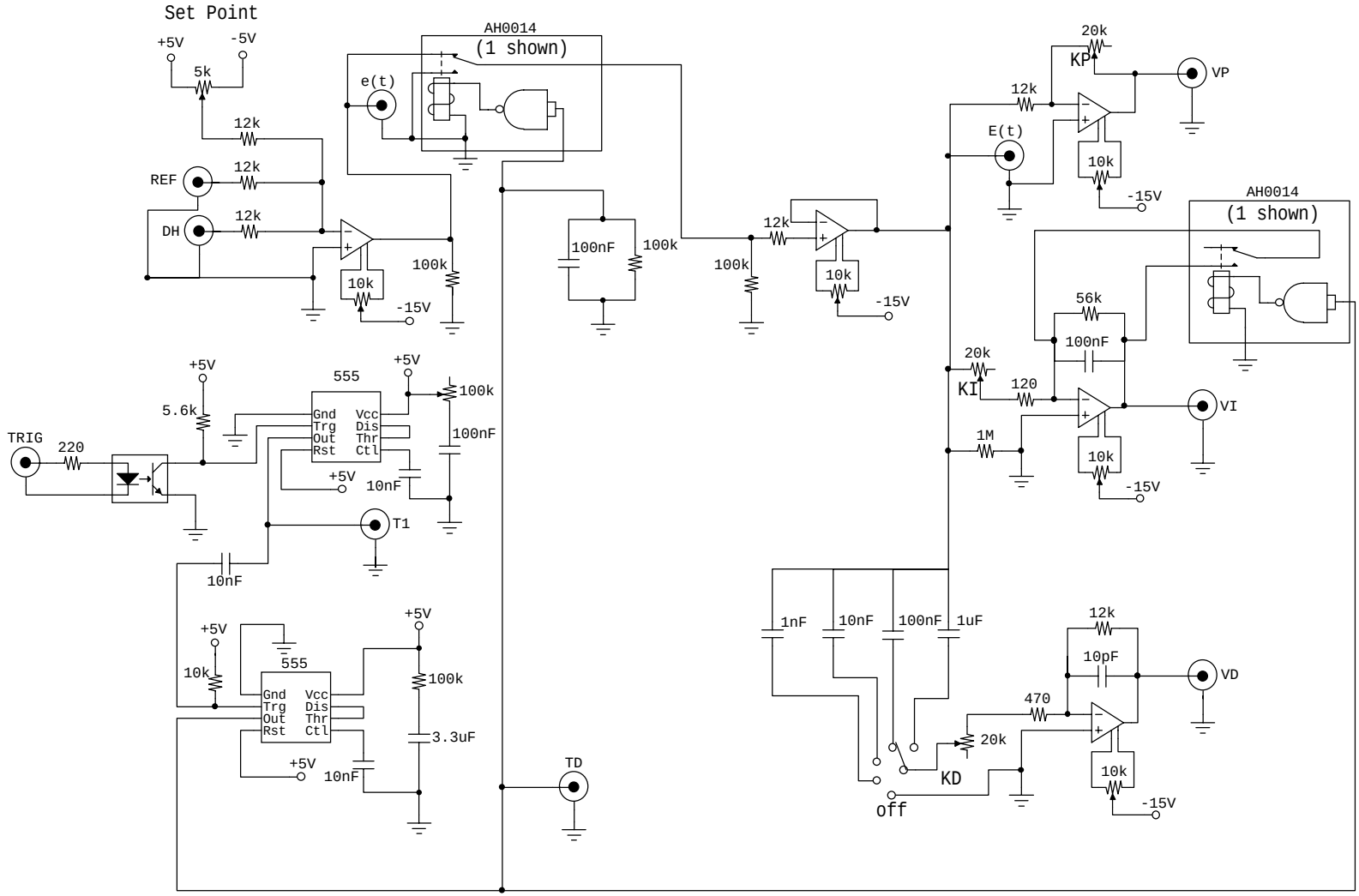

Figure 3.3 Original PID controller – input stage.

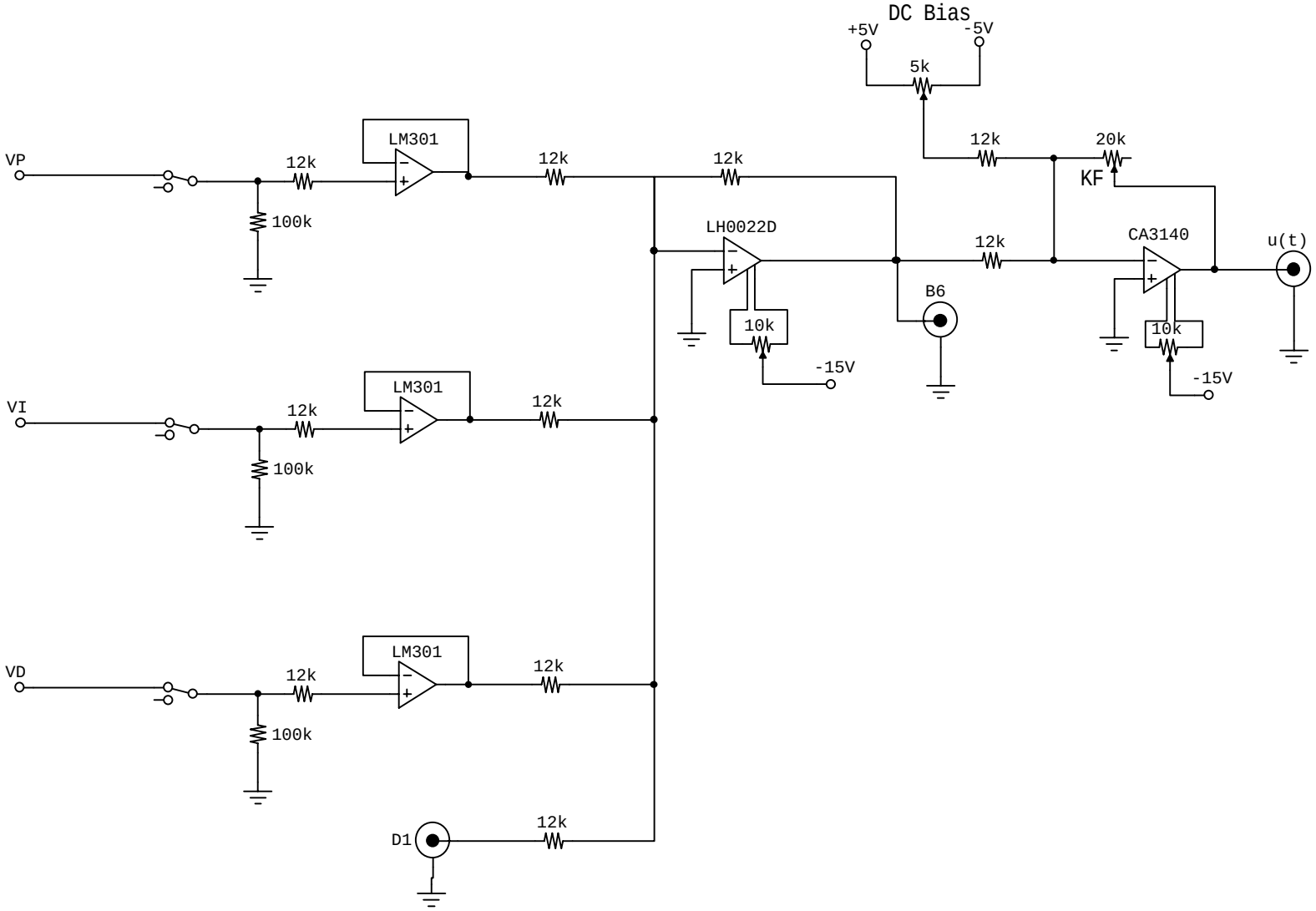

Figure 3.4 Original PID controller – summed output stage.

whenever the T_D signal is low. Like the proportional gain, the integral gain of the PID controller can be adjusted by a ten-turn potentiometer over the range: $-467 \leq K_I \leq -2.7$. The time constant of this integrator is: $\tau_I = 5.6$ ms.

The third path performs the differentiation, and has the following transfer function.

$$\frac{V_D}{E} = \frac{K_D s}{(\tau_{D1} s + 1)(\tau_{D2} s + 1)} \tag{3.2}$$

Note that this modified form of differentiation is used in order to help reduce the sensitivity to noise. This modified form of differentiation reduces to ideal differentiation in the case where τ_{D1} and τ_{D2} are much smaller than the discharge time, as they may then be neglected. Both the gain and the time constant of the differential branch can be adjusted. The gain can only take the following values: $K_D = -12 \times [10^{-3}, 10^{-4}, 10^{-5}, 10^{-6}]$. The time constant, τ_{D1}, can be adjusted using a ten-turn potentiometer over the range: $(0.47 \text{ ms} \leq \tau_{D1} \leq 20 \text{ ms}) \times [10^{0}, 10^{-1}, 10^{-2}, 10^{-3}]$ depending on the value of the differential gain. The time constant, τ_{D2}, is fixed at 0.12 μs.

The proportional, integral and differential signals are then passed through unity gain buffers before being summed by an active mixer. In order to facilitate the pre-programming of the initial stages of the discharge, an additional input to the mixer is provided; this input is used to apply an externally generated waveform, as discussed earlier. Finally, the summed signal is passed to a variable gain active mixer where it is added to a DC Bias level. Appropriate adjustment of the DC Bias level facilitates the breakdown of the hydrogen gas filling the discharge chamber by helping to compensate for stray fields. The gain of this active mixer can be adjusted by a ten-turn potentiometer

from: $-4.2 \leq K_F \leq 0.0$. The resulting signal is the control signal, u(t), and is passed on to the actuator circuit.

The actuator circuit uses a bipolar, 30 V, battery bank and a transistor array designed to supply ±800 A in 10 A steps. This system was proposed in Reference [15], and the reader is referred to that reference for a complete description of the circuit implementation. The transfer function of this actuator is approximately given by [15] as:

$$G_a = \frac{I_{VF}}{U} \approx \frac{K_a}{(1+\tau_a s)} \quad AV^{-1} \tag{3.3}$$

Equation 3.3 appears to represent a LTI system; however when one considers that the response time of the actuator, τ_a, is approximately given by [15] as:

$$\tau_a \approx \frac{L_{VF}}{R_{VF} + \frac{R_{eff}}{n}} \quad s \tag{3.4}$$

where L_{VF} and R_{VF} are respectively the inductance and resistance of the vertical feedback windings, R_{eff} is the effective load resistance, and n is the number of transistors that are switched on at a particular instant, then it becomes clear that this is only an LTI system if τ_a along with the relevant circuit inductance and resistances are assumed to be constant. Figure 3.5 shows the actual response of the actuator circuit for different magnitudes of a square wave control signal, u(t). It should also be no ticed from Figure 3.5 that the time constant of the actuator circuit is much shorter during the decay phase than it is during the storage phase for this actuator, another nonlinearity that is difficult to model and was, therefore, neglected in favour of obtaining the simple model described by Equation 3.3. It should also be pointed out that given the non-constant and relatively long rise time of the actuator circuit, as indicated in Figure 3.5, any digital controller designed for use

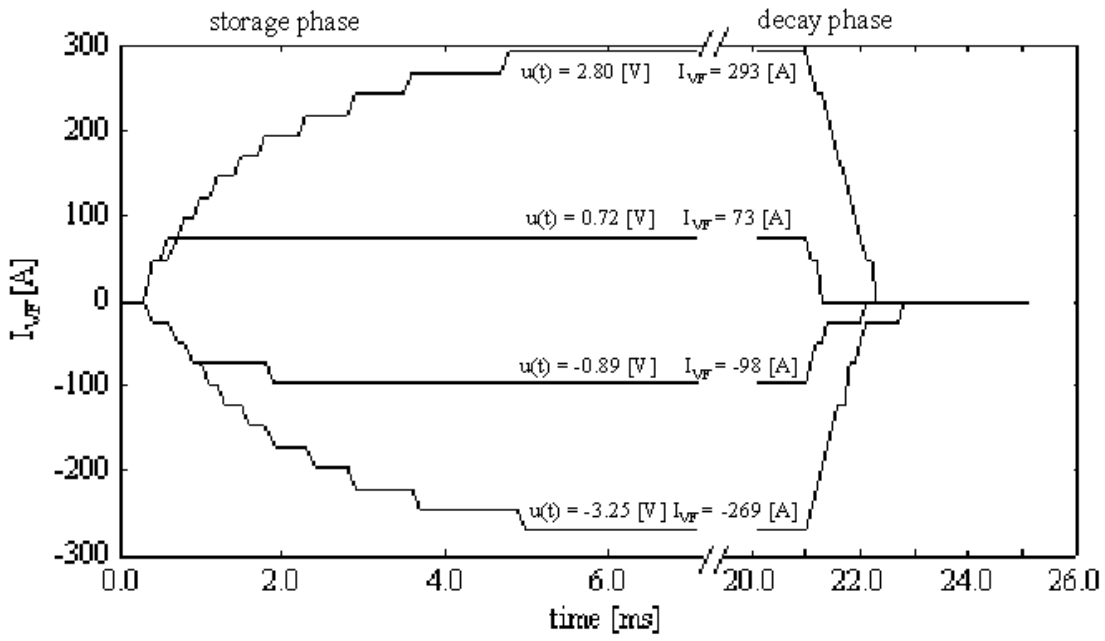

Figure 3.5 Evolution of the vertical feedback current, I_{VF}, for various values of the magnitude of a square wave control signal, u(t).

with STOR-M will be capable of providing a good quality of control over the horizontal position of the plasma column in STOR-M as long as it can arrive at a control decision faster than the actuator can implement it; hence, the choice of 800 μs was made as the maximum time permitted between successive control decisions as outlined in Section 2.6. Furthermore, it should be pointed out that the actuator circuit is not actually capable of supplying ±800 A; rather, it saturates at around $I_{VF} \approx \pm 350$ A. This represents another nonlinearity of the circuit that was not included in the model for the sake of simplifying the design of the existing analog PID controller.

Given the difficulty associated with modelling this relatively simple actuator device, it is not surprising that obtaining a practical model of a complicated device, such as the STOR-M tokamak itself, or even the control of the horizontal position of the plasma column within the STOR-M tokamak, is a very difficult task. Clearly, if a high

quality controller could be developed that would not rely upon a model of the system under control, then this controller would represent a great advantage over the traditional analog PID controllers. A fuzzy logic based controller is such a controller; this is the main motivation for the research presented in this thesis. For if a fuzzy controller is capable of providing a high quality of control over the horizontal position of the plasma column in the STOR-M tokamak, then it might be suitable for application to control other tokamak discharge parameters, and perhaps, more importantly, a fuzzy controller might be suitable for use on larger, reactor relevant, tokamak devices.

3.2.3 Requisite Hardware Modifications

When STOR-M was first configured for 1.5 cycle, A.C. operation, the ability to add up to two more externally generated signals was incorporated into the PID controller circuit. These signals were necessary in order to account for the differences in the stray fields produced during each of the three half cycles. These three, externally generated stray field compensating signals were each produced using a separate signal generator. These signal generators were gated and set to produce a square wave pulse. In order to obtain a good discharge, the delay, width, and magnitude of each of the three pulses had to be optimized. It was decided that this process could be made easier if a single arbitrary signal generator was developed to replace the three separate signal generators.

The author produced an Arbitrary Signal Generator (ASG) using Borland Turbo C++ version 3.0 and the PCL-711B data acquisition card (to be described in Section 4.3.1). In order to interface this ASG with the existing PID controller, several hardware modifications were required. The ASG was designed in such a way that not only was it capable of outputting an arbitrary waveform, but it also had a VETO signal which could

be used to override the output of the PID controller by forcing the T_D signal to be low. As mentioned, whenever the T_D signal is low, the integrator of the PID controller is reset. In this way the arbitrary waveform can either be added to or completely replace the PID control signal, a feature that was not present in the existing PID controller circuit. The modified PID control circuit is shown in Figure 3.6 and Figure 3.7. It should be pointed out that three undergraduate students performed the modifications made to the PID controller as part of the EP 425.3 course offered at the University of Saskatchewan. These modifications were reported in [60] and are repeated here for completeness. This work was guided in part by the author.

The arbitrary waveform was passed through the final stages of the PID controller by using the original external signal input connection. Appropriate logic was implemented so that the VETO signal produced by the ASG could disable the PID controller at any time during the discharge. As can be seen from Figure 3.6, the PID controller only operates when the VETO signal is low and T_D is simultaneously high. Figure 3.8 shows the time evolution of the relevant signals of the modified PID controller. From Figures 3.3, 3.4, 3.6 and 3.7 it should also be clear that the modifications made to the existing PID controller were made in such a way that the modifications could be completely reversed simply by throwing a switch: the mode switch. Furthermore, these hardware modifications permit the implementation of any type of digital control algorithm simply by replacing the ASG program with an appropriate control algorithm. In the case of the research presented in this thesis, a fuzzy logic based controller was implemented and will be discussed in detail in Chapter 4.

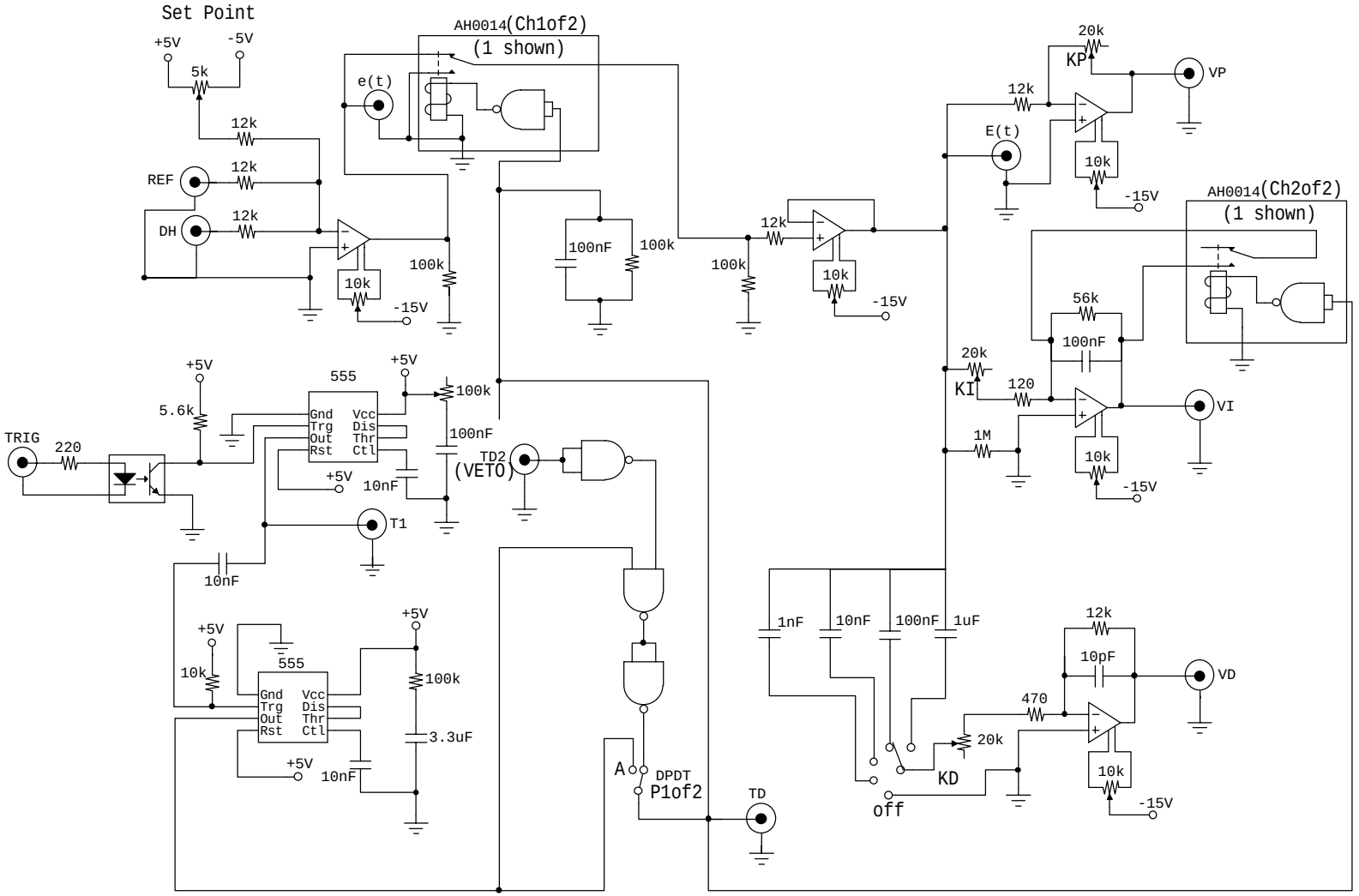

Figure 3.6 Modified PID controller – input stage.

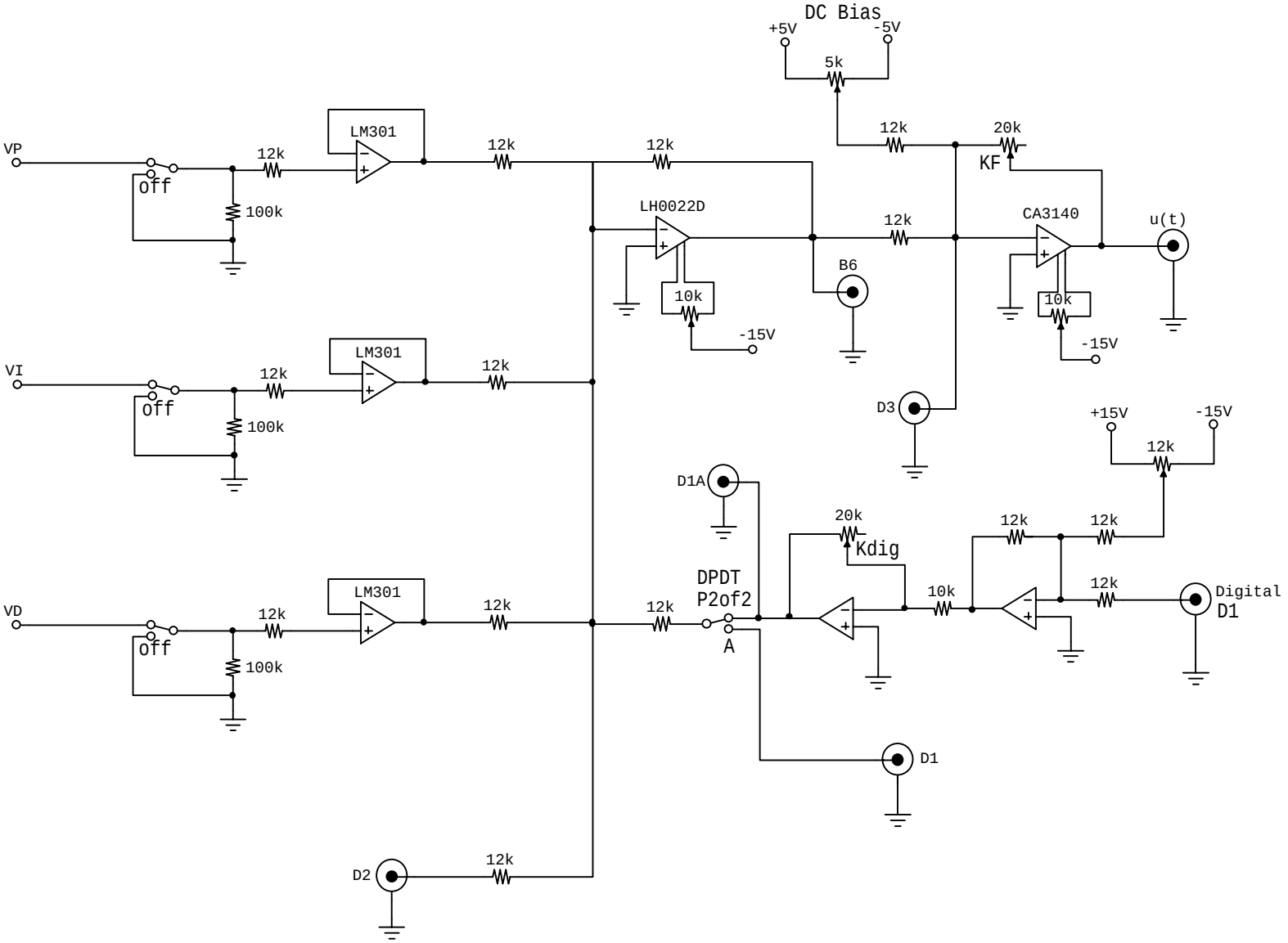

Figure 3.7 Modified PID controller – summed output stage.

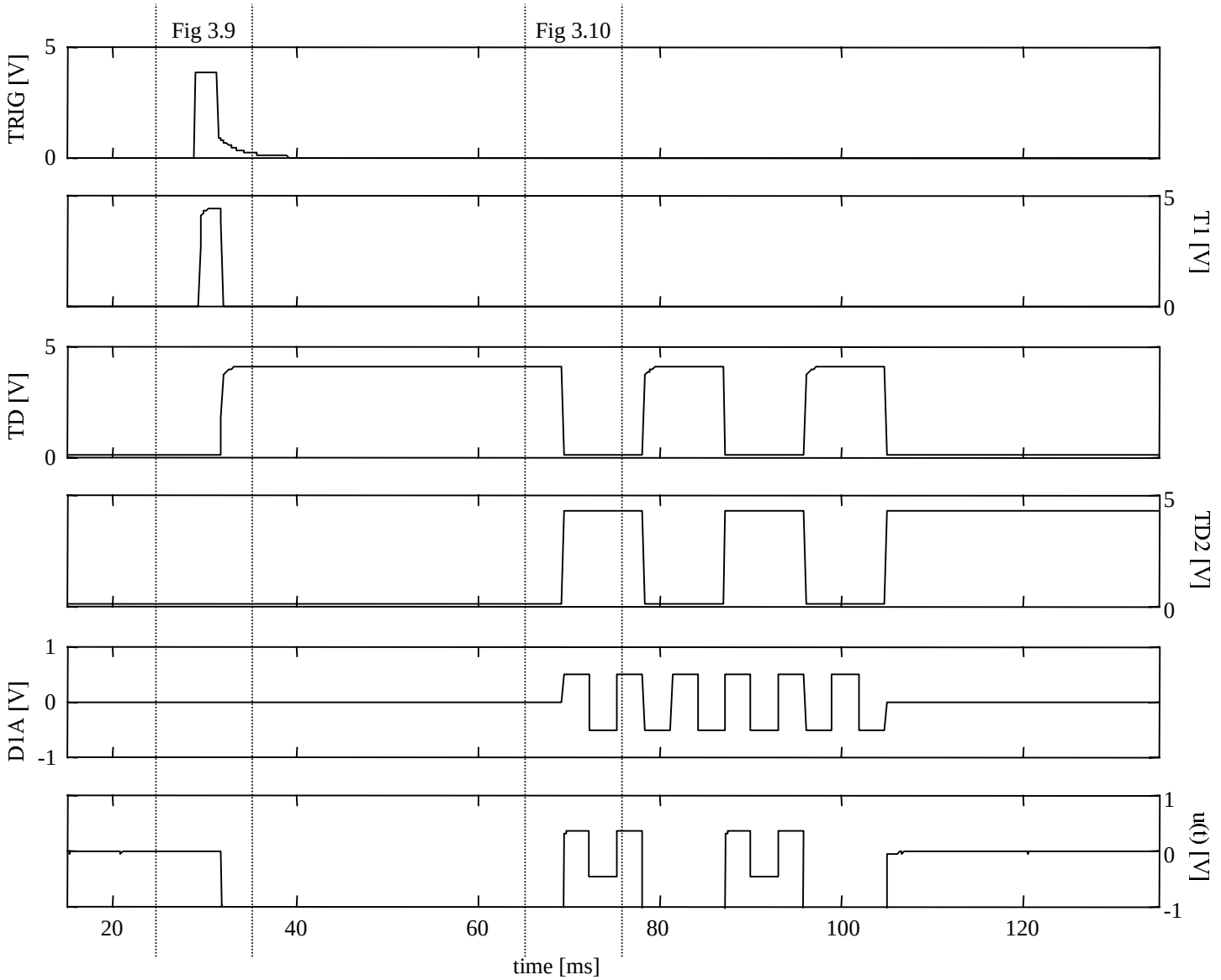

Figure 3.8 Temporal evolution of the modified controller signals.

3.3 Performance Validation

The performance of the modified PID controller was verified offline using the ASG program written by the author. During this round of testing the performance of both the modified hardware and the PCL-711B itself were verified. The modified PID controller was installed in a NIM crate, and the various signal lines were connected to it. The VETO signal was connected to channel 14 of the digital output port of the PCL-711B, and the Digital D1 signal was connected to the digital to analog converter port of the PCL-711B. The ASG program operated on a PC 486 – 66 MHz, in which the PCL-711B was installed.

With the mode switch set for digital, the gains and the offsets of the modified PID controller were adjusted and the output calibrated. The analog output of the PCL-711B varies from 0 V to 10 V; thus, the Digital Offset had to be adjusted in order to permit D1A to vary from –5 V to 5 V. This was accomplished by setting the PCL-711B to output 5 V and adjusting the Digital Offset until the D1A signal was 0.00 V. The digital gain, K_{dig}, was then adjusted such that D1A became 5.00 V when the PCL-711B was set to output 10 V. After this adjustment, it was verified that D1A was still 0.00 V when the PCL-711B was set to output 5 V and also that D1A was equal to –5.00 V when the PCL-711B was set to output 0 V. The pacer clock of the PCL-711B data acquisition card was set at 25 kHz. The ASG program was triggered by a trigger signal connected to channel 0 of the PCL-711B; the triggering of the PCL-711B will be discussed further in Section 4.3.1.

The next step of the validation of the performance of the modified PID controller was performed in order to ensure that the logic associated with the VETO signal was

working well and also to ensure that the ASG program did in fact function as intended. With this in mind the ASG program was set to override the PID controller after a delay of about 40 ms from the time that the modified PID controller was triggered. After this delay, the VETO signal would then alternate between high and low, staying in each state for about 6 ms. During this time, the ASG program was set to output a bipolar square wave train having a magnitude of 0.5 V, a period of 2 ms, and a duty cycle of 50%. The relevant signals of the modified PID controller are shown in Figure 3.8. Figure 3.9 shows signals during the time interval just before, during, and just after the arrival of the trigger pulse.

In Figures 3.8 and 3.9 it can be seen that the modified PID controller behaves as designed. The delay T1 goes high 677.6 μs after the trigger to the modified PID controller, TRIG, goes high. The signal T_D (enable/reset) goes high 6.8 μs from the falling edge of T1. Note that T_D goes high because the VETO (TD2) was initially set to be low by the ASG program. About 3.0 μs later, the control signal, u(t), then begins to become nonzero; that is, it is attempting to control the position of the plasma column.

After the pre-programmed delay of about 40 ms, as mentioned above, the ASG program sets the VETO (TD2) high. Figure 3.10 shows a zoomed in view of the relevant signals during a 10 ms window surrounding this transition. Within about 0.2 μs the signal T_D (enable/reset) goes low, as indicated in Figure 3.10. The ASG program sets the output signal (D1A) to 0.5 V within 21.0 μs of TD2 being set high. It can also be seen in Figure 3.10 that as the square wave pulse output by the ASG goes from 0.5 V to –0.5 V, the control signal goes from: $u(t) \approx 0.5$ V to $u(t) \approx -0.5$ V within 0.8 μs, essentially instantaneously when one considers the response time of the actuator circuit.

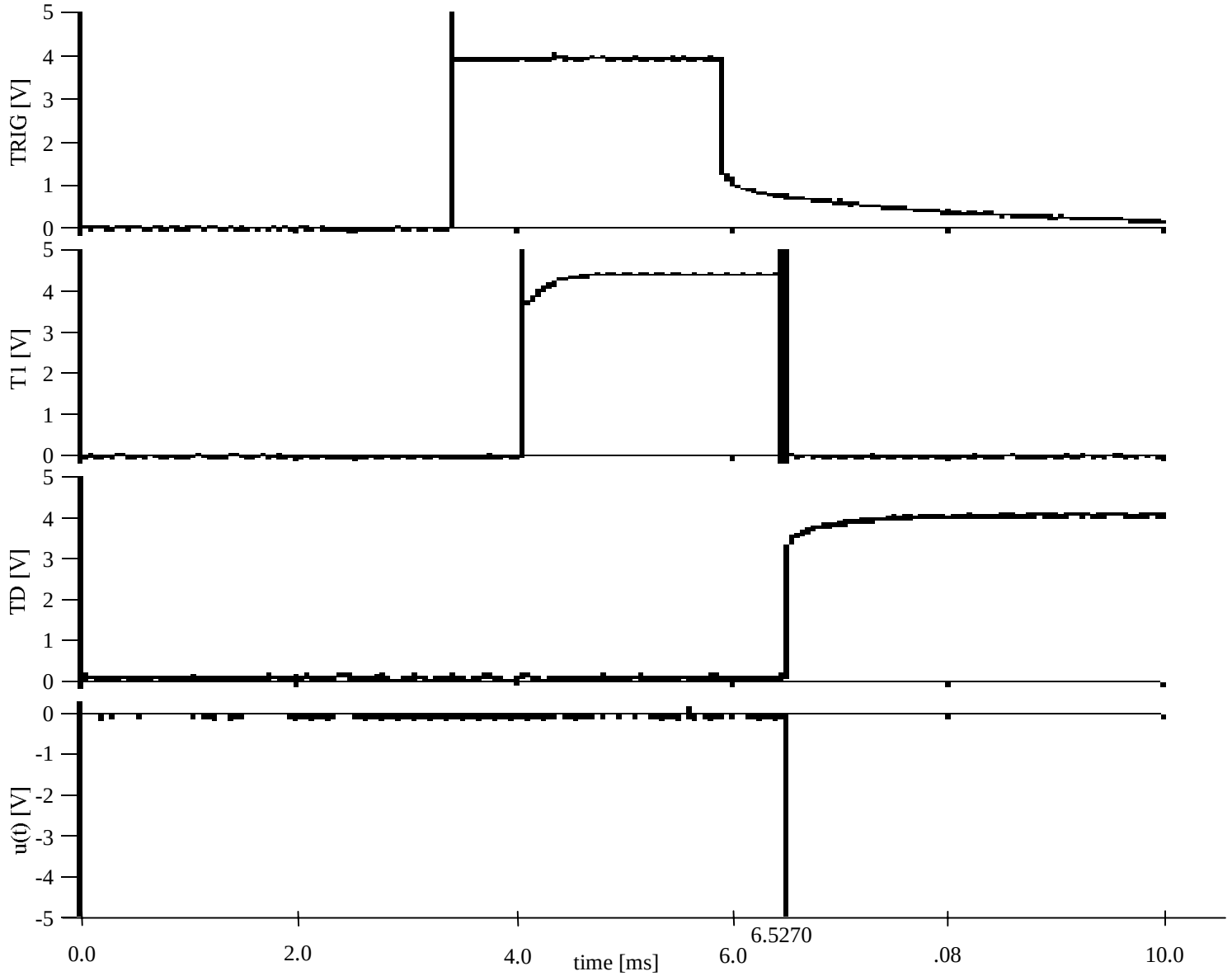

Figure 3.9 Zoomed in view of the temporal evolution of the modified controller signals during triggering.

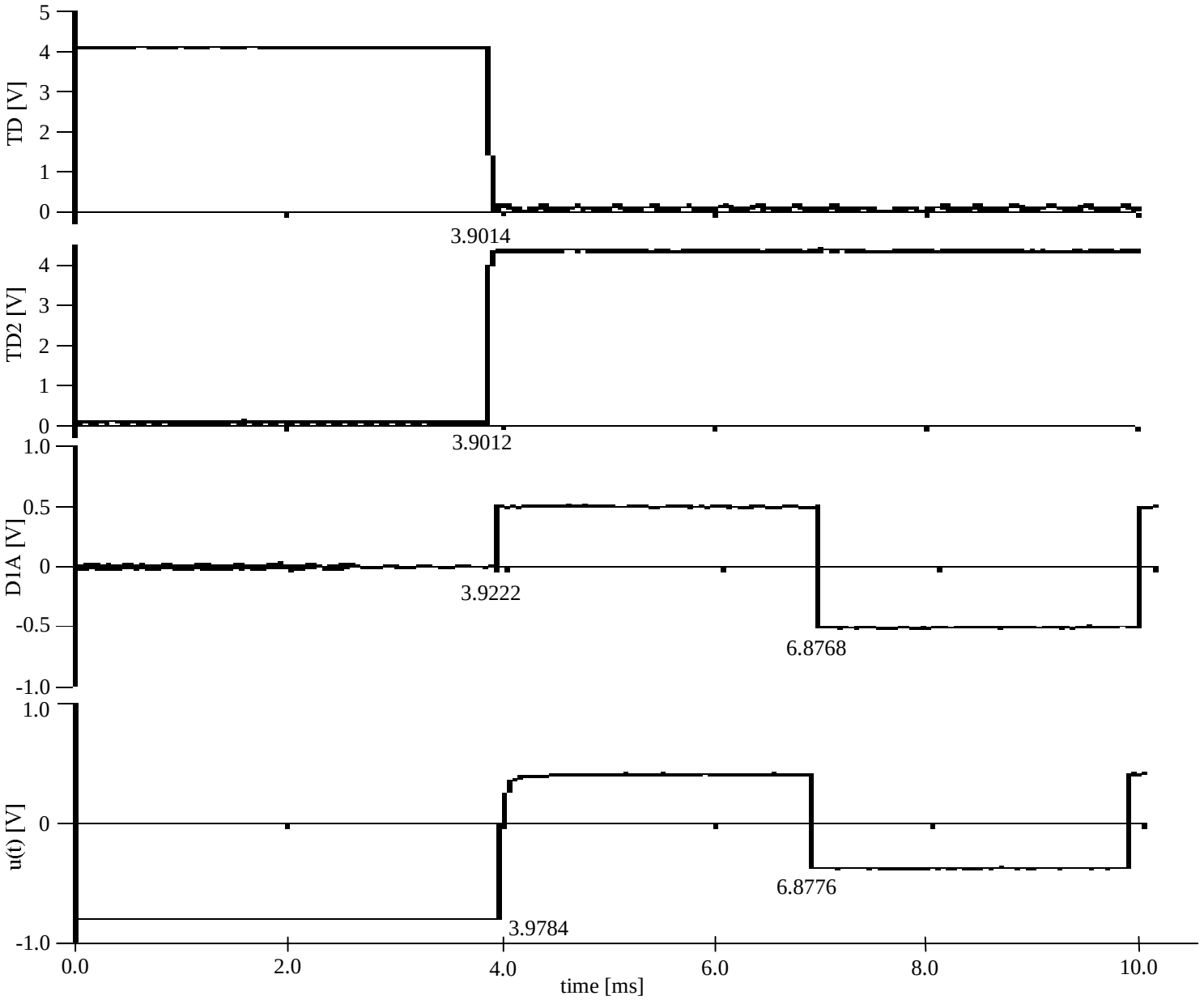

Figure 3.10 Zoomed in view of the temporal evolution of the modified controller signals during VETO by the ASG program.

This test was repeated several times (as were several variations of it), and in every case the modified PID controller performed as expected, with little deviation from the results just presented; that is, the ASG program and the modified PID controller reliably and repeatedly functioned as desired.

Having successfully verified the performance of the modified PID controller hardware as well as the interface between the PCL-711B and the controller, the modified PID control system was ready to be put into service. The modified PID controller was applied to both the normal and A.C. modes of STOR-M operation with the use of the ASG software. The performance of the modified PID controller will be discussed in detail in Chapter 5.

3.4 Summary

The existing analog PID controller used to control the horizontal position of the plasma column in the STOR-M tokamak has been described. In particular the operation of an analog PID controller has been considered and its applicability to the problem of controlling the position of the plasma in STOR-M examined. Some drawbacks, or limitations, of this approach were presented and a possible solution to these drawbacks using a digital computer was proposed. The implementation of this solution and the requisite hardware modifications were also discussed. Finally, the performance of the modified hardware was validated, and the modified PID controller was shown to be suitable for service on STOR-M.

4. FUZZY CONTROLLER

4.1 Overview

To overcome the difficulties inherent in controlling a system that is both non-linear and time varying, a controller based on fuzzy logic was implemented. Fuzzy controllers are known for their ability to provide very good control of this type of system [84]. Fuzzy controllers are particularly suited to applications where it is not necessary to find the global optimum solution, that is, where a near optimum solution is sufficient. This is the case here. Fuzzy controllers have their origin in the concept of fuzzy sets, which was first proposed by Zadeh in 1965 [81]. The concept was quickly expanded and there exist today extensive theories related to fuzzy sets and their corresponding fuzzy logic. While mathematically more complicated than classical sets, fuzzy sets provide a more natural representation of the world.

The notion of a group of objects, or set, is second nature to us; we are used to thinking of things as belonging, or not belonging, to a particular group. It was from this everyday experience that classical set theory was born. According to classical set theory, there are only two possibilities; either an element *x* does or does not belong to a set A. Our everyday experiences, however, tell us that the world is not so easily described. Most often, an element *x* is more accurately described as only partially belonging to a set A; that is, the element *x* has some degree of membership in a particular set. Furthermore, the degree with which a particular element belongs to a given set may be somewhat subjective. Consider as an example the statement "This room is cold." According to

classical set theory for any room there can only be two possibilities. Either the room is "cold" or it is "not cold." Fuzzy set theory is more general. One person may say that the room is "cold," while another person may claim that the room is merely "cool," that is; it is neither "cold" nor "not cold," but instead it is a bit of both. Fuzzy set theory provides a mathematical tool for implementing the reality that the temperature of a room might be deemed cool, in which case it only partially belongs to the set of "cold" rooms. Fuzzy set theory is merely a generalization of classical set theory. While fuzzy sets permit a more realistic representation of reality, they present a higher computational burden, and thus they are not suited for every application.

Classical sets are typically represented either by listing all of the elements of the set or by stating some membership rule. According to the listing method, all of the non-zero elements of a particular set are listed. For example, a set A may be described by:

$$A = \{x_1, x_3, x_5, x_6\} \tag{4.1}$$

The order in which the elements are listed is not important, and each element should be listed only once. The same set can also be described by a membership rule, where the members of the set are any elements that satisfy one or more properties [84]. For example, using the membership rule method, the set A could equivalently be described by:

$$A = \{x | x \text{ satisfies some property or properties}\} \tag{4.2}$$

which reads A contains all elements x such that x satisfies some property or properties [84]. A classical set is said to be crisp since its membership function can only take on two values: 0 or 1.

Like classical sets, a fuzzy set can also be described by some membership rule or rules, typically referred to as the membership function. Unlike classical sets, however, a fuzzy set cannot in general be described by simply listing the elements of the fuzzy set, as every element does not necessarily belong wholly to any set. Thus, in order to describe a fuzzy set by listing its elements, an ordered pair consisting of the element x and its degree of membership in **A** is used. In this way the fuzzy set **A** representing the classical set A would be described by:

$$\mathbf{A} = \{(x_1,1),(x_3,1),(x_5,1),(x_6,1),\} \tag{4.3}$$

However, given the increased flexibility of the fuzzy set, it may be more realistic for the fuzzy set **A** to be written as:

$$\mathbf{A} = \{(x_1,1),(x_2,0.3),(x_3,0.95),(x_5,0.8),(x_6,1),\} \tag{4.4}$$

Thus, the fuzzy set **A** provides a more accurate picture of the domain over which it is defined. Note the inclusion of x_2 in **A** that was excluded from A.

A fuzzy set could be equivalently described by its membership function as follows [88]:

$$\mathbf{A} = \{(x,\mu_{\mathbf{A}}(x))|x \in A, \mu_{\mathbf{A}}(x) \in [0,1]\} \tag{4.5}$$

where $\mu_{\mathbf{A}}(x)$ is the membership function that describes the degree of membership of element x in the fuzzy set **A** and which can take any value in the range [0,1]. Equation 4.5 reads that **A** contains all elements x, to a degree $\mu_{\mathbf{A}}(x)$ such that x satisfies some property or properties, and the degree of membership lies somewhere in the range of real numbers from 0 to 1 inclusive. Thus, a fuzzy set may be thought of as a function defined over a domain A that maps A into the range [0,1]. In the case of a classical set, the membership function is:

$$\mu_A(x) = \begin{cases} 1 & x \in A, \\ 0 & x \notin A \end{cases} \tag{4.6}$$

It should be pointed out that in this thesis upper case letters are used to denote all sets, with fuzzy sets being distinguished from classical sets by the use of boldface type. It should also be mentioned that the membership function of a fuzzy set is often referred to as its characteristic function. Furthermore, it is customary for the membership function to be normalized, so that at least one $x \in A$ attains the maximum degree of membership of 1. All of the fuzzy sets described in this thesis, with the exception of the aggregated fuzzy set described in Section 4.2.2, are normalized. As with classical set theory, fuzzy set theory includes rules describing the relationship between fuzzy sets. Properties such as the conjugate of a fuzzy set and the union and the intersection of two or more fuzzy sets are defined, and in the special case of crisp fuzzy sets, these rules yield the same results as their classical counterparts. For a more detailed discussion of fuzzy set theory the reader is referred to References [81-88].

4.2 Fuzzy Plasma Position Controller

Rather than discussing the properties of a fuzzy controller for a simple arbitrary system, the actual plasma position controller developed by the author will be presented. Like the PID controller discussed in Chapter 3, the fuzzy controller developed uses the plasma position signal, discussed in Section 2.4; however, unlike the PID controller, it has a second input, the plasma current signal, discussed in Section 2.2.

In fuzzy control theory, an input variable is converted into a fuzzy variable by a process known as fuzzification. Each fuzzy variable consists of a group of fuzzy sets. For example, in the plasma position controller that is to be described here, the plasma current will be one of the inputs into the fuzzy controller. The plasma current can be

described by a group of partially overlapping fuzzy sets such as **TINY**, **SMALL**, **MEDIUM**, and **LARGE**, with each set having its own membership function. In this way, for any given value of the plasma current, the degree to which it belongs to each of these sets can be determined, and a control decision based on this information can be obtained. Typical fuzzy controllers have about three to seven fuzzy sets per fuzzy variable [84]. While the membership function of each fuzzy set may take any suitable shape, it is common to restrict the membership functions to triangular, trapezoidal or bell shaped functions in order to reduce the computational burden required to determine the degree of membership associated with a particular value of the input variable, such as the plasma current [84]. In this thesis, only triangular membership functions were employed for the fuzzy sets associated with the input variables. The fuzzification of the two input signals is discussed in Section 4.2.1.

Once the input signals are obtained and fuzzified, the fuzzy logic rules can be applied. In the control algorithm presented here, the fuzzy logic rules take the form of if-then rules. The fuzzy logic rules employed in this controller will be discussed in further detail in Section 4.2.2.

After application of the fuzzy logic rules, a control decision is made. This control decision is in terms of the fuzzy output variable and is described by the aggregated membership function to be discussed in Section 4.2.2. Essentially, each of the fuzzy sets that make up the output variable will have some degree of membership associated with them. Thus, it is necessary to have some defuzzification method. The defuzzification algorithm essentially decodes or maps the control decision from the fuzzy variable to a crisp value of the control signal. The choice of defuzzification algorithm is not unique

[84]. For the controller described here a novel defuzzification algorithm was implemented which is computationally efficient. The defuzzification algorithm will be discussed in detail in Section 4.2.3.

4.2.1 Membership Functions

The fuzzy controller designed to control the horizontal position of the plasma within the STOR-M tokamak has two inputs and one output. The inputs are the horizontal plasma position, ΔH, and the plasma current, I_P, with each of these inputs corresponding to a fuzzy variable. The output is the control decision, u(t), and it also corresponds to a fuzzy variable.

The fuzzy variable associated with the plasma current consists of seven fuzzy sets: **LARGE NEGATIVE**, **MEDIUM NEGATIVE**, **SMALL NEGATIVE**, **TINY**, **SMALL POSITIVE**, **MEDIUM POSITIVE**, and **LARGE POSITIVE**. The membership functions making up the plasma current fuzzy variable are shown in Figure 4.1 (also Figure B.1). The fuzzy controller used the same plasma current membership functions during both normal and A.C. operation of STOR-M.

The fuzzy variable associated with the plasma position signal also consists of seven fuzzy sets: **FAR OUT**, **OUTSIDE**, **JUST OUT**, **VERY GOOD**, **JUST IN**, **INSIDE**, and **FAR IN**. As a result of the stray fields being different when the plasma current is negative than they are when the plasma current is positive, it was necessary to have two definitions for the plasma position fuzzy variable during A.C. operation of STOR-M. The membership functions that make up the fuzzy variable plasma position when the plasma current is positive is shown in Figure 4.2 (also Figure B.2), and those for the case when the plasma current is negative are shown in Figure B.3. The reversal in

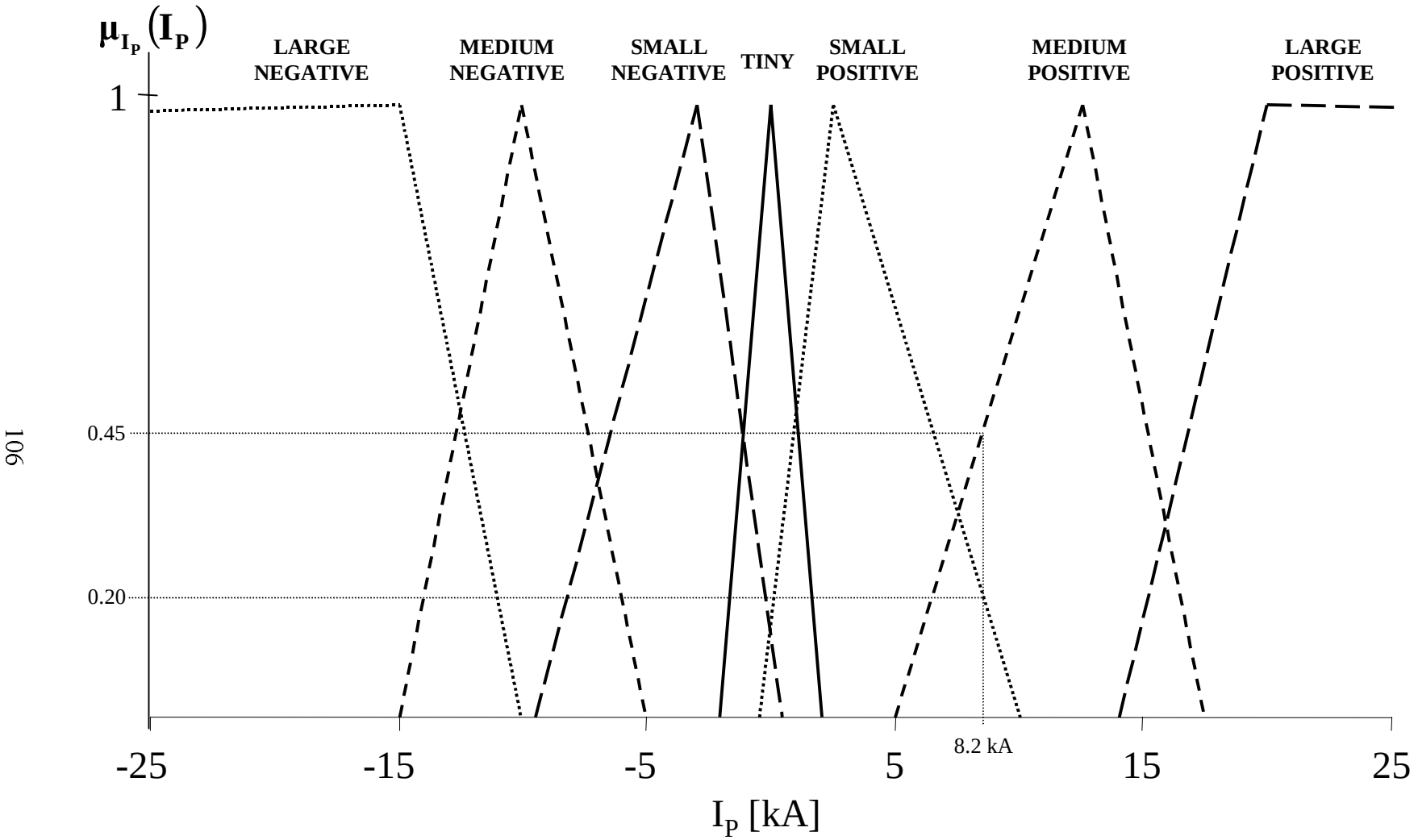

Figure 4.1 Fuzzy membership functions that make up the fuzzy variable representing the plasma current. These fuzzy sets are used for both normal and A.C. operation of STOR-M.

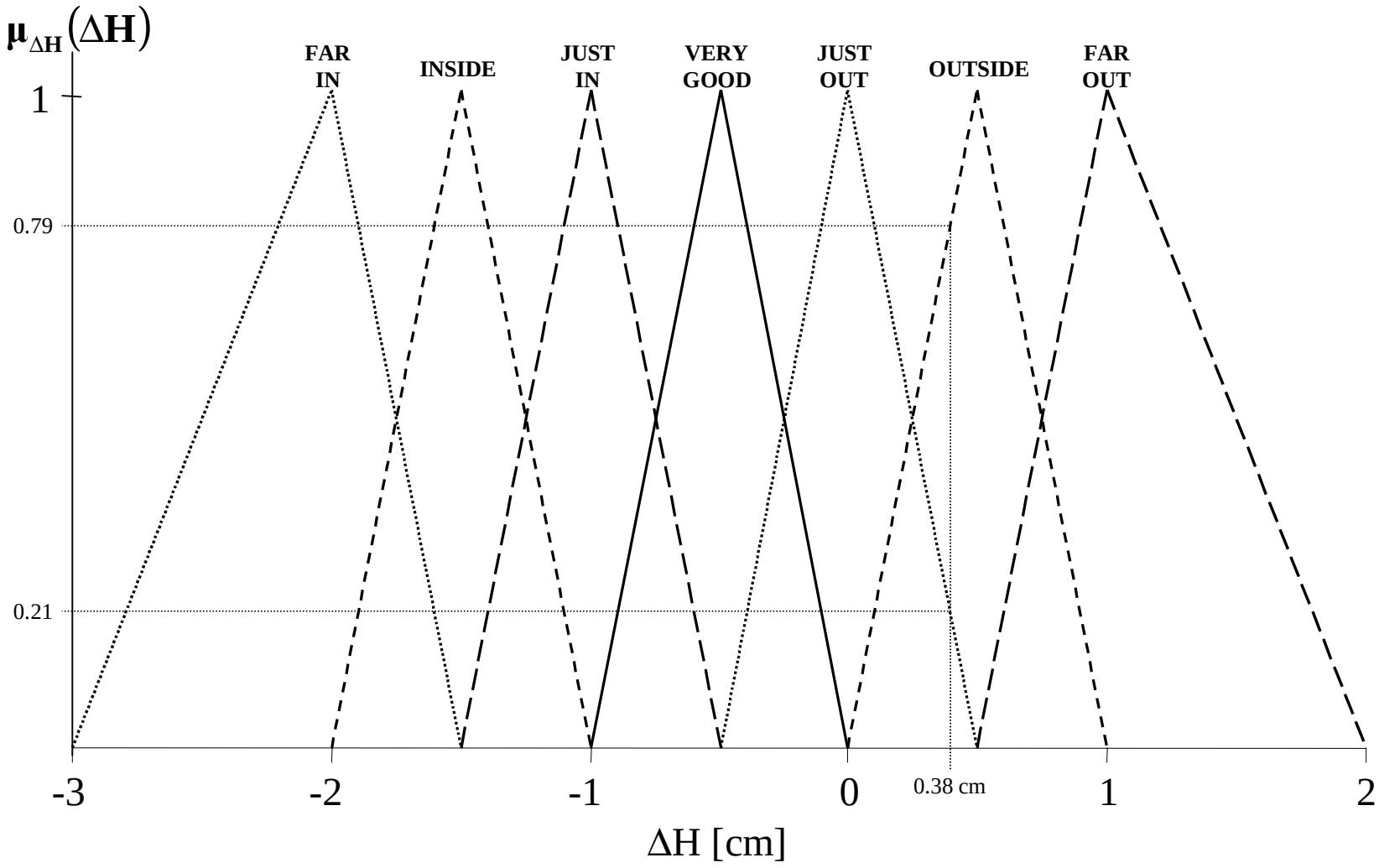

Figure 4.2 Fuzzy membership functions that make up the fuzzy variable representing the plasma position during both the transient region in normal operation and in the positive half cycle in A.C. operation of STOR-M.

the order of the fuzzy sets is due to the change in the direction of the plasma current, and hence, the direction of the Lorentz force acting on the plasma column. Since it was necessary to implement two definitions of the fuzzy variable for A.C operation of STOR-M, it was decided that this could be taken advantage of in order to provide fine control during normal operation. This was accomplished by also using two definitions of the fuzzy variable representing the plasma position in normal operation. In order to accomplish this, the normal mode discharge was broken down into two regions: the transient region and the steady-state region as was discussed in section 2.4.1. During the transient region the same membership functions as those used for the plasma position when the plasma current was positive in the A.C. mode of operation were used. The membership functions used during the steady-state region are shown in Figure B.4.

The fuzzy variable representing the control decision consists of eight fuzzy sets: **HIGH POSITIVE**, **MEDIUM POSITIVE**, **SMALL POSITIVE**, **TINY**, **SMALL NEGATIVE**, **MEDIUM NEGATIVE**, **HIGH NEGATIVE**, and **DC BIAS**. As with the fuzzy variable representing the plasma position, it was necessary to use two definitions for the control decision variable during A.C. operation of STOR-M. The fuzzy membership functions used for the positive half cycle of A.C. operation are shown in Figure 4.3 (also Figure B.5), while those used for the negative half cycle are shown in Figure B.6. The fact that it was necessary to implement two definitions of the control decision variable for A.C. operation was exploited by having a separate group of control decision membership functions for the transient region and the steady-state region during normal operation. The membership functions used during the transient region were identical to those used during the positive half cycle of A.C. operation. The membership

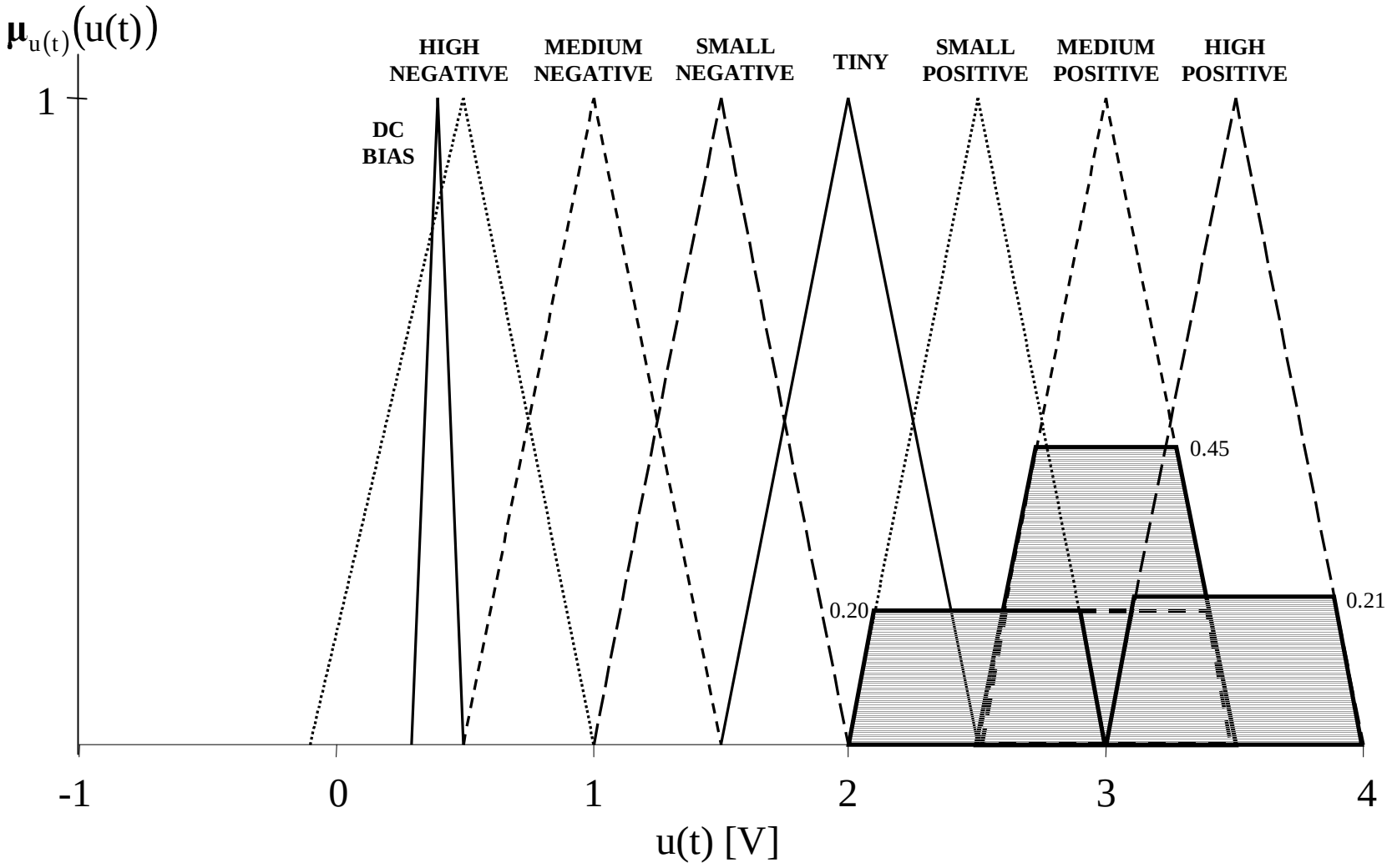

Figure 4.3 Fuzzy membership functions that make up the fuzzy variable representing the control decision during both the transient region in normal operation and in the positive half cycle in A.C. operation of STOR-M.

functions used during the steady-state region are shown in Figure B.7. The implementation of the fuzzy sets is based upon that presented by Rao and Rao [89].

4.2.2 Fuzzy Logic Rules

Having determined the shape of the membership functions, the number of fuzzy sets representing each of the fuzzy variables, and the supporting intervals, or domains, for each of the sets, the fuzzy representation of the control parameters, the inputs and the output, is complete [84]. The next step in the design of the fuzzy logic based controller was the determination of the fuzzy if-then inference rules. The architecture of the fuzzy logic controller described in this thesis is primarily based on that presented by Bojadziev and Bojadziev [84]. The number of fuzzy rules that are required is equal to the product of the number of fuzzy sets that make up the each of the fuzzy input variables. For the fuzzy plasma position controller described here, the input variable representing the plasma current consisted of seven sets, as did the input variable representing the plasma position. Thus, $7 \times 7 = 49$ fuzzy rules were required. The suitable choice of these rules requires the knowledge and experience of someone who is familiar with the behaviour of the system to be controlled. The fuzzy inference rules are organized in a decision table as shown in Table 4.1.

As an example of how to read the decision table, consider the following example. Suppose that at some sampling interval during the positive half cycle of A.C. operation, the plasma current is measured to be 8.2 kA and the plasma position is measured to be 0.38 cm outside. As can be seen in Figure 4.1, evaluation of the membership functions making up the fuzzy input variable representing the plasma current shows that the current value of the plasma current is **SMALL POSITIVE** to degree $\mu_{I_{PSP}} = 0.20$, and

Table 4.1 Fuzzy decision table.

ΔH	I_P	Large Negative	Medium Negative	Small Negative	Tiny	Small Positive	Medium Positive	Large Positive
	Far Outside	DC Bias	DC Bias	DC Bias	DC Bias	Medium Positive	High Positive	High Positive
	Outside	DC Bias	DC Bias	DC Bias	DC Bias	**Medium Positive**	**High Positive**	High Positive
	Just Outside	DC Bias	DC Bias	DC Bias	DC Bias	**Small Positive**	**Medium Positive**	High Positive
	Very Good	DC Bias	DC Bias	DC Bias	DC Bias	Small Positive	Small Positive	High Positive
	Just Inside	DC Bias	DC Bias	DC Bias	DC Bias	Tiny	Tiny	Medium Positive
	Inside	DC Bias	DC Bias	DC Bias	DC Bias	Small Negative	Small Negative	Medium Positive
	Far Inside	DC Bias	DC Bias	DC Bias	DC Bias	Small Negative	Small Negative	Medium Positive

MEDIUM POSITIVE to degree $\mu_{I_{PMP}} = 0.45$. This value of plasma current corresponds to a degree of membership of zero in all of the other fuzzy sets making up the fuzzy variable representing the plasma current. During the same sampling interval, evaluation of the membership functions making up the fuzzy input variable representing the plasma position shows that the current value of the plasma position is **JUST OUT** to degree $\mu_{\Delta H_{JO}} = 0.21$, and **OUTSIDE** to degree $\mu_{\Delta H_{O}} = 0.79$, as can be seen in Figure 4.2. This value of plasma position corresponds to a degree of membership of zero in all of the other fuzzy sets making up the fuzzy variable representing the plasma position.

The fuzzy rules that this particular combination of inputs correspond to are highlighted in the decision table shown in Table 4.1 and can be read from the decision table by finding the intersection of the column associated with the fuzzy set of interest corresponding to the plasma current, with the row associated with the fuzzy set of interest corresponding to the plasma position. For example, the rule "if the plasma current is **SMALL POSITIVE** and the plasma position is **JUST OUTSIDE** then the control decision is **SMALL POSITIVE**" can be found on the decision table shown in Table 4.1 by finding the intersection between the column associated with the **SMALL POSITIVE** fuzzy set corresponding to the plasma current with the row associated with the fuzzy set **JUST OUTSIDE** corresponding to the plasma position. At this intersection is the output decision **SMALL POSITIVE**. However, it must be pointed out that the degree to which the control decision belongs to the set **SMALL POSITIVE** still must be determined.

For every sampling interval, the degrees of membership of the present value of both the plasma current and the plasma position must be evaluated for each of the fuzzy sets that make up their respective fuzzy variables. This process forms the largest

computational burden of the fuzzy logic control algorithm. The desire to reduce this computational burden was the primary reason for the decision to use triangular membership functions exclusively for the input variables in the controller described here. Fortunately, as can be seen in Figure 4.1 and Figure 4.2, none of the fuzzy input variables have more than three fuzzy sets overlapping for any actual value of the input variable. Thus the degree of membership of the current value of the input variables in most of their fuzzy sets will be zero. By taking advantage of this fact, the computation of the degree of membership in each set is accelerated, as the degree of membership for only those sets for which the degree of membership will be nonzero are computed. In addition, this fact is also used to speed up the evaluation of the fuzzy inference rules, as only those rules that correspond to nonzero values of membership functions need to be evaluated. That is, there will be at most only nine fuzzy inference rules that fire (need to be evaluated). The fuzzy logic controller described in this thesis only evaluates those rules that are fired at each sampling interval.

In following the above example we have the rule "if the plasma current is **SMALL POSITIVE** and the plasma position is **JUST OUTSIDE**, then the control decision is **SMALL POSITIVE**." In fuzzy logic the min operator defines the conjunction, or intersection, of two fuzzy sets [83]. Thus, if we define the rule strength $\alpha_{i,j}$ of the application of a particular rule as:

$$\alpha_{i,j} = \min\left(\mu_{\mathbf{I}_{\mathbf{P}_i}}, \mu_{\Delta \mathbf{H}_j}\right) \tag{4.7}$$

where $i \in [\mathbf{LP}, \mathbf{MP}, \mathbf{SP}, \mathbf{T}, \mathbf{SN}, \mathbf{MN}, \mathbf{LN}]$ corresponds to the fuzzy sets that make up the fuzzy variable associated with the plasma current, and $j \in [\mathbf{FO}, \mathbf{O}, \mathbf{JO}, \mathbf{VG}, \mathbf{JI}, \mathbf{I}, \mathbf{FI}]$ corresponds to the fuzzy sets that make up the fuzzy variable associated with the plasma

position, then for the rule being considered, $\alpha_{\mathbf{SP,JO}} = \min(0.20, 0.21) = 0.20$.

Furthermore, it is clear that for all the rules where at least one of the degrees of membership in the corresponding fuzzy sets are zero the min operator will produce a result of zero, and therefore, these rules do not need to be analyzed. The intersection of the i^{th} column and the j^{th} row of the decision table contains the corresponding fuzzy output decision. The rule strength table is formed by substituting in the result of Equation 4.7 for each of the i equals one to seven (the number of fuzzy sets making up the fuzzy variable representing the plasma current) columns and the j equals one to seven (the number of fuzzy sets making up the fuzzy variable representing the plasma position) rows of the decision table. Since most of the cells will contain zero, only the nonzero values need to be evaluated. The rule strength table corresponding to our example is presented in Table 4.2.

Table 4.2 Fuzzy rule strength table.

		I_P						
		LN	MN	SN	Tiny	SP	MP	LP
ΔH	FO	0	0	0	0	0	0	0
	O	0	0	0	0	$\min(0.20, \mu_{\mathbf{u(t)_{MP}}})$	$\min(0.21, \mu_{\mathbf{u(t)_{HP}}})$	0
	JO	0	0	0	0	$\min(0.20, \mu_{\mathbf{u(t)_{SP}}})$	$\min(0.45, \mu_{\mathbf{u(t)_{MP}}})$	0
	VG	0	0	0	0	0	0	0
	JI	0	0	0	0	0	0	0
	I	0	0	0	0	0	0	0
	FI	0	0	0	0	0	0	0

The question of what the fuzzy control decision should be remains to be answered. According to Bojadziev and Bojadziev [84], the control decision that results from each rule is given by the conjunction operation applied to the rule strength and the conclusion of the if-then statement; that is:

$$\text{control decision} = \min\left(\alpha_{i,j}, \mu_{\mathbf{u(t)_k}}\right) \tag{4.8}$$

where $k \in [\mathbf{HP}, \mathbf{MP}, \mathbf{SP}, \mathbf{T}, \mathbf{SN}, \mathbf{MN}, \mathbf{HN}, \mathbf{DCB}]$ corresponds to the fuzzy sets that make up the fuzzy variable associated with the control decision. It should be pointed out that in Equation 4.8 the min operation is being performed on a number and a membership function. For the rule being considered:

$$\text{control decision} = \min\left(\alpha_{\mathbf{SP,JO}}, \mu_{\mathbf{u(t)_{SP}}}\right) = \min\left(0.20, \mu_{\mathbf{u(t)_{SP}}}\right) \tag{4.9}$$

This is shown graphically in Figure 4.4a where the control decision is represented by the shaded trapezoid. The result is a clipped fuzzy set, or more accurately a nonnormalized fuzzy set. The control decisions for the four rules that have fired in our example are shown in Figure 4.3. In order to combine the results of the rules that have fired, the fuzzy sets of the output fuzzy variable are aggregated using the max operator [84]. In the case of our example this takes the form of:

$$\mu_{\mathbf{agg}} = \max\left(\min\left(0.20, \mu_{\mathbf{u(t)_{MP}}}\right), \min\left(0.21, \mu_{\mathbf{u(t)_{HP}}}\right), \min\left(0.20, \mu_{\mathbf{u(t)_{SP}}}\right), \min\left(0.45, \mu_{\mathbf{u(t)_{MP}}}\right)\right) \tag{4.10}$$

where $\mu_{\mathbf{agg}}$ is the overall, aggregated, membership function of the fuzzy output variable. Here, the max operator is being performed on the fuzzy sets, and the result is shown in Figure 4.4b. In order to arrive at a crisp value for the control decision, this aggregated fuzzy membership function must now be defuzzified.

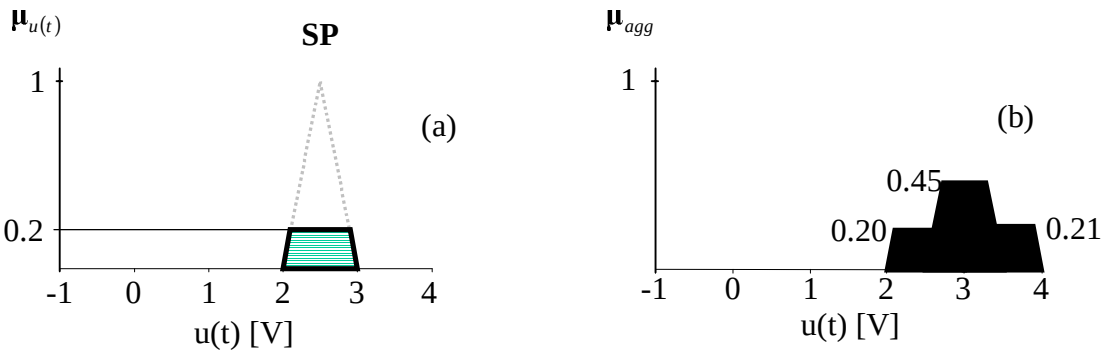

Figure 4.4 Fuzzy rule evaluation (a), and the formation of the aggregated fuzzy membership function (b).

4.2.3 Defuzzification

Once the aggregated fuzzy set representing the fuzzy output variable has been determined, an actual crisp control decision must be made. The process of decoding the output to produce an actual value for the control signal is referred to as defuzzification. For the control algorithm presented here, the primary goal was to obtain a high quality control decision in a computationally efficient manner. As a result, a novel defuzzification algorithm based on the center of gravity defuzzification technique [84] was implemented. This novel, approximate center of gravity defuzzification algorithm is described below.

In the center of gravity defuzzification technique, the crisp value of the output is given by the center of gravity of the aggregated membership function, that is, the horizontal component of the geometric center of the aggregated fuzzy membership function shown in Figure 4.4b. An approach similar to this was implemented here. Rather than applying Equation 4.9 to obtain an overall aggregated membership function, the max operator was applied separately to each of the fuzzy sets making up the fuzzy output variable for which the degree of membership was nonzero. Thus, instead of obtaining a single aggregated membership by applying Equation 4.9, there were as many

membership functions obtained as there were nonzero fuzzy sets making up the fuzzy output variable. Each of the resulting membership functions is trapezoidal. The final aggregated membership function consisted, then, of these membership functions which were allowed to overlap. The final control decision was obtained by finding the center of gravity of this modified aggregated membership function. The primary differences between this technique and the center of gravity technique lie in the overlapping of the fuzzy sets as well as the ease of computation. As a consequence of the overlapping of fuzzy sets, the crisp output decision will be pulled towards those regions in which there is overlap. In a physical system, the overlapping of two fuzzy sets is equivalent to a doubling of the mass density of the overlapping regions. While it is not strictly correct to have an aggregated fuzzy membership function that consists of overlapping sets, the result is computationally simple, and intuitively sensible.

4.3 Implementation of the Fuzzy Controller

The fuzzy logic controller described here was entirely designed, implemented, and evaluated by the author. The fuzzy controller was implemented in hardware using a data acquisition card, to be discussed in Section 4.3.1.1, as the interface between the controller and the sensors and the actuator. A block diagram of the fuzzy control system that was developed is shown in Figure 4.5. Clearly, the fuzzy controller forms a closed loop control system. One of the design requirements imposed upon this fuzzy controller was that it be implemented without disturbing the existing control system. This restriction and the required system modifications were discussed in section 3.2.3. All of the software required to implement the fuzzy controller and to interface with the data

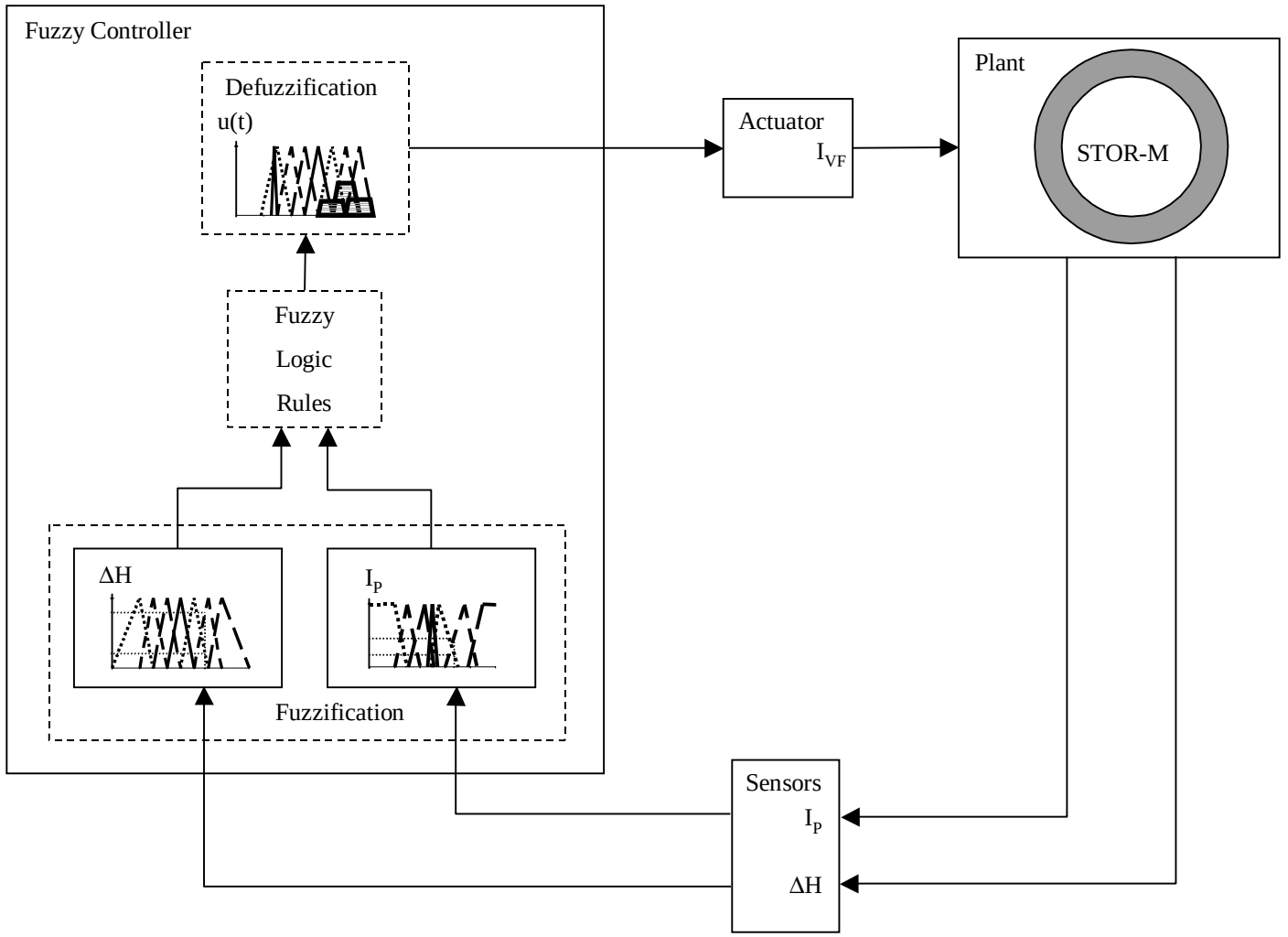

Figure 4.5 Fuzzy plasma position controller.

acquisition card was produced by the author, with the exception of the data acquisition card's drivers, which were supplied by the manufacturer of the data acquisition card.

4.3.1 Hardware Implementation

The hardware implementation of the fuzzy logic based controller was facilitated by the modifications made to the existing analog PID controller, as was discussed in Section 3.2. The fuzzy logic based plasma position controller consisted of the Advantech PCL-711B data acquisition card which was placed in a 486 PC operating at 66 MHz running in DOS mode. The PCL-711B has one 16-bit digital input port, one 16-bit digital output port, eight 12-bit resolution analog to digital converters that accept single-ended analog inputs, a single 12-bit resolution digital to analog converter, and an on-board programmable pacer clock. For greater detail about the PCL-711B and its drivers the reader is referred to References [90 and 91].

For the fuzzy plasma position controller, three analog inputs were used. The plasma current signal, discussed in Section 2.2.2.1, was connected to channel 1 of the analog to digital converter port. The plasma position signal, discussed in Section 2.2.2.3 and Section 2.4, was connected to channel 2 of the analog to digital converter port. The third analog signal that was input to the PCL-711B was a trigger signal, which was connected to channel 0 of the analog to digital converter port. The trigger signal was connected to an analog to digital converter rather than a digital input port so that a suitable trigger threshold could be set. The magnitude of the trigger signal is typically about 3.2 V but may be as low as 2.2 V. The trigger threshold of the fuzzy logic based plasma position controller was set to 1.5 V.

The fuzzy controller had two outputs: a digital output and an analog output. A digital output signal was used as the VETO signal, as discussed in Section 3.2.3. The analog output was the control signal, u(t), which was sent to the actuator circuit discussed in Section 3.2.2. The digital to analog converter of the PCL-711B was jumper selected to have an output range of 0 to 10 V, which was offset to a control signal between –5 V and 5 V as was discussed in Section 3.3.

4.3.2 Software Implementation

The fuzzy logic based plasma position controller was implemented in software using Borland Turbo C++ version 3.0. With the exception of the PCL-711B drivers, provided by the manufacturer, all of the software was written and validated by the author. In writing the software, every effort was made to produce computationally efficient code. To this end, the object-oriented structure of C++ was taken advantage of; furthermore, pointers were used extensively, and memory was allocated dynamically. The result was computationally efficient, reliable and modular code.

The fuzzy membership functions for the fuzzy sets representing the fuzzy input variables and the fuzzy output variable were restricted to triangular shaped membership functions. Prior to beginning the control cycle, the fuzzy controller reads the membership information from a text file. In this way, the membership functions for each fuzzy set associated with a particular fuzzy variable could be modified without the need for recompilation. In fact, as the memory for the fuzzy variables was allocated dynamically, the operator was even free to change the number of fuzzy sets used to define a particular fuzzy input variable. Examples of the text files containing the definitions of the fuzzy variables are given in Figure B.8 and Figure B.9 for use during

the normal and A.C. modes of STOR-M operation respectively. The fuzzy controller also checks for inconsistencies or errors in the fuzzy variable definition file. At each sampling interval, every membership function associated with each of the two fuzzy input variables is evaluated. The fuzzy controller keeps track of which fuzzy sets have nonzero degrees of membership for the current value of the input variables.

The fuzzy logic rules are read into the controller from a text file such as those shown in Figure B.10 and Figure B.11 for the normal and A.C. modes of STOR-M operation respectively. The fuzzy logic rules in this text file are in the form of the decision table discussed above. The control program also checks for inconsistencies and errors in the text file and echoes the decision table to the screen so that the operator can view it prior to the beginning of the control cycle.

When the control cycle is operating, the fuzzy logic rules are evaluated at each sampling interval. Since the fuzzy controller keeps a record of which fuzzy sets have nonzero degrees of membership during the sampling interval, only those fuzzy rules that will result in nonzero rule strength are evaluated. In addition, if more than one of the fuzzy logic rules results in a particular fuzzy set of the control decision variable, only the one with the maximum rule strength is recorded, thereby inherently implementing the aggregation process of the modified center of gravity defuzzification algorithm. The routine that applies the fuzzy logic rules keeps track of which fuzzy sets of the output variable have nonzero rule strength.

The aggregation process of the defuzzification algorithm is performed while the fuzzy logic rules are being applied. After application of the fuzzy logic rules, and the aggregation process, the modified center of gravity defuzzification technique is applied.

The resulting crisp value of the control decision is output by the digital to analog converter of the PCL-711B. Once the control decision has been outputted, the control cycle recommences with the sampling of the input variables. The control cycle continues for 250 iterations, approximately 65 ms, after which time a shot counter is incremented and the fuzzy controller waits for another trigger signal.

4.3.3 Performance Validation

Before the fuzzy controller was applied to control the STOR-M tokamak, its performance was evaluated using a signal generator to simulate the plasma position and the plasma current input signals. During the initial validation procedure, the fuzzy control algorithm was modified so that it would record the sampled value of the two input signals and the fuzzy sets to which the input variables had a nonzero degree of membership, as well as the corresponding degree of membership. The fuzzy controller would also record the rule strength for the appropriate rules that fire as a result of the input signals and the crisp value of the control decision. The values were recorded in an ASCII text file. In order to verify the fuzzy control algorithm, the fuzzy values for each sampling interval were computed using MATLAB and compared with those recorded by the fuzzy controller. In every case the crisp values of the control decision agreed to at least the 3rd decimal place, that is, to the nearest millivolt. For example, when the plasma position was 4.0 mm inside and the plasma current was 3.5 kA, the fuzzy controller determined that the control decision should have been -0.401984 V, while MATLAB gave a value of -0.4020 V. Considering that the digital to analog converter of the PCL-711B has 12-bit resolution, corresponding to a resolution of 2.44 mV, this accuracy is more than sufficient.

Having verified that the fuzzy control algorithm performed as expected, the next step in the performance validation process was determining the speed of the algorithm. In order to accomplish this, a signal generator was again used to simulate the plasma position and the plasma current input signals. During these tests, the trigger signal, the simulated plasma current input signal, the crisp output decision signal, and the veto signal were monitored and recorded using a LeCroy 9314M quad 300 MHz storage oscilloscope with 8-bit resolution. In addition, the pacer clock of the PCL-711B was programmed to operate at 25 kHz. Typical results of an entire simulated STOR-M discharge are shown in Figure 4.6. In this test, the fuzzy controller, upon receiving a trigger, would raise the veto signal and then begin the control process until 250 control cycles had been performed. After the 250^{th} control cycle, the veto signal was lowered, and the fuzzy controller awaited another trigger signal. From Figure 4.6 it can be seen that the fuzzy controller required approximately 65 ms in order to perform 250 control cycles. This corresponds to an average of 0.260 ms per control cycle. As the typical discharge in STOR-M lasts for about 50 ms, the number of control cycles to perform was deemed appropriate.

Since the number of fuzzy sets corresponding to each of the input variables that have nonzero degrees of membership associated with them varies from control cycle to control cycle, the time required per control cycle will also change from control cycle to control cycle. In order to get a better view of the range of variation, as well as the delay time between the trigger signal and the beginning of the first control cycle, this second set of tests was also performed while monitoring only the first 5 ms of the simulated discharge, thereby increasing the sampling period of the LeCroy 9314M from 10 μs to

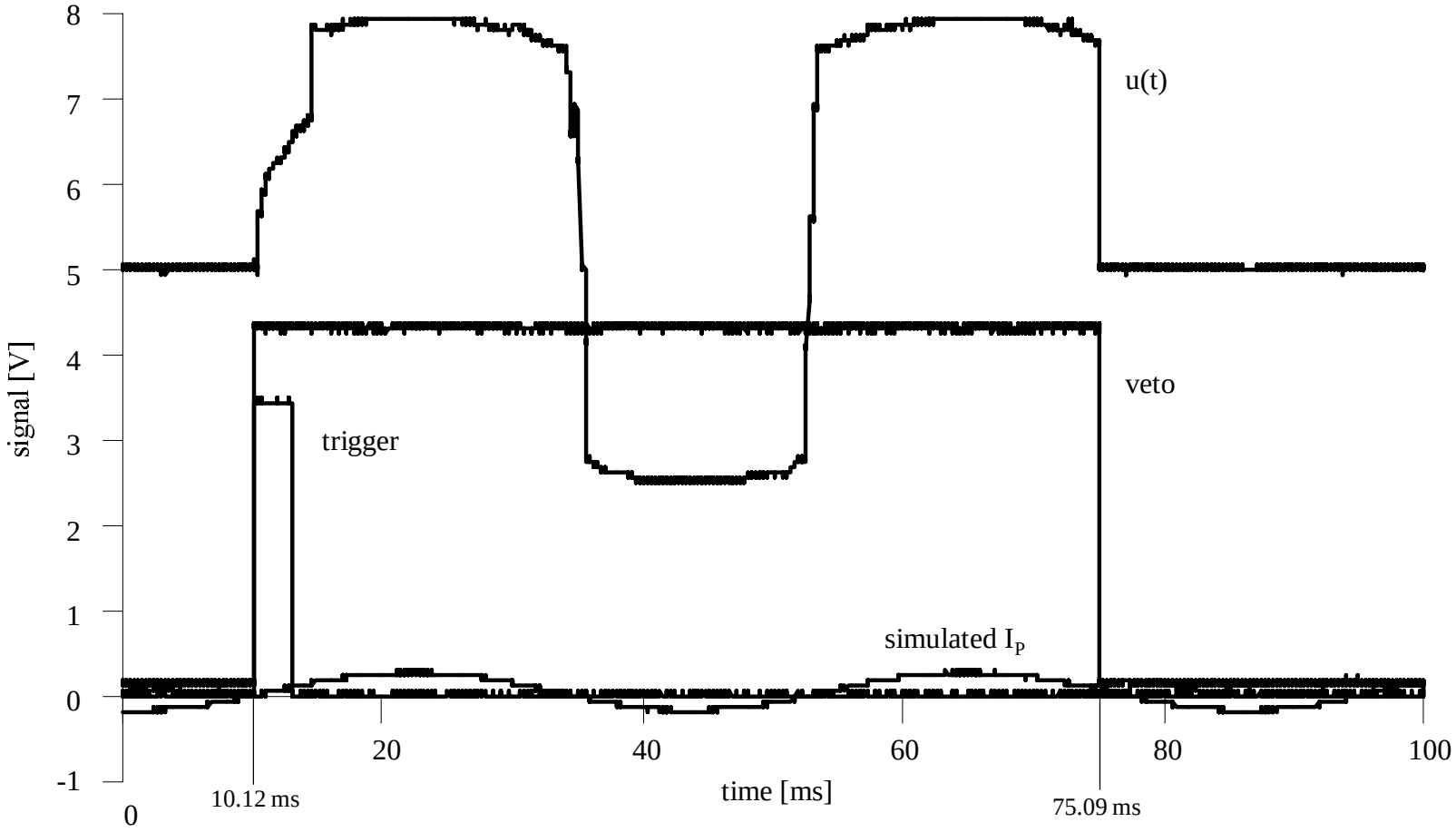

Figure 4.6 Results of a typical trial during the performance validation of the fuzzy logic based plasma position controller.

0.5 μs. Typical results are presented in Figure 4.7. By doing this, it was determined that the average time from the trigger signal going high to the time that the VETO signal goes high was 90.5 μs, and the time required to complete a control cycle varied from a minimum of 255.0 μs to a maximum of 288.0 μs, much less than the maximum permitted time outlined in Section 2.6. Furthermore, the output signal is quite stable during the entire control cycle. The small variations seen in Figure 4.6 and Figure 4.7 typically have a magnitude of 0.0625 V, which corresponds to the bit noise of the LeCroy 9314M storage oscilloscope. Having validated the performance of the fuzzy plasma position controller on a simulated system, the controller was installed for the next step, control of the actual plasma position in the STOR -M tokamak.

4.4 Summary

In this chapter, the fuzzy logic based plasma position controller that was designed and implemented for use with the STOR-M tokamak was described. The hardware and software implementation of this fuzzy logic based controller was discussed in detail. The characteristics of the fuzzy controller that were observed during its performance validation stage were quite satisfactory. In fact, based on the results of the performance validation, it was concluded that the fuzzy controller developed was suitable for application to the control of the plasma position in the STOR-M tokamak. The next step towards this goal involved the installation of the fuzzy logic based controller and its subsequent optimization. The performance of the fuzzy logic controller in actually controlling the plasma position in the STOR-M tokamak is the topic of the next chapter.

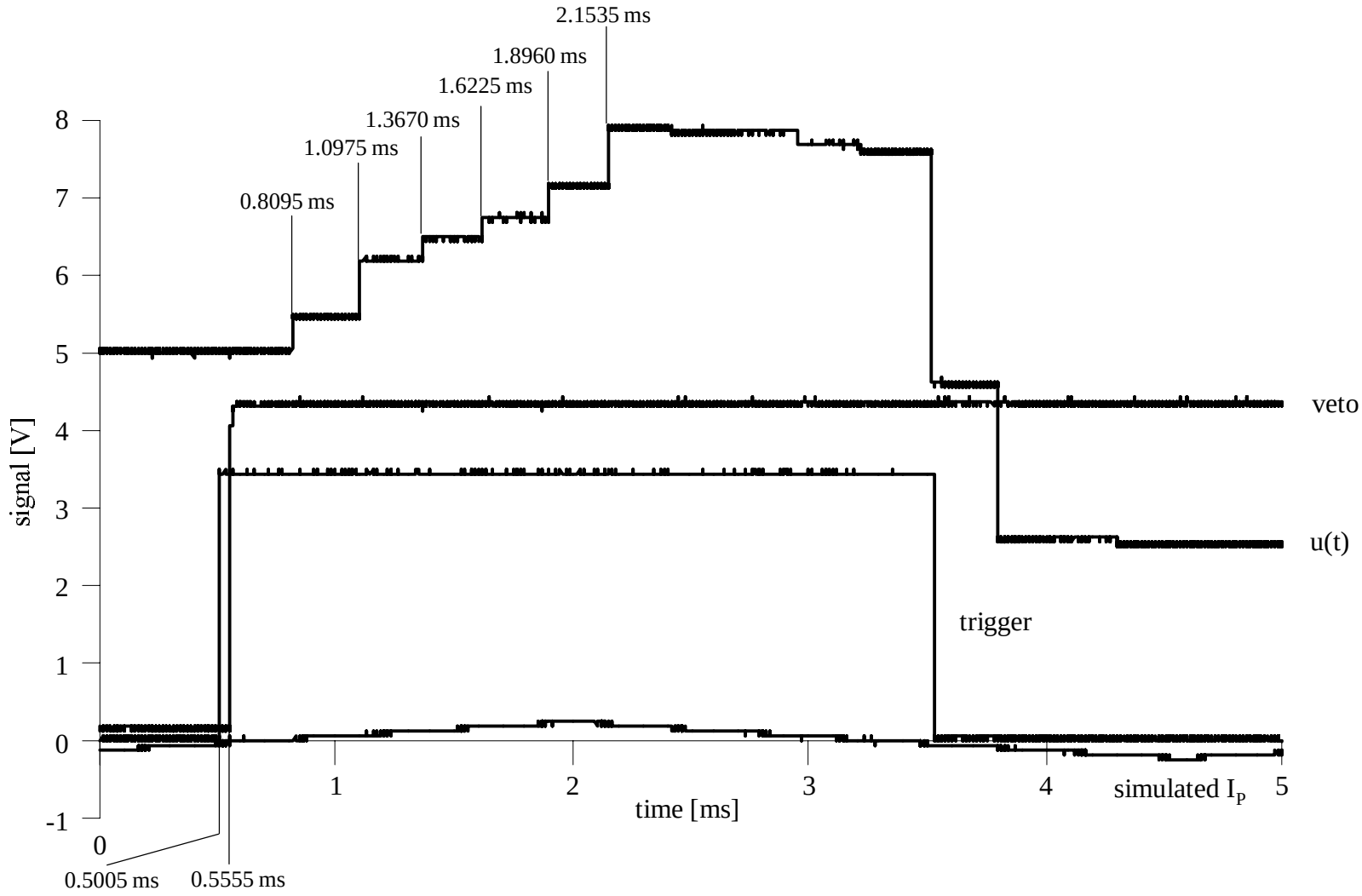

Figure 4.7 First 5 [ms] of a typical trial during the performance validation of the fuzzy logic based plasma position controller.

5. EXPERIMENTAL RESULTS

5.1 Overview

In this chapter, the performance of both the modified PID controller and the fuzzy logic based controller are presented. More specifically, their ability to control the position of the plasma column within the STOR-M tokamak during both the normal mode and the A.C. mode of operation are presented.

5.2 Normal Mode

After successfully validating the performance of the fuzzy logic based controller off-line, it was installed for on-line application to control the position of the plasma column in the STOR-M tokamak. Based on the author's experience, the fuzzy sets describing the fuzzy variables of the controller were defined, and the fuzzy logic rules in the form of the decision table were constructed. These initial definitions required modification before the fuzzy logic based controller was capable of providing a high quality of control over the position of the plasma column. The final fuzzy sets and decision table used during normal mode operation of STOR-M (after this optimization process was completed) are presented in Figures B.1, B.2, B.3, B.4, B.5 and B.7 and Figure B.10 respectively.

The parameters of a typical normal mode discharge using the optimized fuzzy sets and decision table are presented in Figure 5.1. In this figure it is clear that the fuzzy logic based controller is capable of providing a high quality of control over the position of the plasma column in the STOR-M tokamak. To get an indication of the quality of

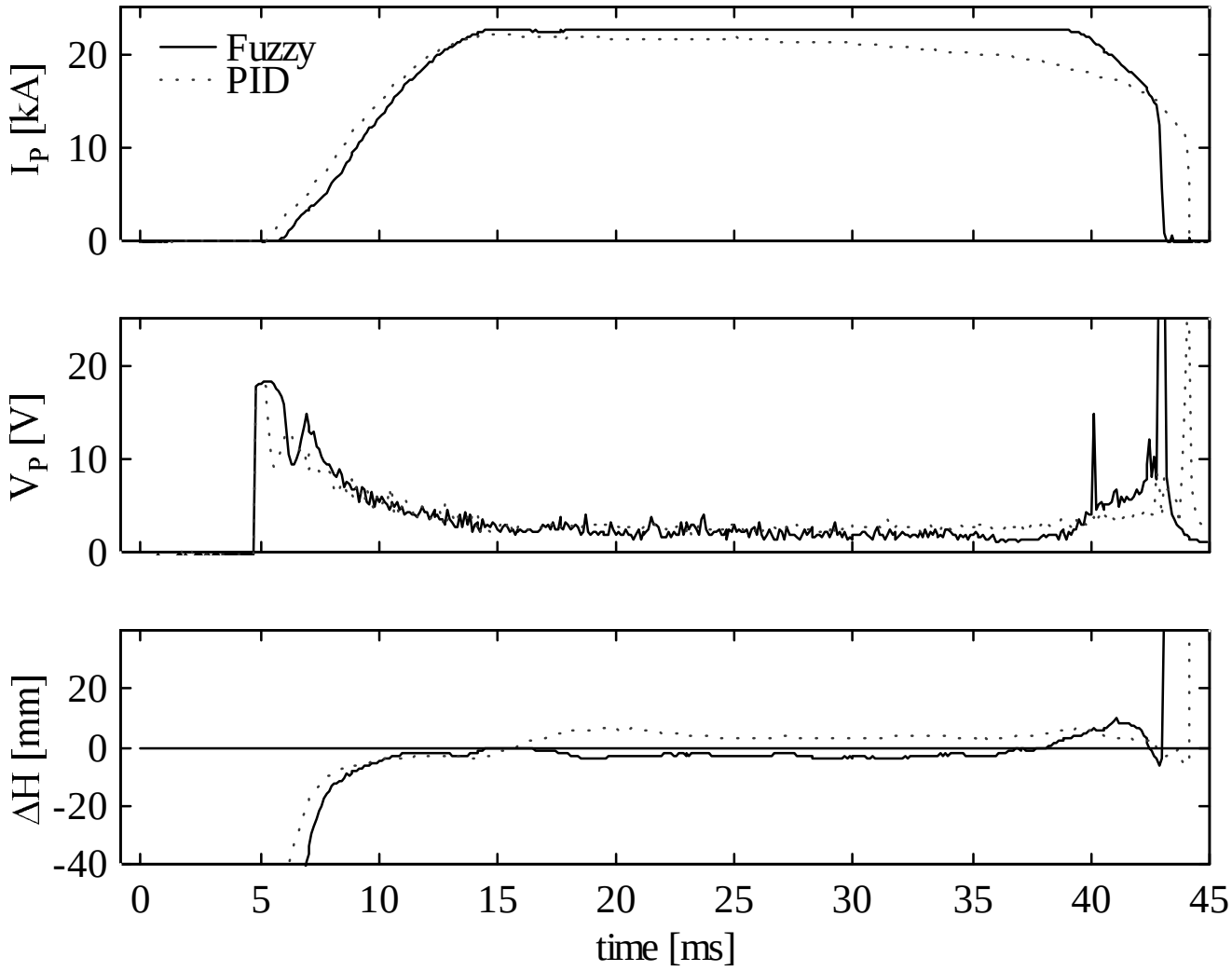

Figure 5.1 Parameters of typical normal mode STOR-M discharges using the fuzzy logic controller and the modified PID controller.

control, the performance of the fuzzy logic based controller is compared with the performance of the modified PID controller.

The parameters of the modified PID controller were optimized during normal mode operation of STOR-M. The typical discharge parameters, using the optimized modified PID controller, are presented in Figure 5.1. The performance of the fuzzy logic controller and the optimized modified PID controller are presented in Figure 5.2. From Figure 5.2 it is clear that both controllers are capable of providing adequate ($\pm$ 5 mm) control over the position of the plasma column during normal mode operation of STOR-M. It should be pointed out, however, that the performance of the fuzzy controller is slightly better, as it maintains the position of the plasma column within acceptable limits for a longer time than the modified PID controller. It should also be pointed out that both controllers were optimized to provide control over the position of the plasma column and not any of the other parameters of the discharge, such as the plasma current profile. It can be seen from Figure 5.1, however, that the plasma current profile when the fuzzy logic based controller is used has a flatter steady-state region.

Figure 5.3 shows the average plasma position during the interval from 20.0 ms to 35.0 ms for 23 consecutive normal mode discharges. The average standard deviation of the plasma position signal over these 23 discharges was 0.8 mm when the fuzzy logic controller was used, and a 1.1 mm when the modified PID controller was used. Thus, the fuzzy logic controller provides a better quality of discharge than the modified PID controller. This is particularly important when conducting experiments to study the properties of tokamak plasmas. Another important feature of both of the fuzzy logic based controller and the modified PID controller was their reliability. Both controllers

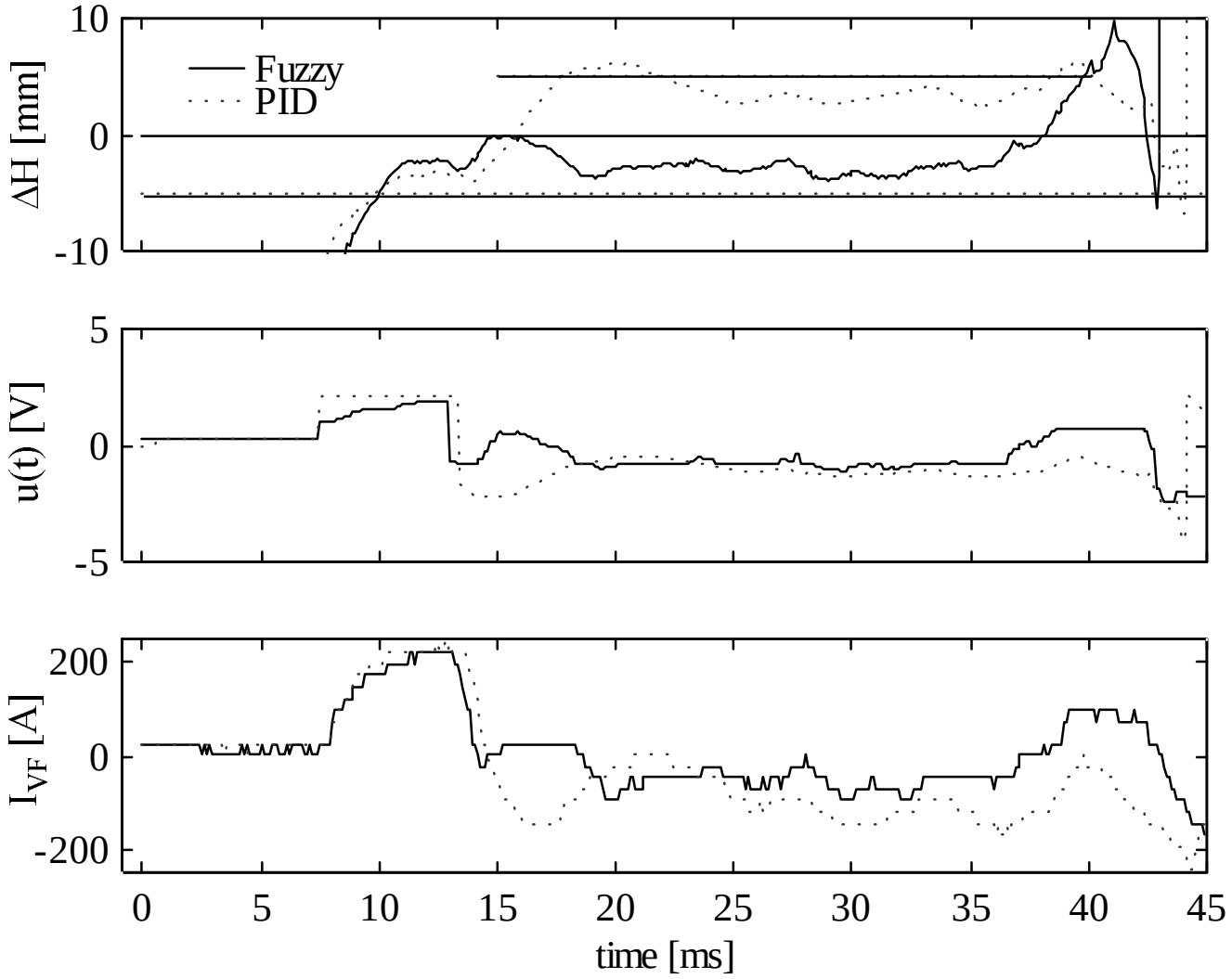

Figure 5.2 Performance of the controllers during normal mode operation of STOR-M.

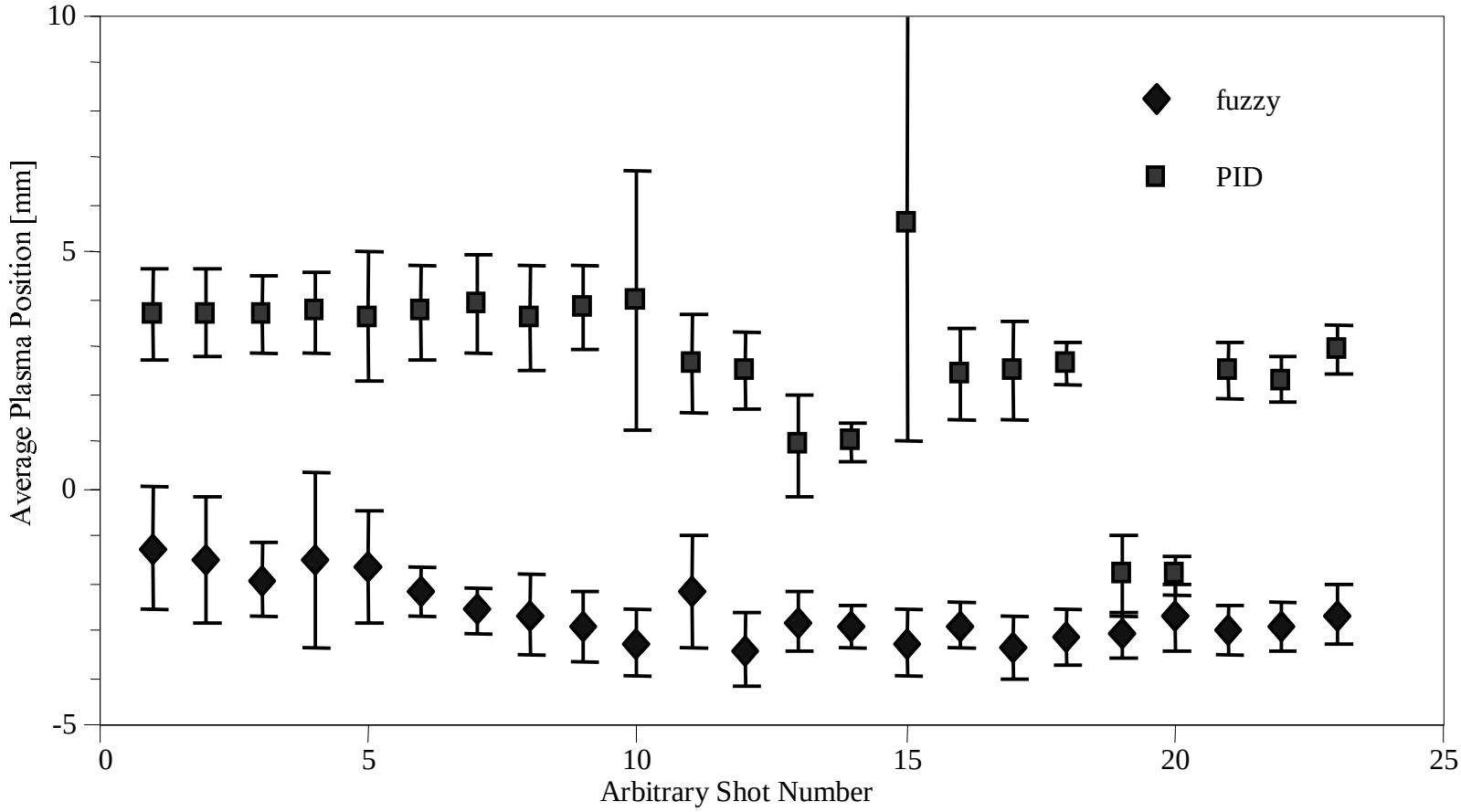

Figure 5.3 Reliability of the fuzzy logic controller and the modified PID controller during normal mode STOR-M discharges.

were capable of providing repeatable discharges parameters throughout the course of a day's operation. However, with the modified PID controller, minor disruptions occurred during both the tenth and the fifteenth discharges as can be seen in Figure 5.3.

When minor disruptions occur, the quality of the subsequent discharge may be affected. A typical minor disruption, corresponding to the fifteenth discharge in Figure 5.3, is shown in Figure 5.4. During disruptions there is often an increase in the release of impurities from the wall of the discharge chamber. This increase in the impurity concentration often degrades the quality of subsequent discharges. Often several additional discharges are required to recondition the plasma following the occurrence of a complete disruption. The occurrence of disruptions makes it difficult to perform experimental studies within the STOR-M tokamak, and is therefore, highly undesirable. The ability of the fuzzy logic controller to permit the STOR-M tokamak to operate without even minor disruptions for many consecutive discharges makes its performance superior to that of the modified PID controller.

5.3 A.C. Mode

The fuzzy logic based plasma position controller was also optimized for use during A.C. operation of STOR-M. Again, based on the author's experience, the fuzzy sets describing the fuzzy variables of the fuzzy logic based controller were defined, and the fuzzy logic rules in the form of the decision table were constructed. These initial definitions also required modification before the fuzzy logic based controller was optimized for providing a high quality of control over the position of the plasma column. The final fuzzy sets, and decision table used during A.C. STOR-M operation are presented in Figures B.1, B.2, B.3, B5 and B.6 and Figure B.11 respectively.

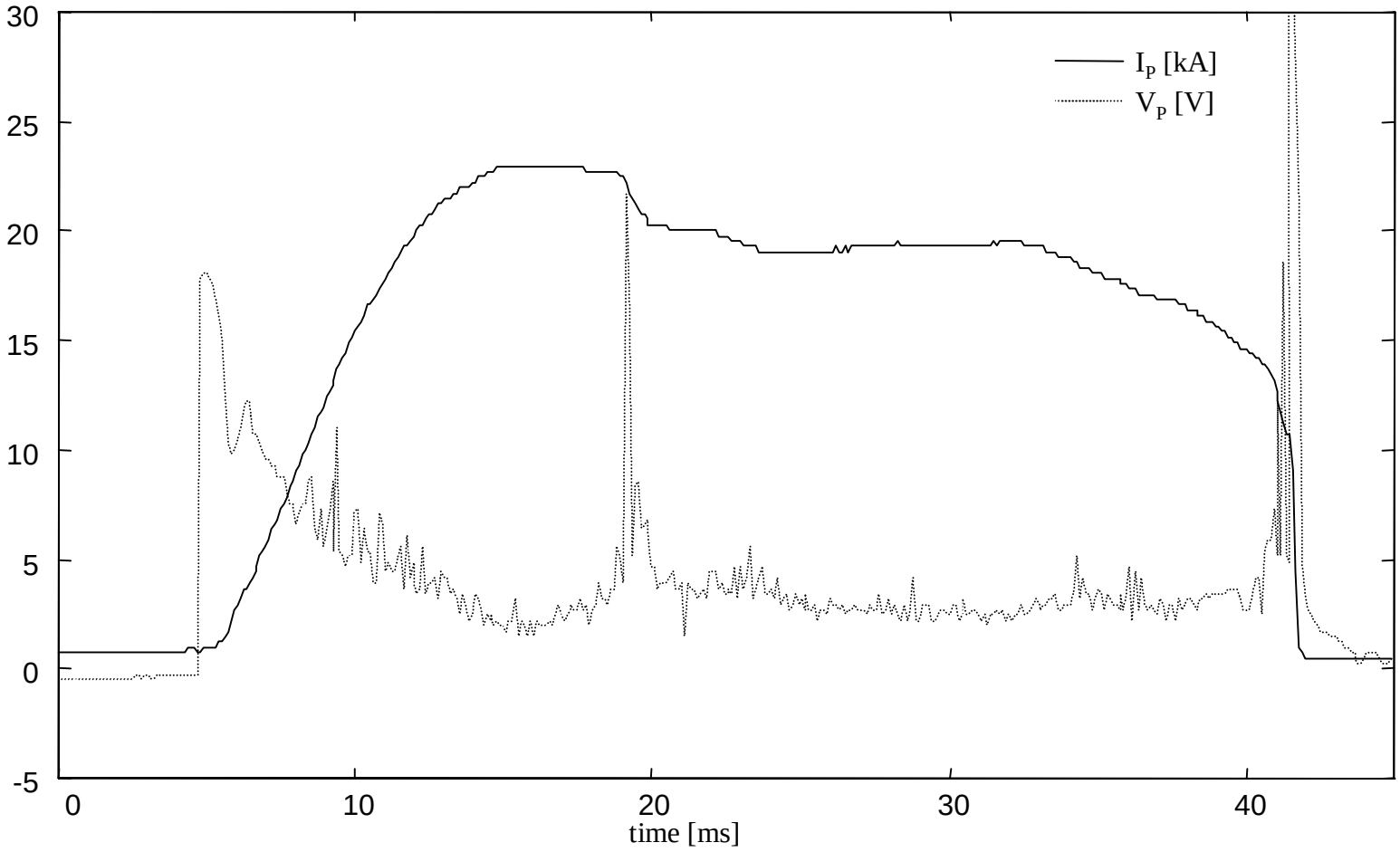

Figure 5.4 A typical normal mode STOR-M discharge with a minor disruption at about 19.5 ms.

In order to evaluate the quality of control provided by the fuzzy logic based controller, the modified PID controller was also optimized for controlling the position of the plasma column during A.C. STOR-M operation. In addition, using the ASG program described in Section 3.2.3, an open-loop pre-programmed controller was also optimized for use during A.C. operation of STOR-M. Figure 5.5 shows the typical discharge parameters using each of the three controllers, and Figure 5.6 shows the plasma position obtained with each of the three controllers during the typical discharges.

From Figure 5.6 it can be seen that strictly from consideration only of the plasma position, the fuzzy logic based controller again provided the highest quality of control. The modified PID controller was not capable of providing a high quality of control over the plasma position during A.C. operation of STOR-M. The average plasma position over the interval from 5.0 ms to 15.0 ms when the modified PID controller was used was –26.6 mm, well beyond the acceptable range of ±5 mm. The average plasma position for ten consecutive discharges where the fuzzy logic controller was used and for seven consecutive discharges where the pre-programmed controller was used are shown in Figure 5.7 for the interval from 5.0 ms to 15.0 ms. The average standard deviation of the plasma position signal during these discharges over the interval from 5.0 ms to 15 ms using the fuzzy logic controller was 2.6 mm. The quality of control using the open-loop pre-programmed controller was not quite as good as that provided by the fuzzy logic based control, the average standard deviation of the plasma position signal was 3.0 mm during the interval from 5.0 ms to 15.0 ms for the seven consecutive discharges, but it was still acceptable.

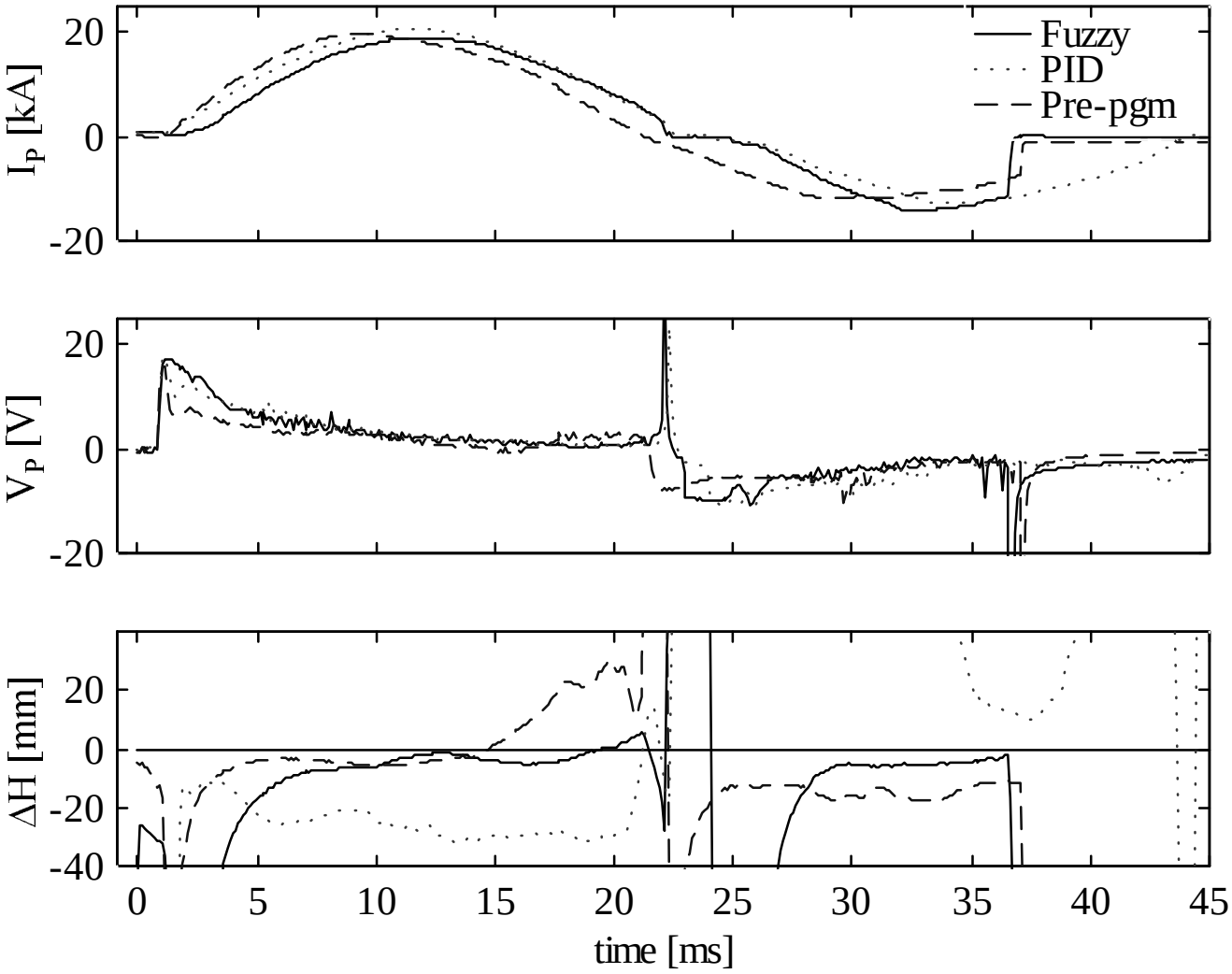

Figure 5.5 Parameters of typical A.C. mode STOR-M discharges using the fuzzy logic controller, the modified PID controller, and the pre-programmed controller.

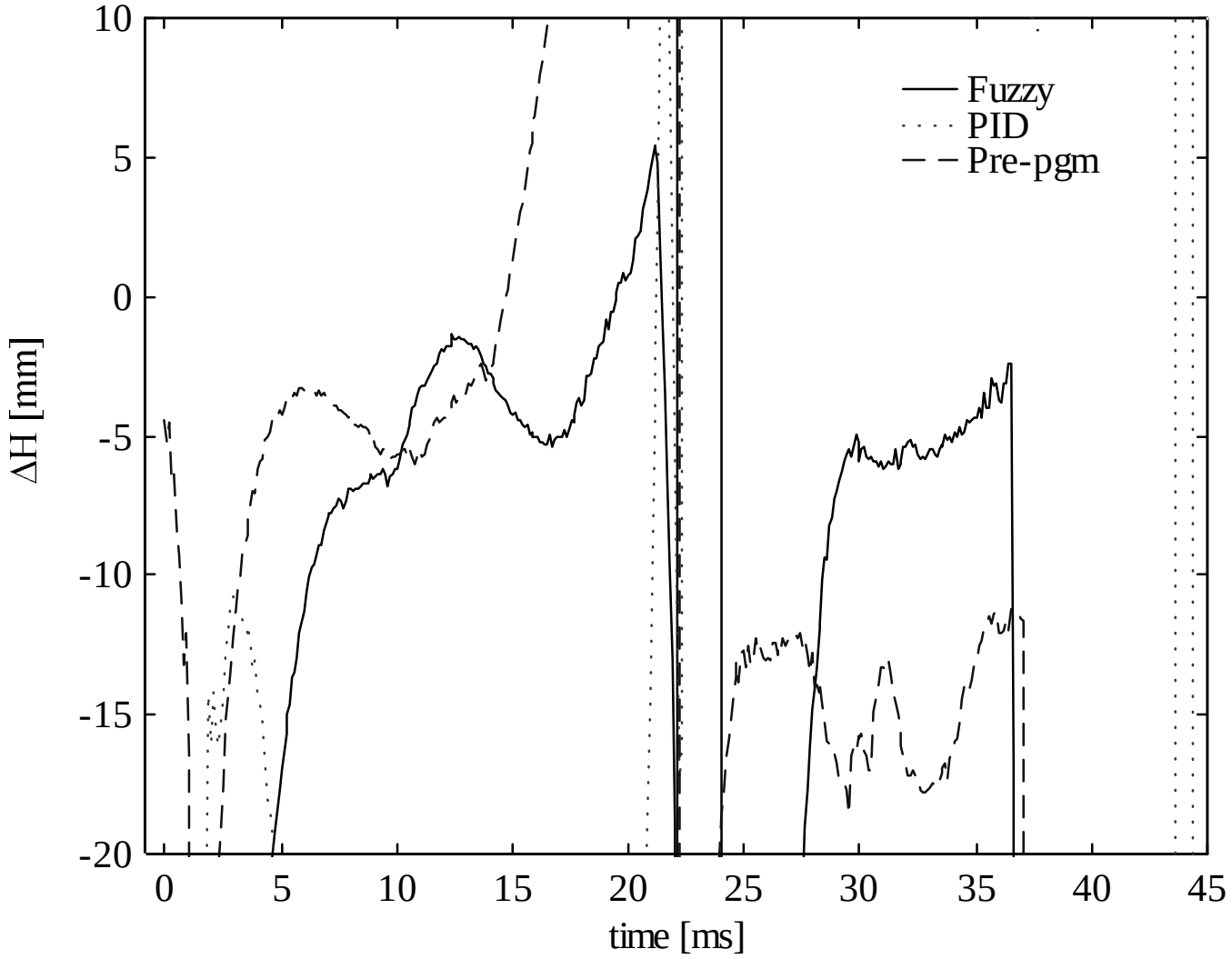

Figure 5.6 Performance of the controllers during A.C. mode operation of STOR-M.

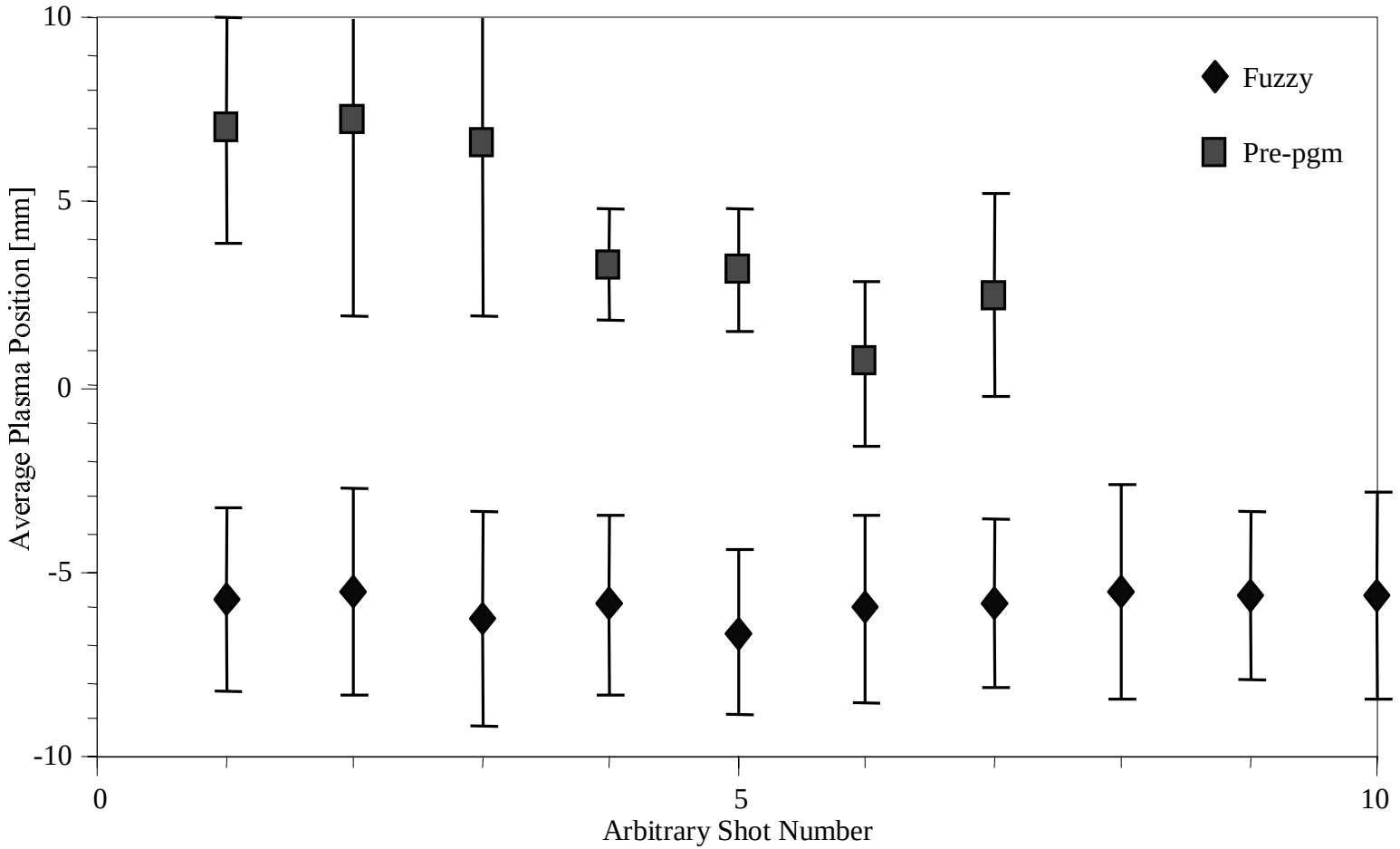

Figure 5.7 Reliability of the fuzzy logic controller and the pre-programmed controller during A.C. mode STOR-M discharges.

When one considers the overall quality of the discharge, the open-loop pre-programmed controller provides the best performance since during A.C. tokamak operation, it is particularly desirable that the current reversal regime be as smooth as possible with minimal dwell time. It should be pointed out, however, that unlike the fuzzy controller and the modified PID controller, the open-loop pre-programmed controller was not optimized with the control of the plasma position in mind, but rather with the goal of obtaining the best possible discharge parameters during the current reversal regime. This makes it clear that there is a trade-off between the optimal temporal plasma current profile and the optimal plasma position during A.C. operation of STOR-M.

It must be pointed out that the quality of discharge obtained with the fuzzy logic controller was highly reproducible, whereas the quality of the discharge obtained with the open-loop pre-programmed controller was not. For example, the eighth discharge in Figure 5.7 suffered a complete disruption, and the plasma required several subsequent discharges to be reconditioned. In fact, complete disruptions occurred at least every seven discharges when the pre-programmed controller was used. Thus, while it was possible to obtain a higher quality of discharge with the pre-programmed controller, these discharges were not highly repeatable from discharge to discharge; thereby making this controller unsuitable for most types of A.C. mode experiments in STOR-M. Clearly the reliability and quality of control provided by the fuzzy logic controller make it more robust and superior to the other controllers that were evaluated.

5.4 Summary

It has been shown that a fuzzy logic based controller is capable of providing a high quality of control over the position of the plasma column within the STOR-M tokamak. Both the fuzzy logic based controller and the modified PID controller were capable of reliably providing high quality of control during normal mode operation of STOR-M. Furthermore, the quality of control as well as the overall quality of discharge during the normal mode of operation was better with the fuzzy logic based controller than it was with the modified PID controller.

During A.C. operation of STOR-M, the fuzzy logic based controller again provided the highest quality of control over the position of the plasma column. The overall quality of the A.C. discharges, however, could best be provided using open-loop pre-programmed control; this quality of control, however, was not reliably repeatable from one discharge to another. Clearly, during A.C. operation, a choice must be made whether a high quality of control is more desirable than a smooth transition between half cycles during the current reversal regime. Overall, the fuzzy logic based controller provided a superior quality of control over the position of the plasma column in the STOR-M tokamak during both normal mode operation and A.C. mode operation of the STOR-M tokamak.

6. CONCLUSIONS

Currently the most viable candidate for ultimate development as a commercial controlled thermonuclear fusion reactor is the tokamak device. A tokamak is a magnetic confinement device. That is, it employs a suitably configured magnetic field to confine extremely high temperature plasma. One of the main requirements of such a device is that it is capable of stably maintaining the equilibrium position of the plasma column within the discharge chamber. It is with this in mind that the resea rch presented in this thesis was undertaken.

For the toroidal geometry of the tokamak, the problem of controlling the position of the plasma column within the discharge chamber is highly nonlinear. In fact, it is even quite difficult just to determine accurately the position of the plasma column. As a consequence, the development of a controller based on traditional control theory requires numerous simplifying approximations to be made. The result is a controller that must be empirically tuned, and that can usually only provide a good quality of control, not optimal control. To improve the control of the plasma parameters within a tokamak device therefore requires extensive system modelling and the implementation of an adaptive controller.

It was thought that much of the problem of system modelling could be avoided if a fuzzy logic based controller could be implemented for the purpose of controlling the position of the plasma column within a tokamak device. To this end, a fuzzy logic based

controller was developed for application to the problem of controlling the position of the plasma column within the STOR-M tokamak.

Traditionally the plasma current within a tokamak is produced by transformer action; this is referred to as inductive current drive. While this is not the only method of producing the plasma within a tokamak device, it is the most common technique. The plasma current in the STOR-M tokamak is produced in this manner. However, the flux capability of the transformer is limited. This results in the pulsed nature of tokamak operation. This pulsed operation requires that a large thermal storage energy system be used with a commercial tokamak reactor in order for it to be capable of continuously producing an electrical output during the reactor downtime. One attractive method of reducing this downtime is to operate the tokamak in A.C. mode. In A.C. tokamak operation there is no need to recharge the transformer flux as after the available flux has been consumed in one direction of plasma current, the plasma current is smoothly reversed in direction. This greatly reduces the downtime to the sum of the plasma current ramp-down time, the dwell time, and the ramp-up time.

One of the important issues related to A.C. operation of a tokamak involves the current reversal regime. It is necessary to maintain control over the position of the plasma during this regime in order to reduce, or even better, to eliminate the dwell time. As a result, one of the primary objectives of the research described in this thesis was to improve the quality of control over the position of the plasma within the discharge chamber. More specifically, the objective was to develop a controller that would be capable of providing near optimal control of the plasma position during all modes of

tokamak operation, particularly during transient conditions such as that which occurs during A.C. operation of the STOR-M tokamak.

The first step that was taken to this end was to modify the existing plasma position control system on STOR-M. These modifications included the implementation of the ability to interface a digital computer with the controller via a data acquisition card. The hardware modifications were accompanied by the development of an Arbitrary Signal Generator that permitted operator intervention over the control signal. This Arbitrary Signal Generator combined with the existing PID controller formed the modified PID controller. This modified PID controller was implemented and applied to the STOR-M tokamak, and its performance was evaluated. It was shown that this controller was capable of providing a good quality of control over the position of the plasma column within the STOR-M tokamak both during normal mode operation and A.C. mode operation.

Having successfully demonstrated the performance of the modified PID controller, it was used as a benchmark against which to evaluate the performance of the fuzzy logic controller that was developed. It was shown that during normal mode operation of the STOR-M tokamak, the fuzzy logic based controller was capable of reliably providing control over the plasma position that was slightly better than that provided by the modified PID controller. Over the interval from 20.0 ms to 35.0 ms the plasma position signal had a standard deviation of 0.8 mm when the fuzzy logic controller was uses, as compared to a standard deviation of 1.1 mm when the modified PID controller was used. Thus, it has been shown that fuzzy logic based controllers are

suitable for application to control the plasma position during normal mode tokamak operation.

In order to evaluate the performance of the fuzzy logic based controller during transient conditions, the fuzzy logic based controller was also applied to the control of the position of the plasma column within STOR-M during A.C. operation. It was again demonstrated that the fuzzy logic based controller reliably provided the highest degree of control over the plasma position. Over the interval from 5.0 ms to 15.0 ms, the standard deviation of the plasma position signal was 2.6 mm when the fuzzy logic controller was used, and the standard deviation was 3.0 mm when the open-loop pre-programmed controller was used. The overall quality of the discharge was slightly better with the open-loop pre-programmed controller than it was with the fuzzy logic based controller. This is due in part to the trade-off between optimizing the controller for control of the plasma position versus optimizing the controller for obtaining the best possible discharge parameters during the current reversal regime of A.C. tokamak operation. The pre-programmed controller could not reliably provide a high quality of control over the position of the plasma column during A.C. mode discharges. The modified PID controller was not capable of providing a high quality of control over the plasma position during A.C. operation of STOR-M. Thus, the fuzzy logic controller is the superior controller.

The research described in this thesis has resulted in the improvement of the quality of control over the position of the plasma column within the STOR-M tokamak over that which was previously available. This is particularly true for the A.C. operation of STOR-M. Furthermore, it was demonstrated that a fuzzy logic based controller could

successfully be applied to the control of the position of the plasma within a tokamak device. This opens up the possibility of applying fuzzy control to other tokamak discharge parameters, potentially providing a marked improvement in the current quality of control available to all aspects of the tokamak discharge. The fuzzy logic based controller presented here was demonstrated to reliably and stably control the position of the plasma column within the STOR-M tokamak during both normal mode and A.C. operation.

REFERENCES

[1] E. Teller, “Fusion”, Volume 1 Magnetic Confinement Part A, Academic Press, Inc., New York, 1981.

[2] L.A. Artsimovich, “Controlled Thermonuclear Reactions”, Gordon and Breach Science Publishers, New York, 1964.

[3] R.A. Serway, “Physics for Scientists and Engineers”, 3rd Edition, Updated Printing, Saunders College Publishing, USA, 1992.

[4] F.F. Chen, “Introduction to Plasma Physics”, Plenum Press, New York, 1981.

[5] W.M. Stacey, Jr., “Fusion An Introduction to the Physics and Technology of Magnetic Confinement Fusion”, John Wiley & Sons, Inc., New York, 1984.

[6] J.G. Cordey, R.J. Goldston and R.R. Parker, “Magnetic Fusion Progress Toward a Tokamak Fusion Reactor”, Physics Today, pp. 22-30, Jan. 1992.

[7] K.M. McGuire, “Review of D-T Results from TFTR”, APS 1994, website: http://w3.pppl.gov/tftr/info/aps13195.pdf, 09/11/01.

[8] M. Keilhacker, A. Gibson, C. Gormezano and P.H. Rebut, “The Scientific Success of JET”, Nuclear Fusion, Volume 41, Number 12, 2001, pp. 1925-1935.

[9] J. Hugill, *Nuclear Fusion Research*, “Plasma Physics and Nuclear Fusion Research, Edited by R.D. Gill, Academic Press Inc., London, 1981.

[10] B.B. Kadomtsev, “Tokamak Plasma: A Complex Physical System”, Institute of Physics Publishing, London, 1992.

[11] K. Miyamoto, “Fundamentals of Plasma Physics and Controlled Fusion”, Iwanami Book Service Center, Tokyo, Japan, 1997.

[12] B.B. Kadomstev, F.S. Troyon, M.L. Watkins, P.H. Rutherford, M. Yoshikawa and V.S. Mukhovatov, “Tokamaks”, Nuclear Fusion, Volume 30, 1990, pp1675-1694.

[13] L. Spitzer Jr., “Physics of Fully Ionized Gases”, Interscience, New York, 1956.

[14] W. Zhang, PPL-137, “Improved Ohmic Confinement Induced by Turbulent Heating and Electrode Biasing in the STOR-M Toakamak”, Ph.D. Thesis, University of Saskatchewan, May, 1993.

[15] M. Emaami-Khonsaari, PPL-112, “Modeling and Control of Plasma Position in the STOR-M Tokamak”, Ph.D. Thesis, University of Saskatchewan, April, 1990.

[16] M. Emaami, O. Mitarai, and S.W. Wolfe, PPL-86, “Electron Density Measurements of Normal and AC Discharges in the STOR-1M Tokamak”, June, 1986.

[17] K.S. Chung and I.H. Hutchinson, Physics Review A, Volume 38, pp. 4721, 1988.

[18] S.W. Wolfe, PPL-101, “The STOR-1M Tokamak: Experiments on Current Reversal and Fast Current Ramping”, Ph.D. Thesis, University of Saskatchewan, July, 1988.

[19] C. Xiao, K.K. Jain, W. Zhang and A. Hirose, Physics of Plasmas, Volume 1, Number 7, July 1994, pp. 2291-2296. Also called: K.K. Jain, C. Xiao, W. Zhang and A. Hirose, PPL-145, “Measurement of Plasma Rotation Velocities with Electrode Biasing in the Saskatchewan Torus - Modified (STOR-M) Tokamak”, March, 1994.

[20] K.C. Mark, “Diamagnetic Measurements on the STOR-1M Tokamak”, M.A.Sc. Thesis, University of Saskatchewan, April, 1993.

[21] M.Emaami et al., “A Controller for Plasma Motion in a Tokamak Based on Model Estimation”, IEEE Transactions on Industrial Electronics, Volume 37, Number 4, August 1990, pp. 317-322.

[22] A. Sarkissian, A. Hirose, O. Mitaria, S. Wolfe and H.M. Skarsgard, “Turbulent Heating Experiment in the STOR-1M Tokamak”, Canadian Journal of Physics, Volume 67, 1989, pp. 884-892.

[23] “Progress Report 1995/96” Plasma Physics Laboratory, University of Saskatchewan, Saskatoon, Saskatchewan.

[24] “Catalog: Aluminum, Stainless Steels, Nickel Alloys” Atlas Alloys, Etobicoke Ontario, 1979.

[25] Design Proposal by High Vacuum Systems Inc. Jan. 7, 1983.

[26] W.Zhang, C. Xiao, L. Zhang and A. Hirose, “Control of the Floating Potential Fluctuations via Limiter Biasing in the Saskatchewan Tours-Modified (STOR-M) Tokamak”, Physics of Plasmas, Volume 1, Number 11, November, 1994, pp. 3646-3651.

[27] “TMP/NT 1000 Turbomolecular Pump & Frequency Converter Manual”, Leybold-Heraeus Vacuum Products Inc., Part Number 722-78-018 Edition C, (PP 313B).

[28] “Trivac “A” Dual Stage Rotary Vane Pump Manual”, Leybold Vacuum Products Inc., Part Number 722-78-001 Edition M, 1993 (PP 320).

[29] “Automatic Pressure Controllers APC-1000 APC-2000 Operation and Maintenance Manual”, Veeco Instruments Inc., Part Number 8290-800, (PP 287).

[30] “Precision Leak Valve PV-10 Operation & Maintenance”, Veeco Instruments Inc., (PP287).

[31] A. Nagashima, A. Funahashi, T. Kawakami, T. Shoji and K. Takahashi, "A 2-mm Wave Digital Interferometer for Tokamak Discharges in the Upgraded DIVA", Japanese Journal of Applied Physics, Volume 17, Number 7, July, 1978, pp. 1263-1270.

[32] "Operation Instructions", ELVA-1, (PP328).

[33] SPEX 1/02, ¾ meter Czerny Turner Scanning Spectrometer, "Operating, Maintenance & Instruction Manual", Spectra Research Ltd., 1969, (PP 169).

[34] V.S. Mukhovatov and V.D. Shafranov, "Plasma Equilibrium in a Tokamak", Nuclear Fusion, Volume 11, 1971, pp. 605-633.

[35] A. Hirose, "Electrodynamics" Lecture Notes for Phys 812.

[36] J. Wesson, "Tokamaks", Oxford University Press, New York, 1987.

[37] L.A. Arzimovich, "Elementary Plasma Physics", Blaisdell Publishing Company, Waltham, Massachusetts, 1965.

[38] M.A. Rothman, "Measurement of Plasma Diamagnetism by a Coil Located Near a Conducting Wall", Plasma Physics, Volume 10, pp. 86-91, 1968.

[39] H. Ninomiya and N. Suzuki, "Estimations of Plasma Position and $\beta_p + l_i/2$ from Magnetic Measurements under High-β Conditions in JFT-2", Japanese Journal of Applied Physics, Volume 21, Number 9, Sept. 1982, pp. 1323-1327.

[40] O. Mitarai, S.W. Wolfe, A. Hirose, and H.M. Skarsgard, "Measurement of the Image Field in the STOR-1M Tokamak", Plasma Physics and Controller Fusion, Volume 27, Number 4, 1985, pp. 395-404.

[41] K. Bhattacharyya and N.R. Ray, "Origin of the Inversion of Up-Down Potential Asymmetry in the Magnetized Toroidal Plasma", Plasma Physics and Controlled Fusion, Volume 43, 2001, pp. 1157-1168.

[42] G.D. Conway et al., “Suppression of Plasma Turbulence During Optimized Shear Configurations in JET”, Physical Review Letters, Volume 84, Number 7, Feb. 2000, pp. 1463-1466.

[43] C.K. Phillips et al., “Scaling of Confinement with Isotopic Content in Deuterium and Tritium Plasmas”, Physical Review Letters, Volume 79, Number 6, Aug. 1997, pp. 1050-1053.

[44] O. Mitarai, S.W. Wolfe, A. Hirose and H.M. Skarsgard, “Alternating Current Tokamak Reactor with Long Pulses”, Fusion Technology, Volume 15, Mar. 1989, pp. 204-213.

[45] N.J. Fisch, “Theory of Current Drive in Plasmas”, Reviews of Modern Physics, Volume 51, Number 1, Jan. 1987, pp. 175-234.

[46] B.J.D. Tubbing et al., “AC Plasma Current Operation in the JET Tokamak”, Nuclear Fusion, Volume 32, Number 6, 1992, pp. 967-972.

[47] O. Mitarai, A. Hirose and H.M. Skarsgard, “An Alternating Current Tokamak Reactor with Ohmic Ignition and Bootstrap Current”, Fusion Technology, Volume 20, Nov. 1991, pp. 285-294.

[48] O. Mitarai, S.W. Wolfe, A. Hirose and H.M. Skarsgard, “Stable AC Tokamak Discharges in the STOR-1M Device”, Bulletin of the APS, Volume 29, Number 8, Oct. 1984, p. 1337.

[49] O. Mitarai, S.W. Wolfe, A. Hirose and H.M. Skarsgard, “Stable AC Tokamak Discharges in the STOR-1M Device”, Nuclear Fusion, Volume 27, Number 4, 1987, pp. 604-608.

[50] O. Mitarai, A. Hirose and H.M. Skarsgard, " Plasma Density at the Current Reversal in the STOR-1M Tokamak with AC Operation", Nuclear Fusion, Volume 32, Number 10, 1992, pp. 1801-1809.

[51] O. Mitarai et al., "Experiments on the Current Rampdown Phase in the STOR-M Tokamak for AC Operation", Plasma Physics and Controlled Fusion, Volume 35, 1993, pp. 711-722.

[52] O. Mitarai el al., "Alternating Current Plasma Operation in the STOR-M Tokamak", Nuclear Fusion, Volume 36, Number 10, 1996, pp. 1335-1343.

[53] O. Mitarai et al., Feedback Control Experiments on 1.0 and 1.5 Cycle AC Operations in the STOR-M Tokamak", Review of Scientific Instruments, Volume 68, Number 7, July 1997, pp. 2711-2716.

[54] X. Yang et al., "Alternating Current Operation with Multicycles in the CT-6B Tokamak", Nuclear Fusion, Volume 36, Number 12, 1996, pp. 1669.

[55] K. Hayashi et al., "Full AC Plasma Current Operation in the CSTN-AC Tokamak", Proceedings of the International Conference on Plasma Physics, Nagoya, Japan, 1996, pp. 1246-1249.

[56] K. Ogata, "Modern Control Engineering", Prentice-Hall Inc., Englewood Cliffs, New Jersey, 1970.

[57] B.C. Kuo, "Automatic Control Systems", 6th Edition, Prentice-Hall Inc., Englewood Cliffs, New Jersey, 1991.

[58] R.C. Dorf, "Modern Control Systems", 5th Edition, Addison-Wesley Publishing Company, Reading, Massachusetts, 1989.

[59] D. Wobschall, “Circuit Design for Electronic Instrumentation Analog and Digital Devices from Sensor to Display”, 2nd Edition, McGraw-Hill Inc., New York, 1987.

[60] C. Friesen, F. Castillo and S. Kohlert, “Modification of a Plasma Position Feedback Control System”, Formal report for EP 425.3, University of Saskatchewan, 2000.

[61] JET Press Release, 31/10/97. http://www.jet.efda.org/pages/content/press-release-1997.html.

[62] JT-60 Team, “Review of JT-60U Experimental Results in 1998”, JAERI 99-048.

[63] T. Miyazima, Transcript from the Artsimovich Memorial Lecture, at the Thirteenth International Conference on Plasma Physics and Controlled Nuclear Fusion Research, held by the IAEA, Washington, D.C., October 1-6, 1990, 08/07/2002/13:24, http://www.ofes.science.doe.gov/More_HTML/Artsimovich/Miyazima.1990.html.

[64] J. Morelli, A. Singh, C. Xiao and A. Hirose, “Mach Probe and Limiter Current Measurements in the STOR-M Tokamak”, Presented at the 43rd Annual Meeting of the Division of Plasma Physics of the American Physical Society, Long Beach, California, October 2001.

[65] L. Schott, “Electrical Probes”, Chapter 11 of “Plasma Diagnostics”, North-Holland Publishing Company, Amsterdam, 1968.

[66] A. Hirose “STOR-M Technical Memorandum No. 5”, May 5, 1982.

[67] W. Zhang, C. Xiao, G.D. Conway, A. Sarkissian, H.M. Skarsgard, L. Zhang and A. Hirose, “Improved Confinement and Edge Plasma Fluctuations in the STOR-M Tokamak”, Physics of Fluids B, Volume 4, Number 10, October, 1992, pp. 3277—3284.

[68] R. Albanese and G. Ambrosino, “Current, Position, and Shape Control of Tokamak Plasmas: A Literature Review”, Proceedings of the 2000 IEEE International Conference on Control Applications, Anchorage, Alaska, Sept. 25-27, 2000, pp. 385-394.

[69] J.B. Lister et al., “Can Better Modelling Improve Tokamak Control?”, Proceedings of the 36th Conference on Decision and Control, San Diego, California, Dec., 1997, pp. 3679-3684.

[70] R. Albanese et al., “An Integrated Approach to the Control of Magnetically Confined Plasmas”, Fusion Engineering and Design, Volume 56-57, 2001, pp. 705-709.

[71] A. Portone et al., “Dynamic Control of Plasma Position and Shape in ITER”, Fusion Technology, Volume 32, Nov., 1997, pp. 374-389.

[72] M.A. Firestone, J.W. Morrow-Jones and T.K. Mau, “Comprehensive Feedback Control of a Tokamak Fusion Reactor”, Fusion Technology, Volume 32, Nov., 1997, pp. 390-403.

[73] C.G. Windsor, T.N. Todd, D.L. Trotman and M.E.U. Smith, “Real-Time Electronic Neural Networks for ITER-Like Multiparameter Equilibrium Reconstruction and Control in COMPASS-D”, Fusion Technology, Volume 32, Nov., 1997, pp. 416-430.

[74] T. Wijnands and G. Martin, “An Advanced Plasma Control System for Tore Supra”, Fusion Technology, Volume 32, Nov., 1997, pp. 471-486.

[75] J. Dahlburg, Chair, FESAC Subcommittee, Electronic Mail from the Division of Plasma Physics of the American Physical Society, “FESAC Subcommittee on Integrated Simulation Initiative”, Tue., Apr. 30, 2002.

[76] K. Yamazaki et al., “Construction of the Central Control System for the Large Helical Device (LHD) Fusion Experiment”, International Conference on Accelerator and Large Experimental Physics Control Systems, Beijing, China, Nov. 1997.

[77] K. Yamazaki et al., “Overview of the Large Helical Device (LHD) Control System and Its First Operation”, The Second Workshop on PCs and Particle Accelerator Control, Tsukuba, Japan, Jan. 1999.

[78] K. Yamazaki, H. Yamada, K.Y. Watanabe, K. Nishimura, O. Motojima, and the LHD Control Group, “Present Status of the Large Helical Device (LHD) and Its Central Control System”, International Workshop on Controls for Small- and Medium- Scale Accelerators, Tukuba, Japan, Nov. 1996.

[79] Y.-S. Na, Y.-M. Jeon, S.H. Hong and Y.S. Hwang, “Real-Time Extraction of Plasma Equillibrium Parameters in KSTAR Tokamak Using Statistical Methods”, Review of Scientific Instruments, Volume 72, Number 2, Feb. 2001, pp. 1400-1405.

[80] Y.-M. Jeon, Y.-S. Na, M.-R. Kim and Y.S. Hwang, “Newly Developed Double Neural Network Concept for Reliable Fast Plasma Position Control”, Review of Scientific Instruments, Volume 72, Number 1, Jan. 2001, pp. 513-516.

[81] L.A. Zadeh, “Fuzzy Sets”, Information and Control, Volume 8, Number 3, 1965, pp. 338-353.

[82] A. Kaufmann and M.M. Gupta, “Introduction to Fuzzy Arithmetic Theory and Applications”, Van Nostrand Reinhold Company Inc., New York, 1985.

[83] M. Mareš, “Computation over Fuzzy Quantities”, CRC Press Inc., Boca Raton, Florida, 1994.

[84] G. Bojadziev and M. Bojadziev, “Fuzzy Sets, Fuzzy Logic, Applications”, Advances in Fuzzy Systems – Applications and Theory, volume 5., World Scientific Publishing Co. Pte. Ltd., Singapore, 1995.

[85] A. Kandel, :Fuzzy Expert Systems”, CRC Press, Inc., USA, 1992.

[86] M.M. Gupta and T. Yamakawa Editors, “Fuzzy Computing Theory, Hardware, and Applications”, Elsevier Science Publishers B.V., Amsterdam, 1988.

[87] H.X. Li and V.C. Yen, “Fuzzy Sets and Fuzzy Decision-Making”, CRC Press, Inc., USA, 1995.

[88] A. Kandel, “Fuzzy Mathematical Techniques with Applications”, Addison-Wesley Publishing Company, USA, 1986.

[89] V. Rao and H. Rao, “C++ Neural Networks and Fuzzy Logic”, 2nd Edition, MIS:Press, 1995.

[90] “PCL-711B PC-MultiLab CARD USER’S MANUAL”, Part Number 2003711020 Revision A2, Advantech Co., Ltd., 1993.

[91] “PCL-LabCard Software Driver User’s Manual”, Part Number 2003000060 2nd Edition, Advantech Co., Ltd., 1994.

[92] K.A.W. Marcelle et al., “Steam Turbine Fuzzy Logic Cyclic Control Method and Apparatus Therefor”, United States Patent, Patent Number 5,517,424, May 14, 1996.

[93] K.H. Abdul-Rahman and S.M. Shahidehpour, “A Fuzzy-Based Optimal Reactive Power Control”, IEEE Transactions on Power Systems, Volume 8, Number 2, May 1993, pp. 662-670.

[94] K. Tomsovic, “A Fuzzy Linear Programming Approach to the Reactive Power/Voltage Control Problem”, IEEE Transactions on Power Systems, Volume 7, Number 1, Feb. 1992, pp. 287-293.

APPENDIX A – STOR-M PARAMTERS

Typical Operating Parameters:

- Toroidal Magnetic Field ($B_\phi \approx 0.7$ Tesla)
- Vertical Magnetic Field ($B_V \approx 60$ Gauss)
- Plasma Current ($I_P \approx 25$ kA)
- Loop Voltage ($V_P \approx 3$ V)
- Average Electron density ($n_e \approx 10^{19}$ m^{-3})
- Average Electron Temperature ($T_e \approx 150$ eV)
- Average Ion Temperature ($T_i \approx 50$ eV)
- Energy Confinement Time ($\tau_E \approx 2$ ms)
- Discharge Duration

  < 200 ms during normal operation (35 ms typical)

  ≈ 20 ms per half cycle during ac operation
- Hydrogen Plasma
- Minor radius (a = 11.5 cm)
- Major radius (R = 46 cm)
- Wall thickness (d_w = 0.156 inch)

APPENDIX B – FUZZY LOGIC CONTROLLER PARAMETERS

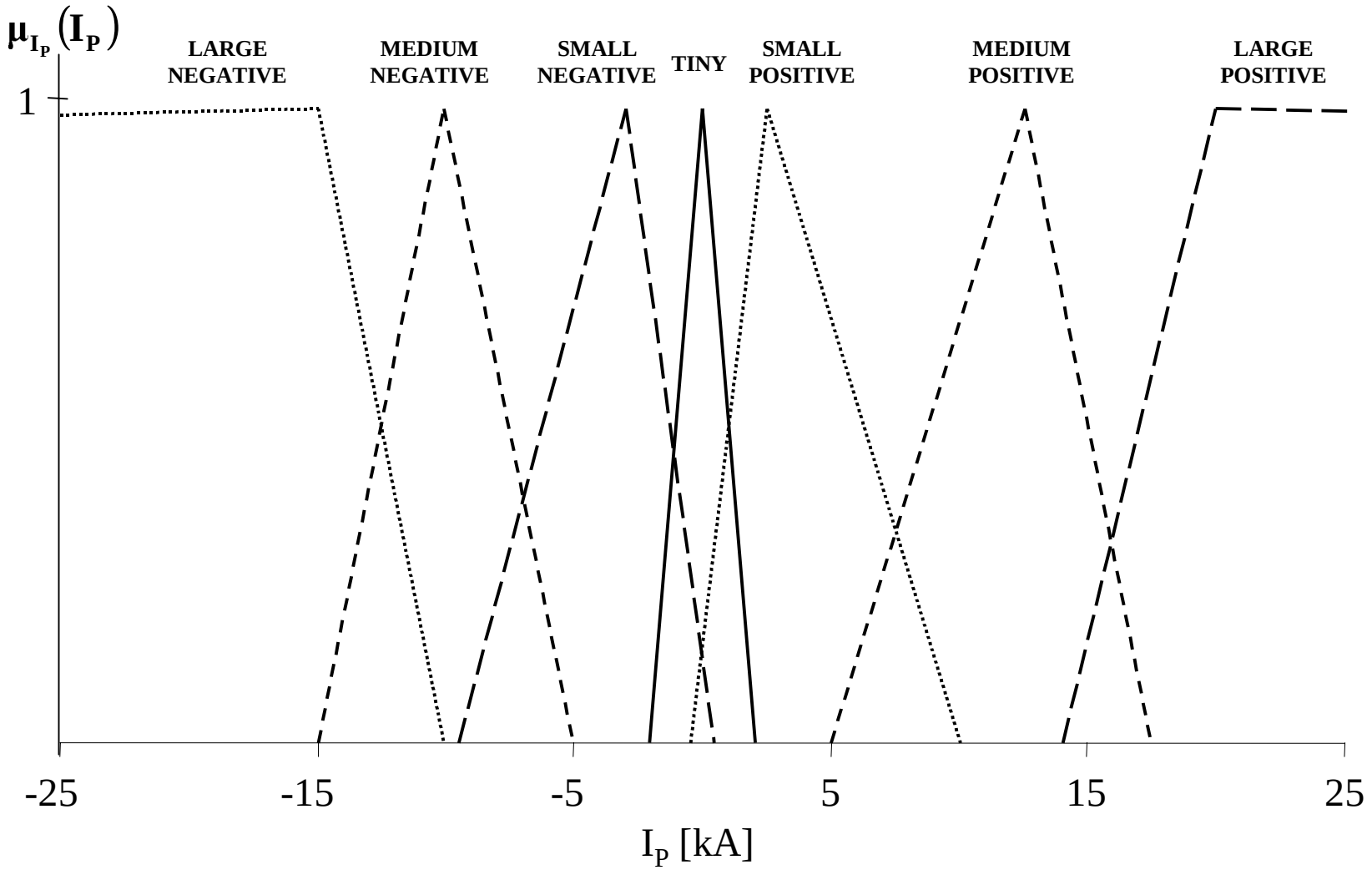

Figure B.1 Fuzzy membership functions that make up the fuzzy variable representing the plasma current. These fuzzy sets are used for both the normal and the A.C. modes of STOR-M operation.

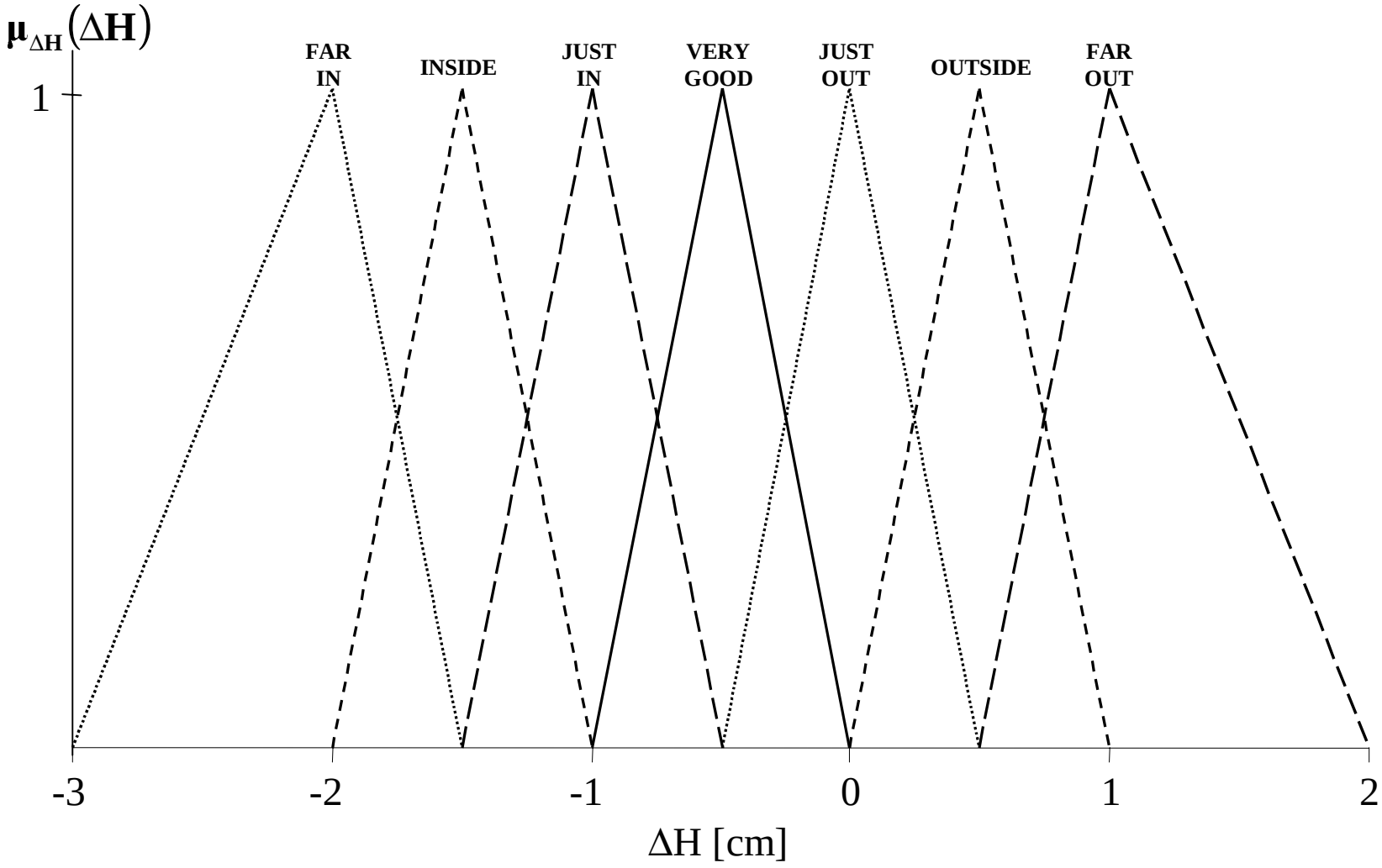

Figure B.2 Fuzzy membership functions that make up the fuzzy variable representing the plasma position during both the transient region in normal operation and the positive half cycle in A.C. operation of STOR-M.

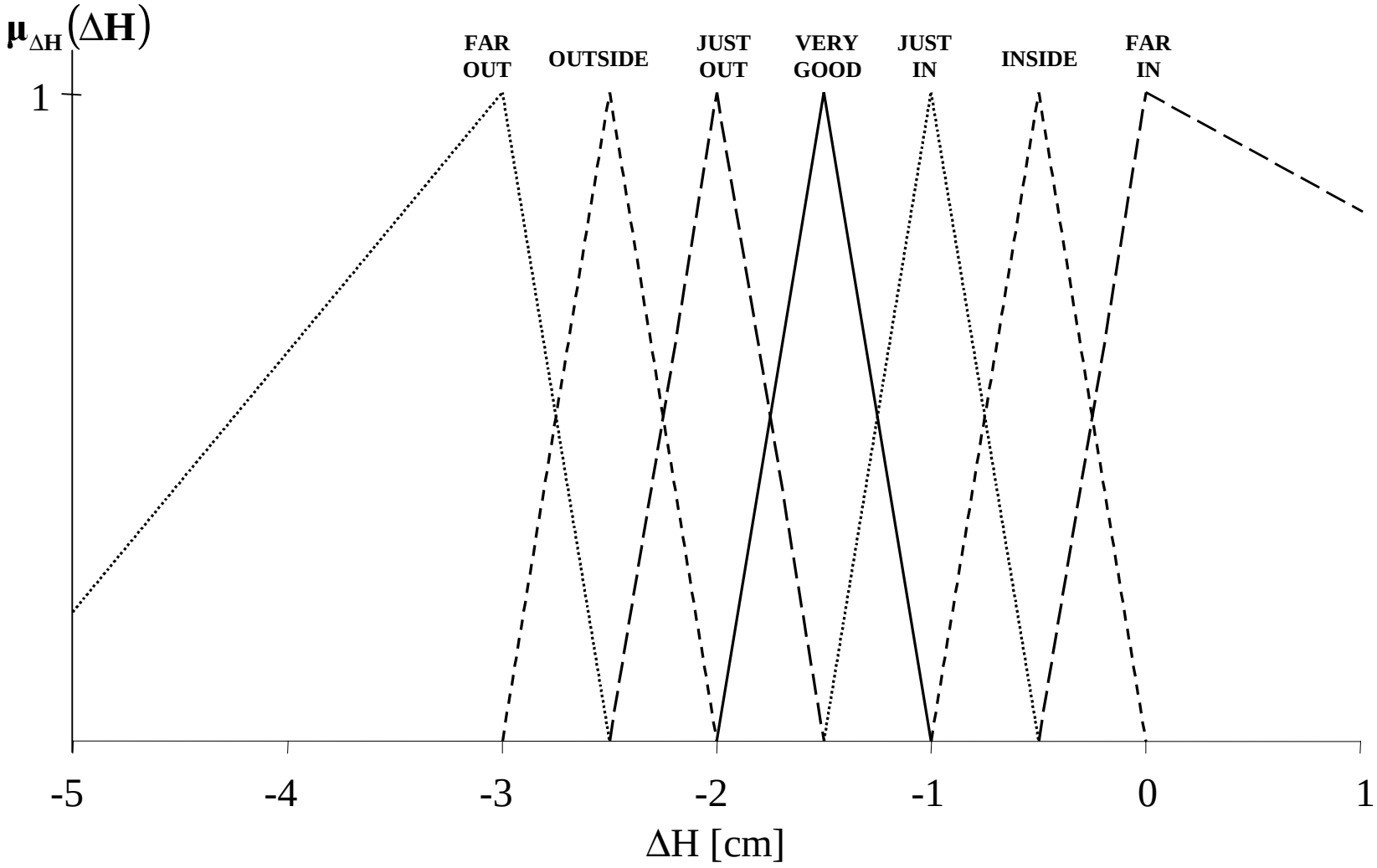

Figure B.3 Fuzzy membership functions that make up the fuzzy variable representing the plasma position during the negative half cycle in A.C. operation of STOR-M.

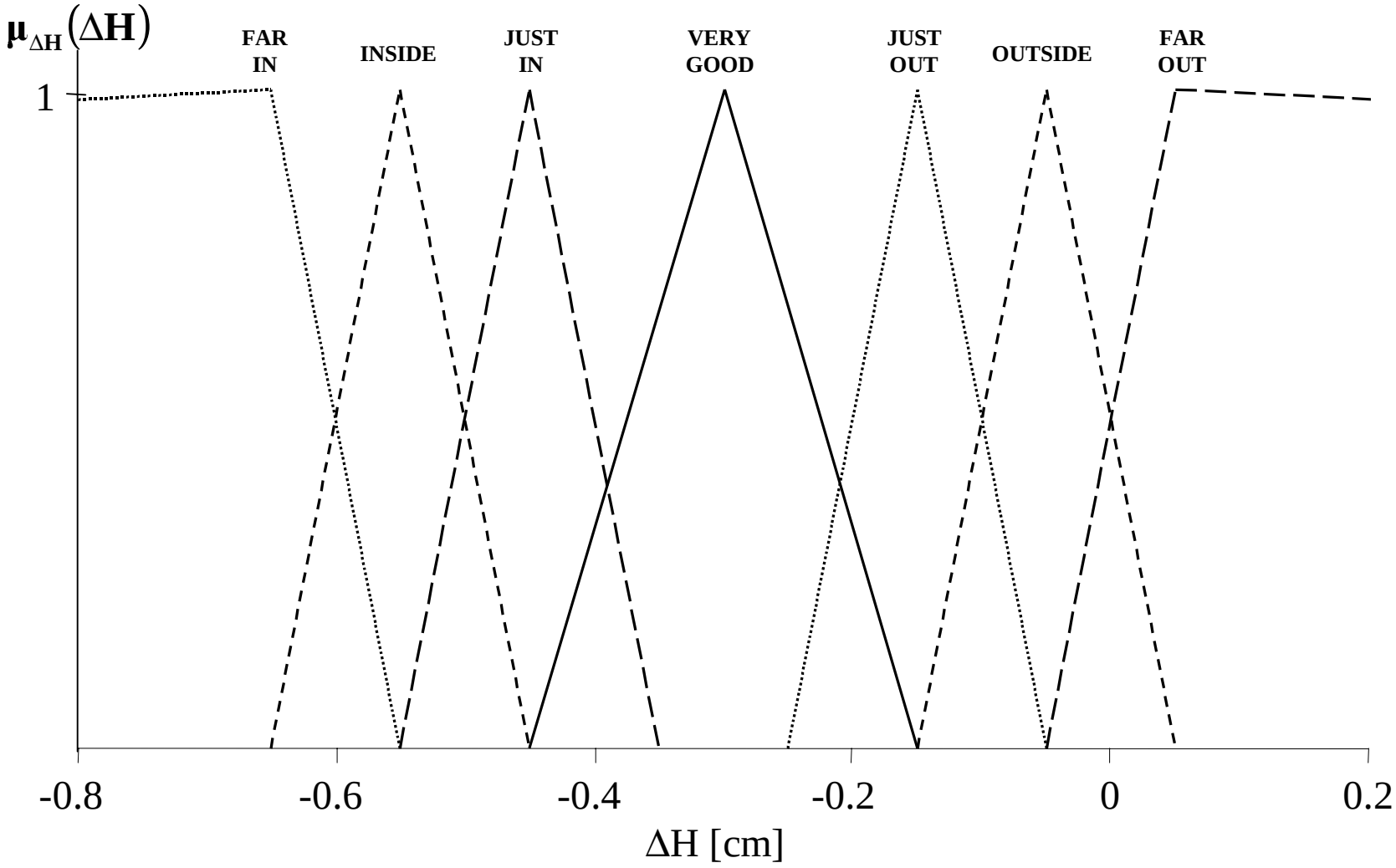

Figure B.4 Fuzzy membership functions that make up the fuzzy variable representing the plasma position during the steady-state region in normal operation of STOR-M.

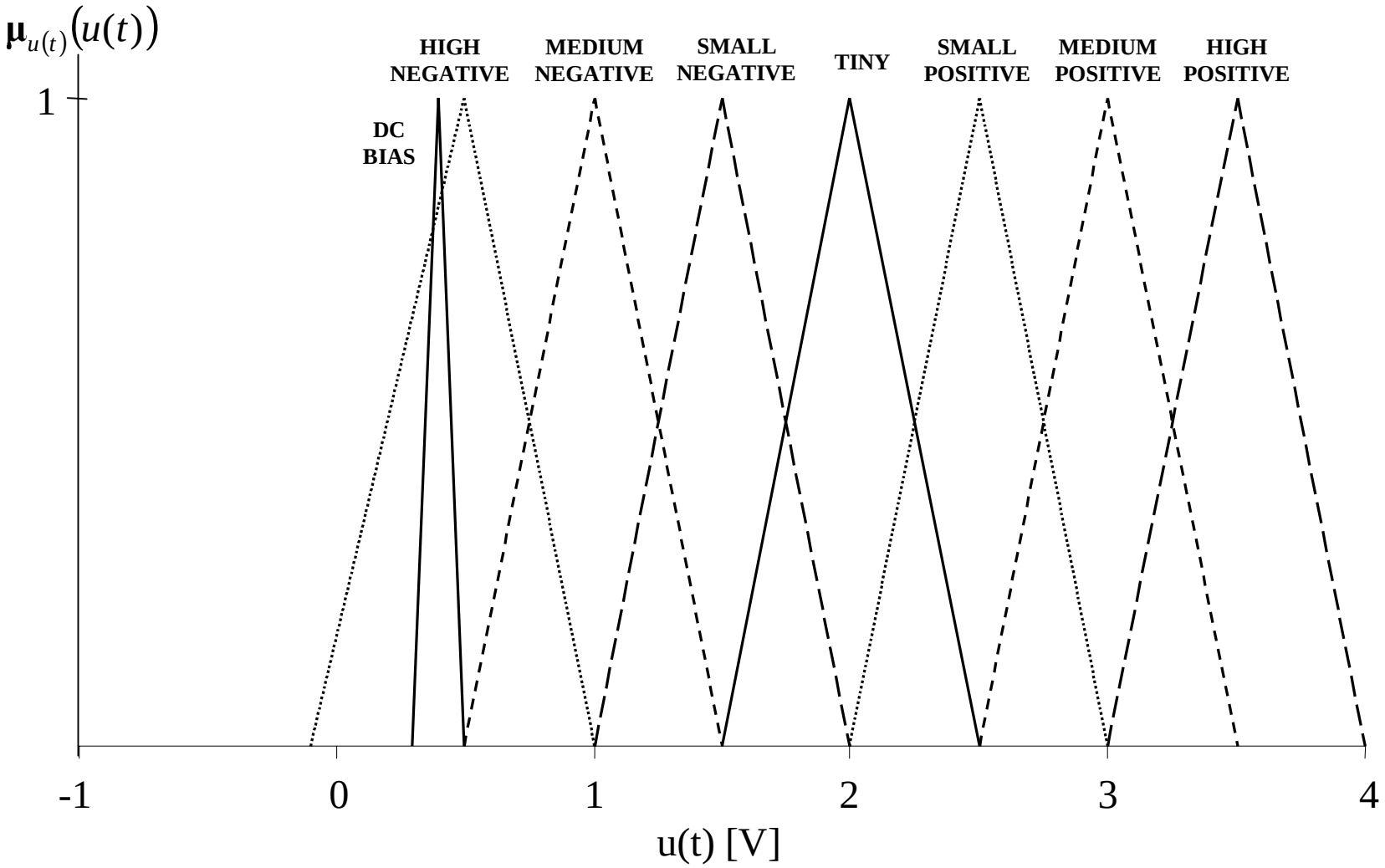

Figure B.5 Fuzzy membership functions that make up the fuzzy variable representing the control decision during both the transient region in normal operation and positive half cycle in A.C. operation of STOR-M.

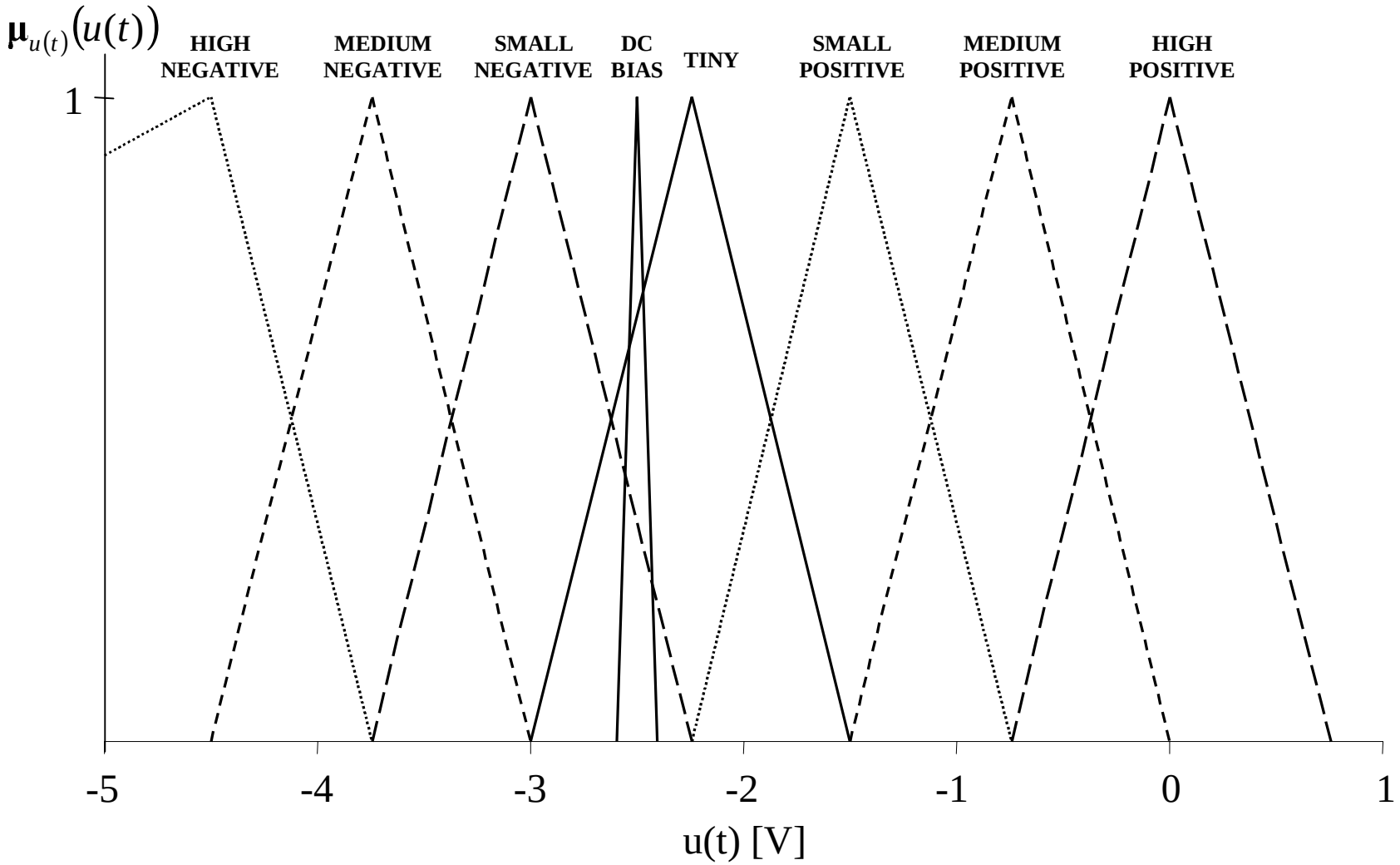

Figure B.6 Fuzzy membership functions that make up the fuzzy variable representing the control decision during the negative half cycle in A.C. operation of STOR-M.

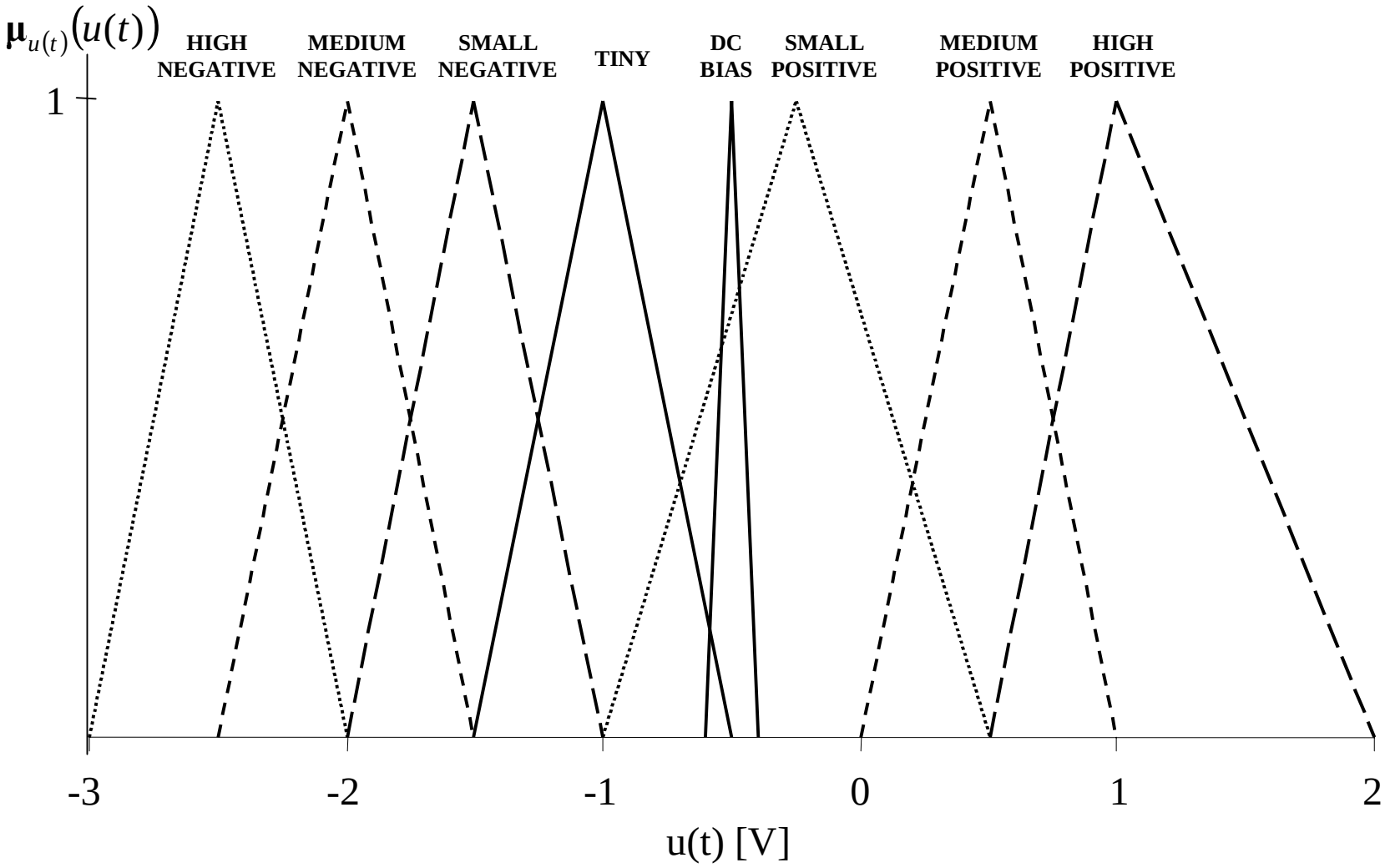

Figure B.7 Fuzzy membership functions that make up the fuzzy variable representing the control decision during the steady-state region in normal operation of STOR-M.

```
Comments: This is a sample file containing fuzzy membership
information.
The values of "lowval", "midval", and "highval" are the values of
The variable signal and must be within a suitable range.



Variable: Current
Set: large_neg  lowval: -10.0   midval: -0.150  highval: -0.100
Set: med_neg    lowval: -0.150  midval: -0.100  highval: -0.050
Set: small_neg  lowval: -0.095  midval: -0.030  highval: 0.005
Set: tiny       lowval: -0.020  midval: 0.0     highval: 0.020
Set: small_pos  lowval: -0.005  midval: 0.025   highval: 0.100
Set: med_pos    lowval: 0.050   midval: 0.125   highval: 0.175
Set: high_pos   lowval: 0.140   midval: 0.200   highval: 10.0
Comments: Fuzzy membership info for the plasma current.


Variable: Pos_Position
Set: far_out    lowval: 0.5     midval: 1.0     highval: 2.0
Set: outside    lowval: 0.0     midval: 0.5     highval: 1.0
Set: just_out   lowval: -0.5    midval: 0.0     highval: 0.5
Set: very_good  lowval: -1.0    midval: -0.5    highval: 0.0
Set: just_in    lowval: -1.5    midval: -1.0    highval: -0.5
Set: inside     lowval: -2.0    midval: -1.5    highval: -1.0
Set: far_in     lowval: -3.0   midval: -2.0    highval: -1.5
Comments: Fuzzy membership info for the position signal when the
plasma current is in region 1.


Variable: Neg_Position
Set: far_in     lowval: -0.050  midval: 0.050  highval: 10.00
Set: inside     lowval: -0.150  midval: -0.050  highval: 0.050
Set: just_in    lowval: -0.250  midval: -0.150  highval: -0.050
Set: very_good  lowval: -0.450  midval: -0.300  highval: -0.150
Set: just_out   lowval: -0.550  midval: -0.450  highval: -0.350
Set: outside    lowval: -0.650  midval: -0.550  highval: -0.450
Set: far_out    lowval: -10.00  midval: -0.650  highval: -0.550
Comments: Fuzzy membership info for the position signal when the
plasma current is in region 2.


Variable: Control_1
Set: high_pos   lowval: 3.0     midval: 3.5     highval: 4.0
Set: med_pos    lowval: 2.5     midval: 3.0     highval: 3.5
Set: small_pos  lowval: 2.0     midval: 2.5     highval: 3.0
Set: tiny       lowval: 1.5     midval: 2.0     highval: 2.5
Set: small_neg  lowval: 1.0     midval: 1.5     highval: 2.0
Set: med_neg    lowval: 0.5     midval: 1.0     highval: 1.5
Set: high_neg   lowval: -0.1    midval: 0.5     highval: 1.0
Set: DC_Bias    lowval: 0.30    midval: 0.40    highval: 0.50
Comments: u(t) fuzzy membership info for use in region 1.
```

```
Variable: Control_2
Set: high_pos   lowval: 0.5    midval: 1.0     highval: 2.00

Set: med_pos    lowval: 0.0    midval: 0.5     highval: 1.0
Set: small_pos  lowval: -1.0   midval: -0.25   highval: 0.50
Set: tiny       lowval: -1.5   midval: -1.0    highval: -0.5
Set: small_neg  lowval: -2.0   midval: -1.5    highval: -1.0
Set: med_neg    lowval: -2.5   midval: -2.0    highval: -1.5
Set: high_neg   lowval: -3.0   midval: -2.5    highval: -2.0
Set: DC_Bias    lowval: -0.60    midval: -0.50    highval: -0.40
Comments: u(t) fuzzy membership info for use in region 2.
```

Figure B.8 Sample fuzzy variable information file for Normal operation.

```
Comments: This is a sample file containing fuzzy membership
information.
The values of "lowval", "midval", and "highval" are the values of the
variable signal and must be within a suitable range.



Variable: Current
Set: large_neg  lowval: -10.0   midval: -0.150  highval: -0.100
Set: med_neg    lowval: -0.150  midval: -0.100  highval: -0.050
Set: small_neg  lowval: -0.095  midval: -0.030  highval: 0.005
Set: tiny       lowval: -0.020  midval: 0.0     highval: 0.020
Set: small_pos  lowval: -0.005  midval: 0.025   highval: 0.100
Set: med_pos    lowval: 0.050   midval: 0.125   highval: 0.175
Set: high_pos   lowval: 0.140   midval: 0.200   highval: 10.0
Comments: Fuzzy membership info for the plasma current.


Variable: Pos_Position
Set: far_out    lowval: 0.5     midval: 1.0     highval: 2.0
Set: outside    lowval: 0.0     midval: 0.5     highval: 1.0
Set: just_out   lowval: -0.5    midval: 0.0     highval: 0.5
Set: very_good  lowval: -1.0    midval: -0.5    highval: 0.0
Set: just_in    lowval: -1.5    midval: -1.0    highval: -0.5
Set: inside     lowval: -2.0    midval: -1.5    highval: -1.0
Set: far_in     lowval: -3.0    midval: -2.0    highval: -1.5
Comments: Fuzzy membership info for the position signal when the
plasma current is in region 1.


Variable: Neg_Position
Set: far_in     lowval: -0.5    midval: 0.0     highval: 5.5
Set: inside     lowval: -1.0    midval: -0.5    highval: 0.0
Set: just_in    lowval: -1.5    midval: -1.0    highval: -0.5
Set: very_good  lowval: -2.0    midval: -1.5    highval: -1.0
Set: just_out   lowval: -2.5    midval: -2.0    highval: -1.5
Set: outside    lowval: -3.0    midval: -2.5    highval: -2.0
Set: far_out    lowval: -5.5    midval: -3.0    highval: -2.5
Comments: Fuzzy membership info for the position signal when the
plasma current is in region 2.


Variable: Control_1
Set: high_pos   lowval: 3.0     midval: 3.5     highval: 4.0
Set: med_pos    lowval: 2.5     midval: 3.0     highval: 3.5
Set: small_pos  lowval: 2.0     midval: 2.5     highval: 3.0
Set: tiny       lowval: 1.5     midval: 2.0     highval: 2.5
Set: small_neg  lowval: 1.0     midval: 1.5     highval: 2.0
Set: med_neg    lowval: 0.5     midval: 1.0     highval: 1.5
Set: high_neg   lowval: -0.1    midval: 0.5     highval: 1.0
Set: DC_Bias    lowval: 0.30    midval: 0.40    highval: 0.50
Comments: u(t) fuzzy membership info for use in region 1.
```

```
Variable: Control_2
Set: high_pos   lowval: -0.75   midval: 0.0     highval: 0.75
Set: med_pos    lowval: -1.50   midval: -0.75   highval: 0.0
Set: small_pos  lowval: -2.25   midval: -1.50   highval: -0.75
Set: tiny       lowval: -3.00   midval: -2.25   highval: -1.50
Set: small_neg  lowval: -3.75   midval: -3.00   highval: -2.25
Set: med_neg    lowval: -4.50   midval: -3.75   highval: -3.00
Set: high_neg   lowval: -10.0   midval: -4.50   highval: -3.75
Set: DC_Bias    lowval: -2.6    midval: -2.5    highval: -2.4
Comments: u(t) fuzzy membership info for use in region 2.
```

Figure B.9 Sample fuzzy variable information file for A.C. operation.

```
first pulse
current in columns
DH1 in rows
         LN       MN       SN       Ty       SP       MP      LP
FO       DC       DC       DC       DC       SN       SP       MP
O        DC       DC       DC       DC       SN       SP       MP
JO       DC       DC       DC       DC       SN       SP       MP
VG       DC       DC       DC       DC       SN       SP       MP
JI       DC       DC       DC       DC       SN       SP       MP
I        DC       DC       DC       DC       SN       SP       MP
FI       DC       DC       DC       DC       SN       SP       MP

second pulse
current in columns
DH2 in rows
         LN       MN       SN       Ty       SP       MP       LP
FI       SN       Ty       SN       LN       LN       LN       LP
I        MN       Ty       SN       LN       LN       LN       MP
JI       MN       Ty       MN       LN       LN       LN       SP
VG       MN       Ty       MN       LN       LN       LN       Ty
JO       LN       SN       MN       LN       LN       LN       SN
O        LN       MN       MN       LN       LN       LN       MN
FO       MN       Ty       MN       LN       LN       LN       LN

Comments:
Enter any comments here.
  The order that DH and Ip labels appear here must be the same as the
order that they appear in vardef.fuz.
  If any changes in the number of fuzzy sets is made, then the file
d_table.cpp must be modified and the program recompiled.
```

Figure B.10 Sample decision table file used for Normal operation.

```
first pulse
current in columns
DH1 in rows
      LN    MN    SN    Ty    SP    MP    LP
FO      DC      DC      DC      DC      MP      LP      LP
O       DC      DC      DC      DC      MP      LP      LP
JO      DC      DC      DC      DC      SP      MP      LP
VG      DC      DC      DC      DC      SP      SP      LP
JI      DC      DC      DC      DC      Ty      Ty      MP
I       DC      DC      DC      DC      SN      SN      MP
FI      DC      DC      DC      DC      SN      SN      MP

second pulse
current in columns
DH2 in rows
      LN    MN    SN    Ty    SP    MP    LP
FI      SN      Ty      SN      DC      SP      LP      LP
I       MN      Ty      SN      DC      SP      LP      LP
JI      MN      Ty      MN      DC      Ty      MP      LP
VG      MN      Ty      MN      DC      Ty      MP      MP
JO      LN      SN      MN      DC      Ty      MP      MP
O       LN      MN      MN      DC      Ty      MP      MP
FO      MN      Ty      MN      DC      Ty      MP      LP

Comments:
Enter any comments here.
  The order that DH and Ip labels appear here must be the same as the
order that they appear in vardef.fuz.
  If any changes in the number of fuzzy sets is made, then the file
d_table.cpp must be modified and the program recompiled.
```

Figure B.11 Sample decision table file used for A.C. operation.